D3.6. Intermediate WP3 scientific report

WP3 – Smart Energy Distribution, Microgrids and Grid of Microgrids

Author: University of Salerno (USA)

September 2023

SMARTGYSUM project has been funded by the European Commission's Horizon 2020 Programme

SMARTGYSUM project has been funded by the European Commission's Horizon 2020 Programme

SMARTGYsum has been funded by the European Union's Horizon 2020 Programme under the Grant Agreement GA 955614

The contents of this publication are the sole responsibility of USA (University of Salerno) and do not necessarily reflect the opinion of the European Union

Versions:

Version No.	Person in charge	Institution (acronym)	Date	Comments
1	Oleksandr Velihorskyi	CNUT	18.06.2023	First template of the deliverable report
2	Giovanni Petrone	USA	10.09.2023	Compilation of chapters, devoted to tasks 3.2, 3.3 and 3.4
3	Oleksandr Velihorskyi	CNUT	13.09.2023	Report about Task 3.1 added
4	Giovanni Petrone	USA	25.09.2023	General compilation of report
5	Oleksandr Velihorskyi	CNUT	30.09.2023	Minor improvements and proofreading
6	Enrique Romero	UEX	05.10.2023	Approval and PDF creation for uploading

SMARTGYSUM project has been funded by the European Commission's Horizon 2020 Programme

Technical References:

Project Acronym	**SmartGYsum**
Project Title	Research and Training Network for Smart and Green Energy Systems and Business Models
Project Coordinator (PC)	Enrique Romero (eromero@unex.es) Universidad de Extremadura (UEX)
Project Duration	1 October 2021 – 30 September 2025

Deliverable No.	D3.6
Dissemination Level	Public
Work Package	WP3 – Smart Energy Distribution, Microgrids and Grid of Microgrids
Tasks	
Lead Beneficiary	5 - USA
Contributing beneficiary (ies)	CNTU, GUT, CAU, KIT
Data due of deliverable	01 October 2023
Actual submission date	01 October 2023

Table of Contents

List of abbreviations

BEN	Beneficiary
Dn	Deliverable (number)
DoA	Description of Action
DS	Doctoral School
ESR	Early Stage Researcher
ETN	European Training Network
GA	Grant Agreement
IRP	Individual Research Project
ITN	Innovative Training Network
MSn	Milestone (number)
MSCA	Marie Sklodowska-Curie Actions
PC	Project Coordinator
REC	Research Ethics Committee
RSC	Recruitment and Secondment Committee
WPn	Work Package (number)

SMARTGYSUM project has been funded by the European Commission's Horizon 2020 Programme

1. Executive summary

The present deliverable provides the first report about the scientific activities done and main results obtained with the implementation of IRPs of ESRs working on workpackage WP3.

WP3 (Smart energy Distribution. Microgrids and grid of microgrids) aims to explore the possibilities of microgrids for energy management to address the challenges of secure energy routing and power quality control, as well as advanced distribution grid management and the use of radial grids. This research is addressed by IRPs identified by 5 to 8.

This deliverable presents the progress of each task highlighting the work done by each of the ESRs involved in this WP, and how they are contributing to achieve the WP outcomes. In particular, the objectives of WP3 are to identify and demonstrate new ways of collaborative distributing electric energy and new operation strategies as well as operating in connected and islanding modes; to design converters and strategies to control microgrids (as optimal operational parts of distribution grids) to manage energy flows and minimize transportation losses; to coordinate the production of different generators with the consumption of different consumers to match generation and consumption in a safety and optimize way; finally to analyse the new opportunities of storage system in microgrids and conventional grids.

This deliverable also illustrates the challenges faced by the different parties and their impact on the main results versus the expected ones.

The ESRs involved in this WP3 are:

- ESR05 (**Mohammadreza Azizi**), recruited and coordinated by Chernihiv Polytechnic National University (CNTU). The individual research project is entitled "Energy Router for Hybrid Microgrids for efficient and robust energy and power management". The IRP objectives are linked to research on the communication performance requirements in wireless networks, as well as to advance in the grid intelligence to understand the energy distribution in the grid and allow real-time decision making.

- ESR06 (**Mykola Lukianov**), recruited and coordinated by Politechnika Gdanska (GUT). The individual research project is entitled "EV chargers, developing an active bidirectional charger able to provide anciallary services". The IRP objectives are linked to develop new power electronics facilities for energy transfer system with improved efficiency and power density and analyse future energy system including wireless charge system for electric vehicles.

- ESR07 (**Mahyar Hassanifar**), recruited and coordinated by Christian-Albrechts-Universitaet Zu Kiel (CAU). The individual research project is entitled "Reliability and availability of Smart Transformers for cost effective and high quality of services in the grid". The IRP objectives are linked to create smart devices in the grid, aimed at enabling autonomous grid management increasing the reliability and the availability of grid services.

- ESR08 (**Gabriele Arena**), recruited and coordinated by Karlsruhe Institut für Technologie (KIT). The individual research project is entitled "Real-time modelling and validation of Distributed Energy Storage Systems and Integration strategies". The IRP objectives are linked to generate and analyse real-time models of Distributed Energy Sustems, to optimize distributed REES through the integration of actual and simulated components, controls and networks, under a wide variety of scenarios, to optimize the computation efforts for the obtention of the models.

The initial results obtained by ESR05 are focused on the comprehensive review of existing topologies of power converters for energy conversion in microgrids and the analysis of existing reliability and protection measures in such systems. In particular three tasks have been carried out: analysis of the energy router structure; analysis of common-ground solutions for energy router; enhancement of reliability and protection in energy router structures These activities includes simulation techniques, analytical calculations and analysis techniques. Successful implementation of that tasks are the basis for the next steps (e.g. design of energy router consisting of power converters).

The results obtained by ESR06 are mainly related to the theoretical part of the research, with a deep study of the problems related to the EV bidirectional charging and its future part in the electrical network structure. The ESR carried out an extensive review of the EV charging technologies,; the ancillary services market for aggregated bidirectional EV charging; the problems associated with EV charger connection points as well as the modern bidirectional EV charger converter topologies. On the basis of the literature review, LV DC traction connection point were chosen, as such that stimulates development of light rail traction transport, increases its overall efficiency and reduces bidirectional EV chargers installation costs. Further research were related to the power exchange between elements of the system and system control algorithm. In the studied simulation model case, with a real tram power profile, voltage peak at the line during tram braking was reduced, which shows that LV DC power quality is improved. As a result, proposed control algorithm with bidirectional EV chargers allows to reduce peak voltage at the LV DC line, reduce peak power consumption form the traction substation and to manage PV batteries and EV batteries to reduce circulating power.

The initial objective of ESR07 has been to comprehensively study the literature about the Smart Transformer (ST) to gain the required knowledge for the next stages of the research. In the initial phase of the research, the ST structures along with potential converter topologies applicable to each architecture and stage are reviewed. Based on insights acquired from this review, the three-stage topology is chosen as a preferred structure for subsequent analysis and the continuation of research. the modular multilevel converter (MMC) is chosen to be used in the ST. To have a deeper understanding of the MMC, the MMC-based topologies are reviewed and compared. Subsequently the research focus shifted towards enhancing the lifetime of the MMC to make it more economically attractive. A new method that simultaneously balances junction temperature and capacitor losses is proposed for integration with the conventional capacitor voltage balancing method. To validate the feasibility of the proposed method, a three-phase MMC is simulated. The proposed method is integrated into the balancing stage and an analysis was conducted between the conventional balancing technique and the proposed strategy. An indepth analysis has been provided to validate the performace of the proposed solution. A test bench, currently in its assessment phase, will be also employed to evaluate the effects of the proposed method.

ESR08 started his research activity by analysing the main characteristic of DC-DC converters and DC networks. In particular, losses and short-circuit behavior of an isolated and a non-isolated DC-DC converter have been studied to understand which one fits better the DC networks of the future. Moreover, the modeling of DC-DC converters through different integration methods has been studied, taking as study case the dual active bridge converter. Finally, the main features and standards of DC fast charging stations have been explored as a case of study of DC networks and the ESR08 is going in the direction of exploring converter topologies and optimization strategies of DC fast charging stations connected to DC microgrids. The use of battery energy storage systems (BESSs) has also been discussed for DC fast charging stations. The use of a BESS can reduce the installation and grid reinforcement costs in areas where the grid infrastructure is weak like countryside and highways. The grounding strategies for DC networks have also been studied to understand the properties of different grounding systems, such as TN-S and TI, and the advantages and disadvantages of different grounding resistances. The experimental setup for the future studies on isolated DC-DC converter topologies for DC fast charging stations has been bought and prepared for tests. It will be used soon to validate the simulated results on the real hardware.

1.1. Objectives of the deliverable

The objective of the intermediate scientific report is to collect the results obtained in the corresponding IRPs included in the WP3.

1.2. Organisation of the deliverable

The present deliverable is based on the report made by the ESRs describing their yearly work towards the WP and Tasks objectives. Overall, the work done is in line with what was expected with no significant deviations with respect to the workplan. Only for ESR05 and ESR08 there are some modification, as described in the following.

ESR05 had some deviation with the initial plan of the project, mainly caused by the war in Ukraine that started 24th of February 2022, just after the candidate selection was completed. ESR05 started his work in remote and it was decided that he has to be hosted by Tallinn University of Technology involved as secondment. Unfortunately, visa application has been rejected for two time (June 2022 and November, 2022). Finally, according with supervisors and

Project Coordinator, it was decided to change initial plan and try academic mobility program to Extremadura University (coordinator of the project). The third attempt of visa application was successful, starting from end of March, 2023, and ESR05 is hosted at University of Extremadura, starting since that date. Nevertheless the mentioned issues only shifted the formal date of recruitment and not affected significantly the obtained results. Despite these issues ESR05 published 2 conference papers and he has been also enrolled to the PhD study program in the specialty "Electric power engineering, electrical engineering, and electromechanics" in Chernihiv Polytechnic National University, he successfully finished the first year of study program and by the decision of Scientific Council of CPNU allowed to transfer to the second year of study.

ESR06 research activies are going forward as planned, he has published a review paper in journal and 2 conference paper. He also received the best abstract award during the conference «XI Konferencja Naukowo-Techniczna –I-MITEL-2023, Sulęcin, kwiecień 12-14, 2023» with the title "LV DC traction substation with connected bidirectional EV chargers and improved functionality". He spent two months of secondment at UEX (February – March 2023) during which, simulation model to verify considered PCI connection schemes and power flow were developed.

Progress in research activities for ESR07 is also following the expected timeline, he published one conference paper and currently is working for submitting a joint publication, which should compare the hybrid transformer and the smart transformer with respect to their grid service provision capability. ESR07 has been also involved in other professional activities such as supervising a student in Master Seminar, teaching assistant in a course named "Renewable Energy Systems", teaching Bachelor Laboratory. ESR07 also undertook his first secondment at the GUT, under the supervision of Prof. Strzelecki

ESR08 has been distinguished for getting 5 conference paper in the first year of the research activities and for receiving the best student award at the AEIT2022 conference in Rome. A first period of secondment in Tallinn (Estonia) has been also completed where he worked the state of the art of DC fast charging stations with the intent to submit a journal review paper on this topic. To this regard, with respect to the initial IRP, the modeling of faults in DC networks was not done because it has been decided to focus on DC fast charging stations for electric vehicles, due to the strategic importance that they have in the future energy grids.

2. General progress of the action

2.1. WP3 Objectives and tasks

WP3 (Smart Energy Distribution, Microgrids and Grid of Microgrids) objectives are:

i. To identify and demonstrate new ways of collaborative distributing electric energy and new operation strategies as well as operating in connected and islanding modes;
ii. To design converters and strategies to control microgrids (as optimal operational parts of distribution grids) to manage energy flows and minimize transportation losses.
iii. To coordinate the production of different generators with the consumption of different consumers to match generation and consumption in a safety and optimize way
iv. To analyse the new opportunities of storage system in microgrids and conventional grids

WP3 (Smart Energy Distribution, Microgrids and Grid of Microgrids) tasks are:

- Task 3.1: Development of Energy Routers for Hybrid Microgrids enhancing efficiency and robustness (USA-CNTU).
- Task 3.2: Development of an Active Bidirectional Energy Charger for providing Ancillary Services. (USA-GUT).
- Task 3.3: Research on the reliability of smart transformers to ensure cost-effective and high-quality services. (USA-CAU).
- Task 3.4: Real time modelling of energy storage system technologies with low computation effort (KIT-OPAL).
- Task 3.4: Elaboration of partial and final scientific reports on Smart Energy Distribution (USA).

2.2. WP3 – Workpackage progress

ESR	Starting date	General evaluation	Status
5	1/08/2022	Work of ESR05 in the first reporting period were done, aimed to fulfil the Objective 3.2 and to complete Task 3.2. Considering current project progress, achieved research project results, and taking into account force majeure issues (war in Ukraine and visa issues for Iranians in Estonia), the work of early-stage researcher Mr. Mohammadreza Azizi under the individual research project "Energy Router for Hybrid Microgrids for efficient and robust energy and power management" can be rated as "good".	In accordance with the plan, with some delay in publication activity.
6	1/06/2022	ESR06, during the first year of the study, conducted a comprehensive review of contemporary literary sources. Additionally, in order to determine the relevance and direction of the research, a series of meetings were held with companies and specialists in the field of traction networks for trains (Pesa) and project partner - Arex, specialists in connecting EV chargers to trolleybus networks. Based on the data obtained, the main problems of connecting bidirectional charging stations to traction networks were identified. Throughout the year, the synthesis and analysis of a system structure enabling the integration of bidirectional charging stations for e-autos and renewable energy sources into traction substations were primarily carried out. The results of the work in the first year also included publications in journals and presentations at conferences.	On going
7	1/08/2022	ESR07 initiated his research on 1st August 2022, under the supervision of Prof. Marco Liserre and Dr. Marius Langwasser, he has been working toward the objectives of the project. In the initial phase, ESR7 focused on the Smart Transformers (ST) and suitable converter topology to be utilized in ST. The modular multilevel converter (MMC) was identified as a potential candidate to exploit in the medium-voltage stage of the ST. An in-depth analysis of the MMC-based topologies was conducted and the results of this investigation were disseminated through a conference paper publication. Since April 2023,	On going

		ESR07 has been dedicated to improving the simulation of the new MMC submodule balancing method. In parallel, he has been engaged in setting up an experimental test bench to validate the feasibility of the proposed approach through practical experimentation. This setup has also required ESR7 to acquire proficiency in VHDL language and system-on-chip (SoC) technology, which is essential for controlling the test bench.	
8	1/04/2022	ESR08 goal is to analyse, model, control and validate DC energy resources in order to obtain a more efficient and sustainable energy distribution. As main test case, he has focused on DC fast charging stations, due to the strategic importance that they have in the future energy grids. On the opposite of slow charging stations, where a lot of research has been done, DC fast charging stations offer still a lot of interesting research questions, that ESR08 will try to reply during his PhD project. In the last 15 months, he focused on the main characteristic of DC-DC converters and DC networks. In particular, losses and short-circuit behavior of an isolated and a non-isolated DC-DC converter have been studied to understand which one fits better the DC networks of the future. Particular focus has been given to the modelling, both from the power electronics side and from the integration methodologies, taking as study case the dual active bridge converter.	On going

3. WP3 Tasks progress

3.1. Task 3.1 – IRP5 "Energy Router for Hybrid Microgrids for efficient and robust energy and power management"

3.1.1. Introduction

The scientific work of IRP5 "Energy Router for Hybrid Microgrids for efficient and robust energy and power management" was done by Mr. Mohammadreza Azizi, recruited by full-time position of Early-stage researcher in Chernihiv Polytechnic National University (Ukraine) under supervision of Dr. Oleksandr Velihorskyi and Dr. Oleksandr Husev. Due to the full-scale invasion of Russian Federation in Ukraine, the start of the contract was postponed from 01.03.2022 to 01.08.2022 with the granted possibility for remote work mode of Mr. Azizi and academic mobility to Estonia (Tallinn University of Technology, where one of co-supervisors is hosted) on the period of war in Ukraine.

Due to problem in getting long-term Estonian visa (two rejected applications and two rejected appeals on decision), the first scientific outcomes were obtained in the period from 1st of August, 2022 to 28th of March, 2023 in remote mode in Iran and partly in Turkey. The next scientific outcomes were reached:

- Review and comparison of isolated dc-dc converters for low power applications for use in the overall energy structure of the router (August-September 2022). The results of this study were presented at the PEMC-2022 conference (September 2022).
- Detailed analysis of Parallel and Redundant operation of two inverters in energy router, working at the "back-to-back" principle. The issue of balancing performance was observed that proposed to be overcome by the modification of the control method by means of "virtual impedance" block in the control structure (October-December 2022).
- To solve grounding issues, using a common-ground inverter in the overall structure of the energy router was proposed. The Energy Router structure was simulated using a common-ground inverter and different working conditions were investigated (January-March 2023). The results of studies and simulation of common-ground inverters in the general structure of Energy Router were collected and presented at the CPE-PowerENG 2023 conference.

After consultations of supervisors with the project coordinator it was decided to establish academic mobility program to University of Extremadura. After getting long-term Spanish visa, the second part of the academic work was done from 29th of March, 2023 to 31st of September, 2023 at the facilities of University of Extremadura. The next scientific outcomes were reached there:

- In the initial stage, the aim was to investigate dc nanogrids and ac nanogrids. By studying relevant references, efficiency comparison criteria were examined and with a fair approach, two ac and dc nanogrids were examined and compared. Due to the fact that the dc nanogrid had higher efficiency in the presence of PV and storage, the energy router that has a dc link to connect PV, energy storage and dc loads, and has an AC link to connect to the AC network and feed electric AC loads, was considered as a suitable solution. Then, the challenges of this structure such as isolation, grounding, etc. were examined. This result work was done in March-May 2023 May and the rest of this work is being implemented and written since the end of August.
- From the beginning of June, according to the approved schedule, the investigation and research on the topics related to reliability and protection improvements, such as grounding, isolation and leakage current in dc and ac systems at the connection point of dc to ac parts have started. This part of the work lasted in June-August. Finally, in September, the work on the preparation of Journal paper on that topic is going on.

As a part of academic mobility short research visit to Tallinn University of Technology was done from June 6th to June 29th, 2023. During that visit, some work was done in the facilities of Power Electronics Group of TalTech. In parallel with research work in laboratory under guidance of co-supervisor Dr. Oleksandr Husev, the participation in 2023 IEEE 17th International Conference on Compatibility, Power Electronics and Power Engineering (CPE-POWERENG), that was held in Tallinn, Estonia, from 14 to 16 June 2023, was also done in that period.

3.1.2. Scientific outcomes

According to the initial study plan of the project in the first year, which included a comprehensive review of existing energy router structures in the microgrids, Studies, and research were conducted on the topic and the following scientific results were obtained during this reporting period.

Introduction

Considering the importance of using renewable resources and the increasing trend of using these resources in the distribution network, the importance of energy management becomes more apparent. In the residential sector, many buildings are equipped with PV and storage units. Having an interface converter that can measure the amount of production, storage and consumption is very beneficial from an economic and technical point of view. Considering that existing solar inverters only momentarily transfer PV power to the grid and do not have energy management capabilities, Energy Router was introduced as a new generation of interface converters with energy management capabilities. In this regard studying different structures of energy routers and improving their capability and removing their challenges in this project is of high importance.

Comparative Evaluation of Isolated dc-dc Converters for Low Power Applications

Among the various dc-dc converters, isolated converters have higher reliability. A high-frequency transformer with low weight and volume in its structure increases the reliability of the converter by creating isolation and can also increase the gain of the converter through the turn ratio. The flyback converter is a widely used structure and is usually used in the low power range. Many researchers have tried to improve the performance of this converter by providing derivatives of it. Snubber circuit design or switching improvements are among these studies. This converter with two differential outputs has been used as a single-stage inverter, while also it is used as the dc-dc booster step in a solar inverter. Another known dc-dc isolated structure is the forward converter. The use of a third winding to reset the circuit and instantaneous conversion of energy through the operation of the transformer are some of the features of this converter. Researchers have also proposed derivative structures to improve this converter. In dual-switch structure, the use of two switches reduces the voltage across the switch, and there are two diodes on the primary side instead of the third winding to reset the circuit. Other commonly used dc-dc isolated converters include push-pull and full-bridge converters . The use of a three-taps transformer and the operation of each of the two switches in each half-cycle are characteristic of the push-pull converter. As in each half-cycle, one of the switches is conducting and the voltage source is empowering, the utilization rate of the voltage source will be higher.

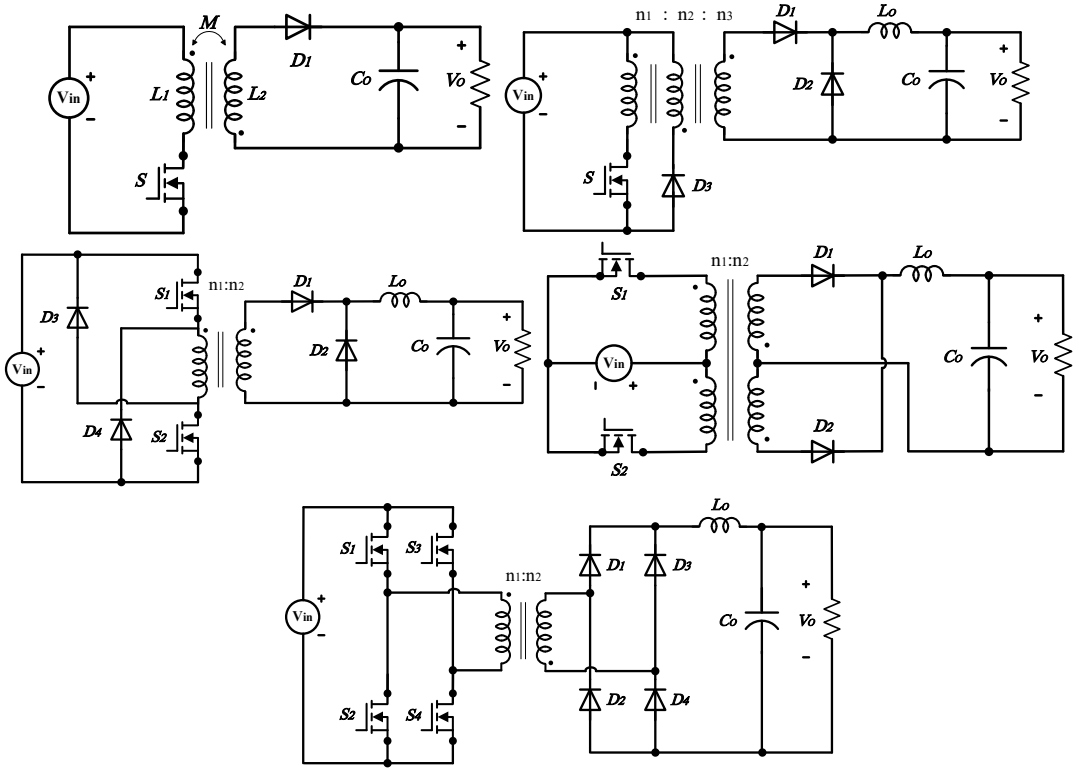

Fig. 3.1.1. Five well-known isolated dc-dc converters. a) Flyback b) Forward c) Dual-Switch Forward d) Push-Pull e) Full-bridge

The full-bridge converter has also been welcomed as a well-known and widely used structure in all power ranges or as a bidirectional converter in many applications. With the development of power electronic converters, these types of isolated converters are still widely used in many low-power applications. Several studies have compared and analyzed some of these converters.

Fig. 3.1.1 shows the five well-known isolated structures including flyback, forward, dual-switch forward (DS-forward), push-pull, and full-bridge converter. The use of high-frequency magnetics in these structures is for primary and secondary isolation, which is associated with increasing gain and the reliability of the converter. To design the elements of these converters, the optimal values of the elements should be calculated by analyzing the performance in different operating modes and extracting the relationships governing them. In this section, by examining the flyback converter, its elements will be designed.

Methodology of Evaluation

In this section, the purpose is to simulate and compare the above converters. Table 3.1.2 lists the specifications of the converter required for evaluation. Due to the gain relationship of the flyback converter based on the buck-boost converter and its duty cycle range, the turn ratio of the coupled inductors in this converter is considered to be 20. The other converters in this study operate based on buck converters. For the stable operation of the forward converters, the duty cycle must be less than 0.5. Due to the gain relationship in these converters, to produce an output voltage of 350V with an input voltage of 24-36V, a higher transformer turn ratio is required. To simulate these two types of forward converters in these simulations, the transformer turn ratio is set to 38. For the two converters of push-pull and full-bridge, the duty cycle is between zero and one. Therefore, in push-pull and full-bridge converters, like flyback, the turn ratio is considered to be 20. In Table 3.1.1, the K coefficient is considered for all converters except flyback. The flyback converter has a continuous magnetizing current and coefficient K in the flyback converter is the ratio of the magnetizing current ripple to the dc value of this current. While for other converters, this coefficient is the ratio of the maximum magnetizing current to the input current difference. This coefficient is assumed to be 0.05 for the flyback converter in the simulation. In the following sections, these converters are examined and compared from different aspects.

Table 3.1.1 - Converter design equations

	Flyback	Forward	DS-forward	Push-pull	Full-bridge
LM	$\frac{D^2V_{in}^2}{2Kf_sP_o}$	$\frac{2(1-2K)f_sL_oD^2V_{in}^2}{2Kf_s^2L_oP_o+Kf_s(1-D)V_o^2}$	$\frac{(1-2K)f_sL_oD^2V_{in}^2}{2Kf_s^2L_oP_o+Kf_s(1-D)V_o^2}$	$\frac{2(1-K)f_sL_oD^2V_{in}^2}{2Kf_s^2L_oP_o+Kf_s(1-D)V_o^2}$	$\frac{(1-2K_1)f_sL_oD^2V_{in}^2}{2Kf_s^2L_oP_o+Kf_s(1-D)V_o^2}$
LO	-	$\frac{(1-D_{\min})V_o^2}{2K_{Lo}f_sP_o}$	$\frac{(1-D_{\min})V_o^2}{2K_{Lo}f_sP_o}$	$\frac{(1-D_{\min})V_o^2}{2K_{Lo}f_sP_o}$	$\frac{(1-D_{\min})V_o^2}{2K_{Lo}f_sP_o}$
CO	$\frac{D_{\max}}{Rf_sK_C}$	$\frac{1-D_{\min}}{8K_Cf_s^2L_o}$	$\frac{1-D_{\min}}{8K_Cf_s^2L_o}$	$\frac{D_{\max}}{8K_Cf_s^2L_o}$	$\frac{D_{\max}}{8K_Cf_s^2L_o}$
VS-max	$V_{in-\max}+\frac{D_{max}V_{in-\min}}{1-D_{max}}$	$(1+n_1/n_2)V_{in}$	V_{in}	$2V_{in}$	V_{in}
IS-max	$\frac{P_o}{\eta DV_{in}}+\Delta I_{L_M}$	$\frac{P_o}{\eta DV_{in}}+\Delta I_{L_M}+\Delta I_{L_o}$	$\frac{P_o}{\eta DV_{in}}+\Delta I_{L_M}+\Delta I_{L_o}$	$\frac{P_o}{\eta DV_{in}}+\Delta I_{L_M}+\Delta I_{L_o}$	$\frac{P_o}{\eta DV_{in}}+\Delta I_{L_M}+\Delta I_{L_o}$
VD1-max	$\frac{n_2}{n_1}\frac{V_{in}}{1-D}$	$\frac{n_2}{n_1}V_{in}$	$\frac{n_2}{n_1}V_{in}$	$2\frac{n_2}{n_1}V_{in}$	$\frac{n_2}{n_1}V_{in}$
ID1-max	$\frac{V_o}{(1-D_{\max})R}$	$\frac{(1-D)V_o}{2f_sL_o}+\frac{V_o}{R}$	$\frac{(1-D)V_o}{2f_sL_o}+\frac{V_o}{R}$	$\frac{(1-D)V_o}{8f_sL_oD}+\frac{V_o}{R}$	$\frac{(1-D)V_o}{8f_sL_oD}+\frac{V_o}{R}$
n2/n1	$\frac{(1-D_{\max})V_o}{V_{in-\max}D_{\max}}$	$\frac{n_3}{n_1}=\frac{V_o}{DV_{in}}$	$\frac{V_o}{DV_g}$	$\frac{V_o}{DV_g}$	$\frac{V_o}{DV_g}$
D	$\frac{V_o}{V_0+(n_2/n_1)V_{in}}$	$\frac{n_1}{n_3}\frac{V_o}{V_{in}}$	$\frac{n_1}{n_2}\frac{V_o}{V_{in}}$	$\frac{n_1}{n_2}\frac{V_o}{V_{in}}$	$\frac{n_1}{n_2}\frac{V_o}{V_{in}}$

Table 3.1.2 - General specifications of simulated converters

Specifications	Value
Input voltage (Vg)	24 V to 36 V
Output voltage (V)	350 V
Output power	200 W
Ripple factor of ILM (K)	0.005
Ripple factor of ILo (KLo)	0.25
Ripple factor of Vo (KC)	0.005
Switching frequency (fsw)	100 kHz

Passive elements design

In this section, according to the extracted relationships for magnetizing inductance, output inductance and output capacitor, the required values of elements in the input voltage range of 24 to 58 V are compared. Due to the converter gain equations, the converter operation is possible at an input voltage higher than 36 V. (58 V, is the case that there are four series batteries in the input, under charging). Fig. 3.1.2 shows the magnetizing inductance curve for the five desired converters. As it turns out, the push-pull converter requires the highest magnetic inductance. The lowest value belongs to the flyback converter which is due to the continuous magnetizing current in this converter. The magnetizing inductance curve for other converters can also be seen in the figure based on their equation in the table and the ripple coefficient considered.

A comparison between the output inductance values for the forwards, push-pull and full-bridge converters is shown in Fig. 3.1.3a. As the input voltage increases, the required duty cycle will decrease and as shown, the inductance required for these converters increases. As it is clear, the forward converters require more inductance at the output. This is due to the lower duty cycle compared to the push-pull and full-bridge converters. It should also be noted that the high value of the output inductance is due to the low output current. Finally, Fig. 3.1.3b compares the required output capacitors which are drawn using the capacitor output relationships for these converters. As can be seen, the flyback converter requires a larger capacitor at the output. As the input voltage increases, the value of the capacitor for the flyback, push-pull and full-bridge converters decreases and is almost constant for the forward converters

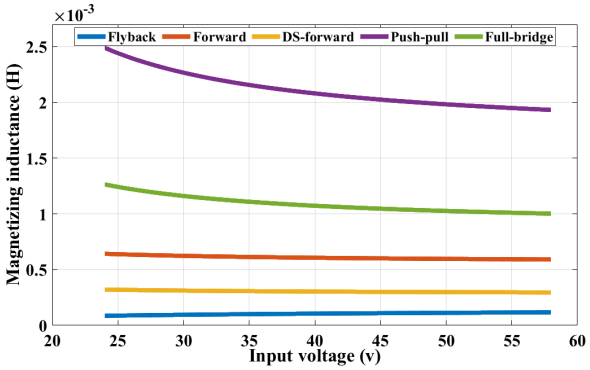

Fig. 3.1.2. Magnetizing inductance in the input voltage range of 24 to 58 V (a), Output inductance in the input voltage range of 24 to 58 V (b)

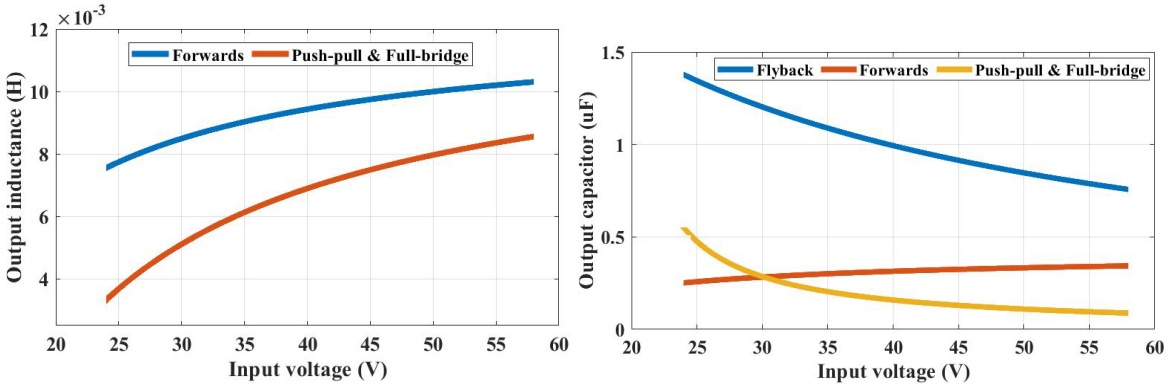

Fig. 3.1.3. Output inductance in the input voltage range of 24 to 58 V (a), Output capacitor in the input voltage range of 24 to 58 V (b).

Energy and sizing

In this section, the aim is to calculate the capacitive and inductive energy of the passive elements in the converters. Since the size of passive elements is determined using their energy, the energy consumed in the capacitor(s) and inductor(s) in these converters will be calculated for each of these converters. According to the design of converters and calculating the values of passive elements and then current and voltage of the circuit, inductor and capacitor energy can be obtained from the well-known energy equations. Fig. 3.1.4 shows the energy of the passive elements of each converter. In this figure, the calculated energy is normalized to maximum energy. As can be seen, the flyback converter needs the most energy in its passive elements. Therefore, in this converter, passive elements should have a larger size. Of course, the structure of the flyback magnetics core is different and there is an air gap in its core structure, working based on the coupling inductors. For the other four converters, the total energy value of the passive elements is much lower. Although push-pull and full-bridge converters have slightly higher total energy due to the larger output capacitor.

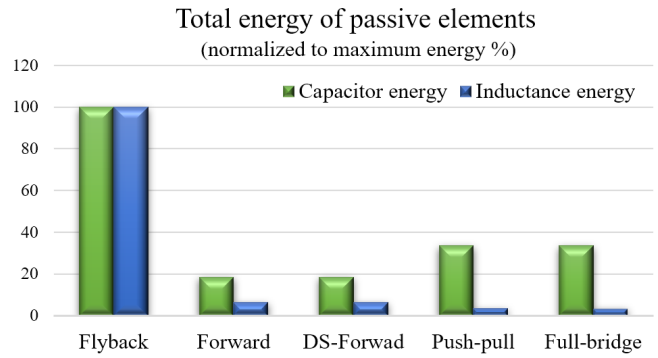

Fig. 3.1.4. The normalized total energy of passive elements in the converters

Selection of semiconductors

In selecting the semiconductor components of the converters, to select the appropriate switch and diode, their tolerable voltage and current must be calculated according to the specifications of the converter. The relationships between the maximum voltage and current of switches and diodes in different converters are given in Table 3.1.1. The current passing through the switches and diodes can be easily calculated through the output load and the transformer conversion ratio. In this section, a comparison is made between the voltage across the switch and the output diode (D1) in the converters. As Fig. 3.1.5a shows, as the input voltage increases, the voltage across the switch increases for all converters. Based on the equations in Table 3.1.1, in DS-forward and full-bridge, the voltage across switch is Vin and for forward and push-pull is 2Vin. For flyback converter, this voltage is in range of Vin to 2Vin and based on its equation.

Fig. 3.1.5b also shows the maximum voltage across the output-side diode (D1). In this figure also, the voltage across the output diode of all converters increases by increasing the input voltage. Based on equations in table and fixed output voltage and turn ratio, this voltage has been calculated. The lowest voltage across the diode is related to the full-bridge converter which is equal to nVin and n in the full-bridge is 20. For a push-pull converter, this voltage has the highest value of 2nVin. For forward converters this voltage is equal to nVin and to reach desirable output voltage, the turn ratio in forward converters was selected to be 38. Finally, for flyback, the voltage across diode is based on its equation in table 3.1.1 and is shown in Fig. 3.1.5b.

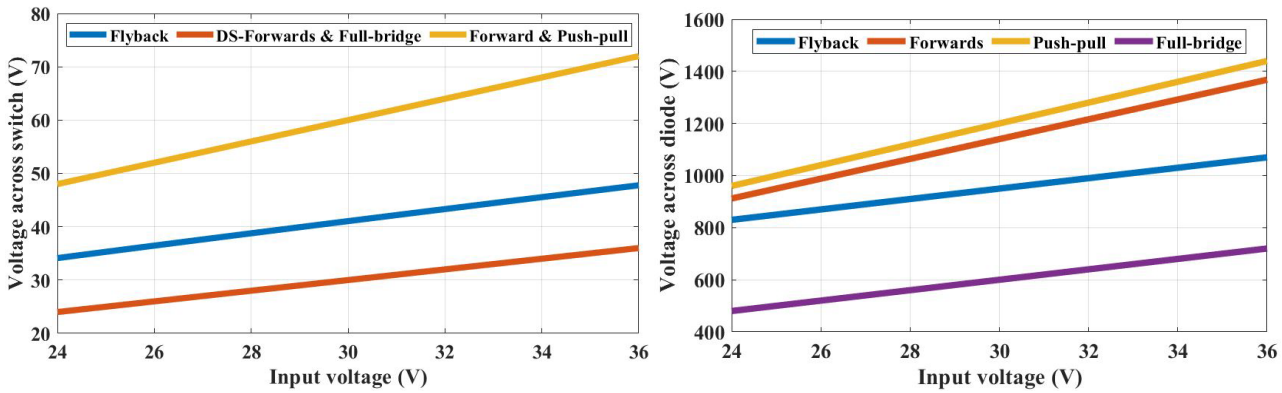

Fig. 3.1.5. The voltage across the switches (a), diodes (b) in the converters

Losses

A comparison has also been made to investigate the semiconductor losses of these converters. In this comparison, switching and conduction losses of switches and conduction losses and forward voltage drop losses of diodes are considered. Due to the different numbers as well as the current and voltage of switches and diodes, their losses in each converter are calculated and compared. To calculate the losses, the conduction resistance value of the Rds-on switch is considered 0.008 Ohms, and the conduction resistance value of the diode is 0.004 Ohms. The average turn-on/off time of the switches is also assumed to be 100ns for calculating switching losses. There is also a voltage drop across each diode of 0.4V. With these assumptions and a switching frequency of 100kHz, Fig.3.1.9 and 3.1.10 show a comparison between losses in different converters for two cases of input voltage. The values of these losses for each section are indicated in the figure.

As can be seen, the major amount of these losses is related to switching losses. By comparing the losses at 24 and 36V input voltages, it can be concluded that at constant output load, at 24V input voltage, due to the lower voltage across the switches, the switching losses are less than that of 36V input voltage for all converters. Due to the constant output power, at 24V input voltage, the input current (initial side of the transformer) will be higher and this will lead to more conduction losses than 36V input voltage. As can be seen in Fig. 3.1.6, the highest losses are related to the switching losses of the forward converters, which is due to the higher current of switches. Although there is only one switch in forward converters, due to the higher voltage across the switch in this converters, switching losses are high. Also, as can be seen, in the DS-forward converter, the losses of two diodes in the primary side of the transformer that passes a high current will lead to relatively high losses. In the push-pull converter, switching and conduction losses are reduced due to the input current being divided between the two paths. In the case of flyback and forward converters, it should be added that the switching losses for these two converters are calculated assuming the presence of snubber circuits that prevent voltage spikes. Of course, these snubber circuits also cause losses, which has a significant impact on the overall efficiency of the converter.

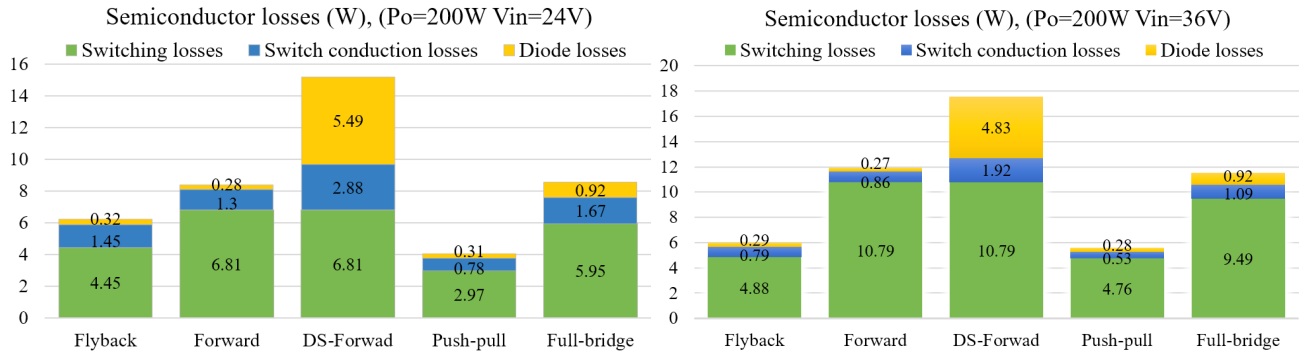

Fig. 3.1.6. Losses in semiconductor devices of the converters in Vin=24 V (a), Vin=36 V (b)

Overall comparison and discussion

In this study, the general equations of five isolated dc-dc converters were extracted and then evaluated for a high step-up low-power application. According to the results, it can be said that the flyback converter has a simpler performance and fewer elements compared to other converters. However, with a high magnetizing current and high energy in the inductance of the magnetic core, this converter requires high consideration, including the air gap in the magnetic core. The other problem is related to the hard switching and voltage spike which need snubber circuits and this will result in additional losses.

The need for three windings in the single-switch forward converter and the high blocking voltage across the switch in this converter has reduced its popularity. Like a flyback converter, this converter also needs snubber circuits to alleviate voltage spikes. Although these problems have been fixed in the DS-forward converter, the presence of two switches and two diodes on the primary side increases the losses. In forward converters, the duty cycle limit is another factor to consider. In high gain applications, the duty cycle limitation in these converters must be overcome by increasing the transformer turn ratio, which in turn increases the size and cost, and on the other hand, also increases the maximum input current. As a result, a switch with a higher current rating will be needed. Given the above, push-pull and full-bridge converters seem to be better options. The advantages of these converters are the absence of limitations in the duty cycle and the reduction of the maximum input current. Also, there is no need for axillary circuits. In the push-pull converter, the presence of two switches with a lower current on the primary side will be associated with a reduction in losses. However, the need for a three tabs transformer in this converter can also be one of its disadvantages.

In the full-bridge converter, none of the above-mentioned problems exist for this converter. The only factor that can be a problem in this converter is the need for a large number of switches and diodes. This will result in losses and increase the size and cost to some extent. However, the cost is approximately equal to the cost of switch/diode(s) and snubber circuits in flyback and forward converters.
For an overall comparison and a better understanding of the above, an illustrative scheme is used in Fig. 3.1.7. In this diagram, four factors of switch and diode losses (PS&D), inductive energy (EL), capacitive energy (EC) and switch voltage stress (VS), have been investigated. The values of these factors are normalized to the maximum value in these converters. It should be noted that this diagram is drawn for input voltage of 36 V. In the case of 24 V input voltage, the results are almost the same and there is only a slight difference in the amount of switch losses. This diagram introduces push-pull and full-bridge converters as relatively superior choices. Although the smaller area in this diagram indicates the overall better performance of the converter, the importance of each of these factors should be considered separately in order to make the best choice. For instance, in some applications, losses may be more important than converter size/weight or vice versa.

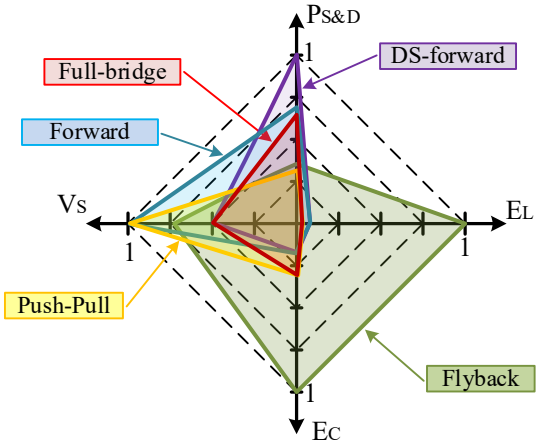

Fig. 3.1.7. Spider diagrams for an overall comparison between five desired converters in Vin=36 V.

Conclusion for Comparative Evaluation of Isolated dc-dc Converters for Low Power Applications
In this study, five isolated converters for a high step-up low-power application were evaluated from different aspects. After examination, it was found that the flyback converter requires a larger capacitor/magnetics and more considerations are required in its coupled inductors design. In terms of losses, with increasing input voltage, switching losses increase and conduction losses decrease at constant output power. The main losses in these converters were related to switching losses, and DS-forward converter had higher losses due to the high current of switches. Push-pull converter with a simpler structure had less losses. For forward converter that only have one switch, switching losses were relatively high due to the high voltage across the switch. Also, in the DS-forward, due to the presence of two diodes on the primary side, the diode losses were relatively high

Back-to-Back Energy Router based on common-ground inverters
In hybrid micro/nanogrid, energy router (ER) has been introduced and developed in the last decade. ER is an interface converter between ac and dc systems. This smart multi-port converter has the ability to manage and optimize energy flow between production, storage system and consumption. ER can feed dc and ac loads and provide ancillary services to the grid. Various structures have been proposed for ER. In the high-power range, a three-stage power converter based on a solid-state transformer (SST) in the middle stage is proposed **Errore. L'origine riferimento non è stata trovata.**. In the low power range, non-isolated hybrid inverters and back-to-back (B2B) structures are among the most prominent solutions.
In the hybrid inverter, PV, storage, and dc loads are connected to the dc port, while ac loads are directly connected to the point of common coupling (PCC). In case of a fault in this structure, in either the grid or ac load, the other part is also affected. In the B2B structure, this problem has been solved. Due to the presence of the main dc link between two inverters, the ac loads of the building are detached from the grid.
Presenting new structures or modifying existed with the aim of improving ER performance is one of the leading research paths. As mentioned, in the hybrid inverter and B2B structure, the inverter has a conventional non-isolated structure (mainly H-bridge). Due to the lack of isolation and the presence of PV in the dc link, leakage

current and safety issues should be resolved. This study proposes the B2B structure of an ER with common-ground inverters. Connecting the negative port of the dc link to the neutral wires of both inverters can solve the problems associated with safety and leakage current. Fig. 3.1.8 shows the general view of the proposed method with the common-ground concept. As seen in Fig. 3.1.8, the negative port of the dc link, the neutral wires of inverters, and the body of the equipment are all connected to each other and grounded. The use of relays R1 to R3 is also considered for switching between on-grid or off-grid states, isolating ac load, or parallel operation and load sharing of inverters, respectively.

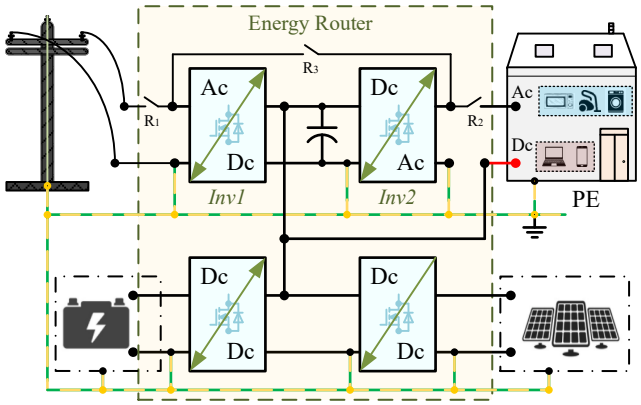

Fig. 3.1.8. Proposed energy router structure with grounding connections.

In existing B2B structures, conventional structures (mainly H-bridge) are used for dc-ac conversion. Due to the absence of isolation, the problems caused by leakage current and safety issues still exist. In addition, this kind of inverter works only in a step-down manner and does not have the ability to increase voltage. Therefore, a suitable alternative should be found for these inverters. Fig. 3.1.9 shows the inverter intended to be replaced with conventional structures. This common-ground inverter uses five switches, an inductor, and a capacitor, and also has the ability to increase/decrease the voltage. In this figure, the input and output passive filter elements are also displayed.

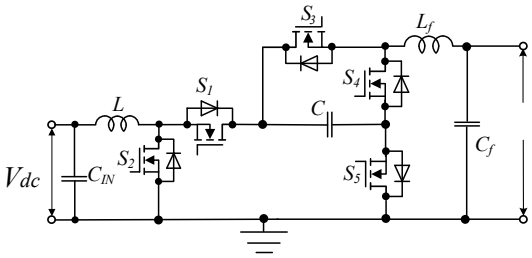

Fig. 3.1.8. The structure of the common-ground inverter intended for use in ER structure.

Energy Router with Common-Ground Inverters

Fig. 3.1.9 shows the overall structure of ER with two common-ground inverters along with their control blocks. It consists of the following blocks: grid-side inverter (Inv1) and LCL filter, load-side inverter (Inv2) and LCL filter, PV interface converter, and interface converter for battery storage.

In this structure, the negative port of the dc link and the neutral wires of both inverters are connected together. Inv1 is located on the grid side and should be able to work bi-directionally. It means that it should draw power from the grid or inject power into it. To control Inv1, two phase-lock-loops (PLL) and a PI controller along with a proportional resonance controller are used to finally produce M and D required by the inverter. PLL1 samples grid voltage and provides synchronization to the primary grid. Additional PLL2 sampling output current (Io), provides a pure sinusoidal reference current that is equal to the fundamental harmonic of the output current. It will provide only a sinusoidal grid current under any shape of the output current. For these two PLLs, the traditional second-order generalized integrator (SOGI) regulator is used. The grid side reference current is derived by means of a simple proportional-integral (PI) controller, in combination with the instantaneous value of the output current. This provides the instantaneous power balance between the output side and the grid side, which, in turn, mitigates the power ripple across the dc-link capacitor and improves the dynamic of the system. Finally, a conventional proportional resonant (PR) is used for grid current control. On the ac-loads side, Inv2 also uses a common-ground structure. For Inv2, there is an MPC controller to generate the modulation index M and a PI controller to generate D. In the MPC controller, the cost function is defined in such a way as to minimize the changes in the output voltage of the inverter near the reference output voltage under any kind of loads. MPC

becomes a feasible instrument for power electronics applications. It should also be mentioned, by applying the proportional coefficient, the condition D>M should always be satisfied in both controllers of Inv1 and Inv2. The PV and storage system are also connected to the dc link through their respective dc-dc converters, and each has its own controllers, which is not the focus of the discussion here. Here, the goal is to focus on the operation of two inverters in grid-connected mode and power exchanges between the load, the dc link, and the grid.

Simulation verification

For the investigation of the performance of two common-ground inverters and comparing them with conventional inverters in ER structure, PLECS software has been used. Firstly, the parameters of passive components were calculated. Table 3.1.1 summarizes the simulation parameters. In the first part, the performance of the proposed structure has been examined in different situations. Then, the THD of the grid current in the states of power injection/receiving in the proposed structure has been compared with the conventional structure First, the performance of overall system in the condition of changing the output load (ac loads) is investigated. To simplify and reduce the situations under consideration in these simulations, it is assumed that constant power is transferred from the battery and PV side to the dc link in this section. It is assumed that the power of 3000 W is given to the dc link from the PV and battery side. At the moment t = 0.7 s, the output load increases from 1000 W to 2000 W. With this increase, the output load current (Io) increases. Then, overall controllers of the system perform the necessary corrections for stable operation. Fig. 3.1.10 shows the dc link voltage, Inv1 and Inv2 output voltage and tenfold current (for a better view). As it can be seen, with the increase of the output load, the voltage of the dc link will drop slightly, but it will still be within the permissible range. (Fig. 3.1.10a). For the output of Inv2, it can also be seen in Fig. 3.1.10b that at the moment of load increase, the inverter current has increased (doubled) and the output voltage has seen a very small drop (between 2-3 V) at this moment. Therefore, as can be seen, after this load change, the control system was able to keep the dc link and output voltage of Inv2 within the allowed range.

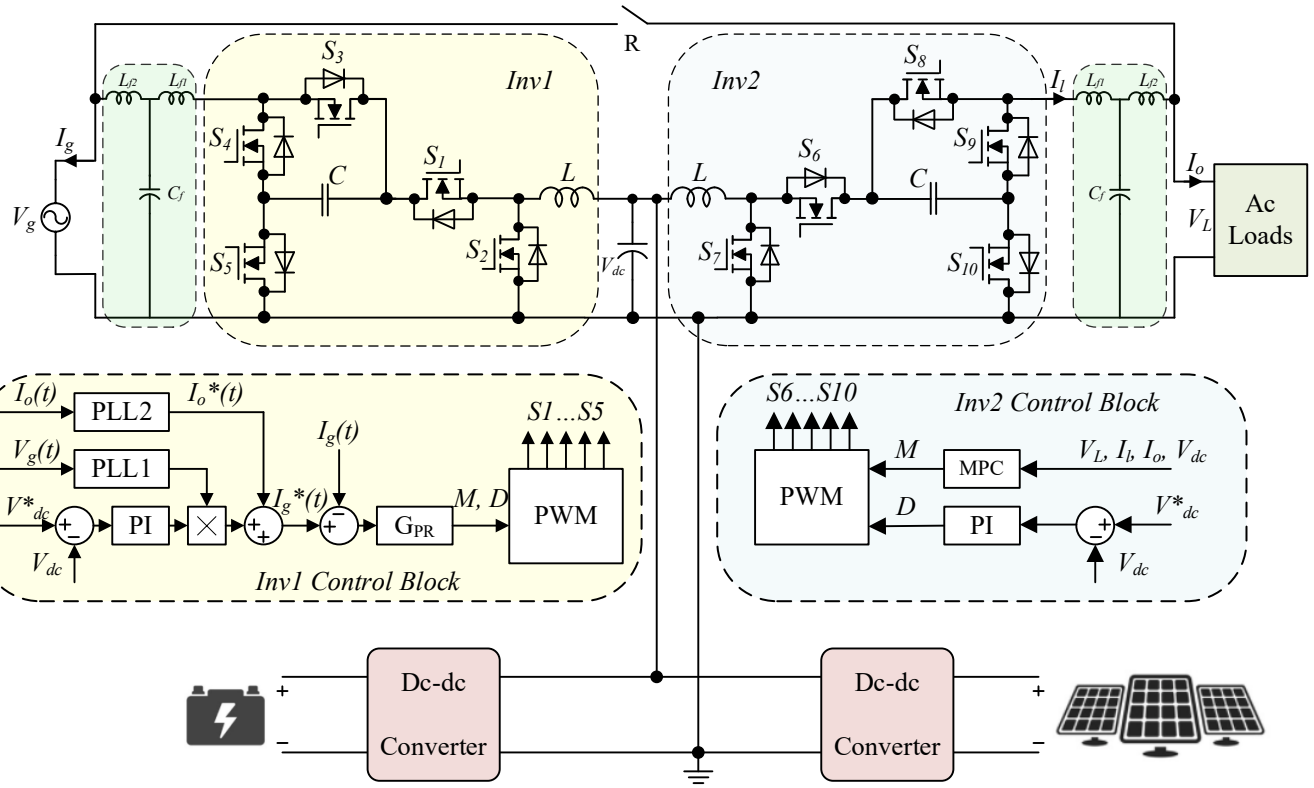

Fig 3.1.9. General schematic of ER with two common-ground inverters and their control block

On the other hand, the power injected into the grid is the difference between dc link power and output load power. At the moment of increasing the output load from 1000 W to 2000 W, the power injected into the grid will decrease due to the constant power of the dc link. Fig. 3.1.10c shows the grid-side voltage and tenfold current. At the moment t=0.7 s, with the increase of the output load, the power injected into the grid has decreased as can be seen. In this figure, the voltage and current before and after changing the output load are in phase and the power factor is unity. Also, the current injected into the grid is sinusoidal and has the minimum possible distortion.

Simulation Parameters.

Table 3.1.3 - Simulation Parameters.

Parameter's name	Value	Units
Output Voltage, VL	230	V
Dc-link voltage, Vdc	400	V
Dc-link capacitor	2000	uF
LCL filter inductance, Lf1(Inv1) and Lf2(Inv2)	1.4	mH
LCL filter capacitance, Cf	9	uF
LCL filter inductance, L2(Inv1) and L2(Inv2)	0.6	mH
Switching frequency, fs	10	kHz
Inverters inductors, L	1	mH
Inverters capacitors, C	200	uF

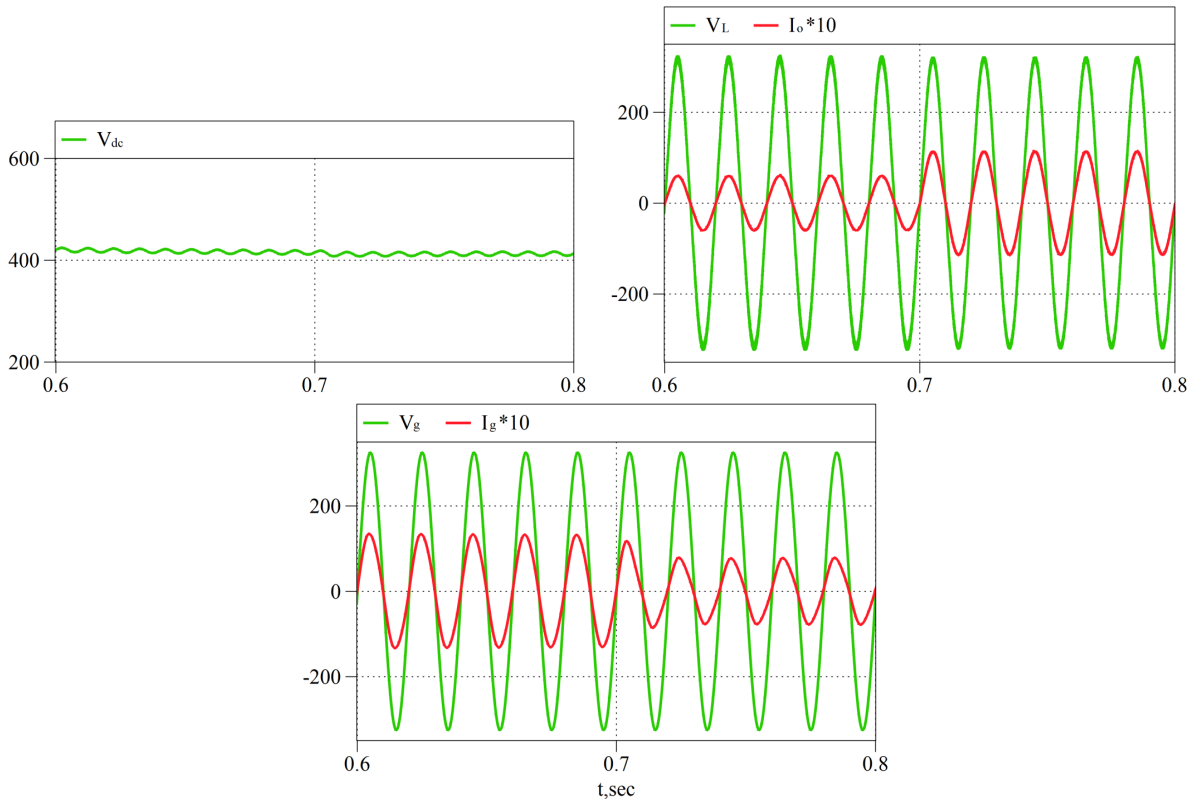

Fig. 3.1.10. Simulation of changing the load from 1000 W to 2000 W at t=0.7 s for ER with common ground inverters: dc-link Vdc (a), load side VL and Io (b), grid side Vg and Ig (c).

Considering that the power of the PV and battery is considered to be 3000 W, if the load power is greater than this value, the Inv1 on the grid side should draw the power difference from the grid to feed the output load. To check this situation, it is assumed that the output load was 2000 W at the beginning, and then at the moment t=0.7 s, the output load increases to 6000 W. Due to the presence of 3000 W of power in the dc link, Inv1 should receive the required power difference from the grid and transfer it to the output load. Fig. 3.1.11a shows the voltage and current of the grid side for this scenario. As can be seen, the extra power available in the dc link (while feeding ac loads) has been injected into the grid before t=0.7 s. With the increase of the output load at t=0.7 s, the power available in the dc link alone cannot feed the ac loads. Then the grid current direction is changed to supply the output load, and power is drawn from the grid. The simulation in this case also confirms the correctness of the bidirectional operation of the alternative inverter. Another point is that in the case of power injection into the grid, the voltage and current are in phase and the power factor is unity, and when the current

direction changes, the voltage and current will have a phase difference of 180 degrees and the power factor will also be close to unity.

For the situation under non-linear loads, the performance of the proposed structure is also considered. Similar to the first case, the power of 3000 W is considered in the dc link. The load-side Inv2 draws 1000 W power for household appliances. In t=0.7 s, a non-linear rectification load of 1000 W is added to the output. With the addition of this load, the current waveform will be distorted. But as seen in Fig. 3.1.11b, the MPC controller produces an output voltage with low distortion. In this case, the THD of the output voltage is close to 3.5%, while in completely similar conditions of non-linear load the application using the H-bridge inverter, the THD value will be close to 3%. Therefore, it can be deduced that the proposed structure has an acceptable performance under non-linear loads.

To further investigate the performance of the proposed ER, the THD of the grid current has been investigated in two modes of using H-bridge inverters and common-ground inverters. This comparison is performed with the same conditions in switching frequency, LCL filter, etc. for both structures based on Table 3.1.1. Here, the comparison has been made for two modes of power injection into the grid and power receiving from it at different power levels. PLECS simulation has been implemented to simulate both structures.

In the first case, to inject power into the grid, the output load power of Inv2 is fixed at the low power of 250 W. The produced power in the dc link has been considered at different levels and comparison has been performed for two modes of using different inverters. Fig. 3.1.12a shows the value of THD in the mode of power injection to the grid for two structures of H-bridge-based (H-B) and common-ground-based (C-G). As can be seen, in all injected powers, with the use of the common-ground inverter, the THD of the current is less and with the increase of dc link power and subsequently the increase of injected power to the grid, the amount of THD slightly decreases. Also, in the H-bridge-based structure with the increase of injected power, THD will decrease. Of course, it should be kept in mind that the LCL filter in these structures is designed for a power range close to 5 kW, and performance at light loads is associated with an increase in THD.

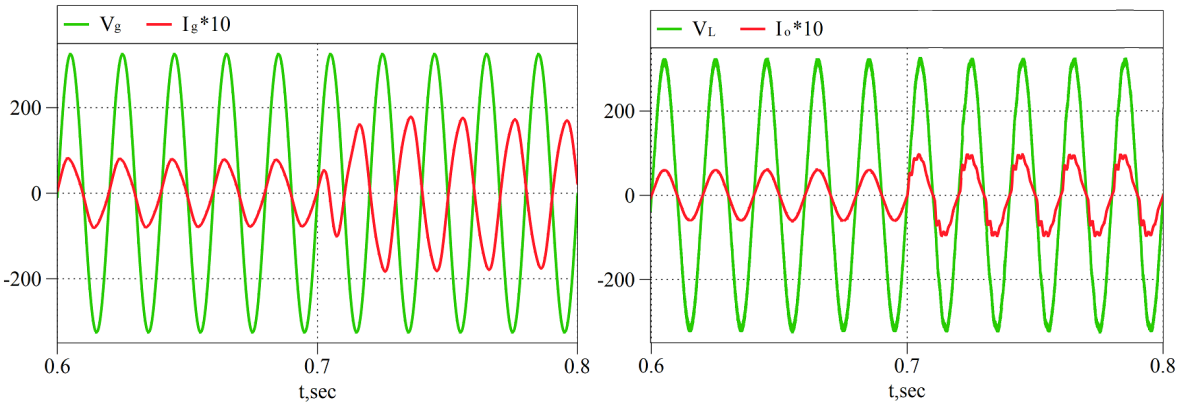

Fig. 3.1.11. The voltage and current of Inv1 when the output load increases from 2000 W to 6000 W at t=0.7 s and the power of the dc link is 3000 W. (a), The voltage and current of the Inv2 when the output inverter feeds 1000 W and at t=0.7 s a non-linear rectification load of 1000 W is added. (b)

In the second case, to check the condition when the power produced in the dc link is insufficient to supply the output loads, the performance of the B2B structures has been checked with H-bridge and common-ground inverters. In this situation, the output power in the dc link is considered fixed at 500 W and the output load power is at different levels. The results of the simulation for the THD of the grid current for H-bridge-based (H-B) and common-ground-based (C-G) structures are shown in Fig. 3.1.12. At low received power from the grid, both structures have relatively larger THD. Although in the H-bridge-based structure, this value is 7.5% and larger than in the common-ground-based structure. As can be seen, in this case also, as the power received from the grid increases, the THD value decreases for both structures and reaches very low values for the rated power. Of course, in this case, the performance of the H-bridge is better at high loads. It can also be concluded that the presented common-ground structure, has a better performance in inverter mode rather than rectification mode.

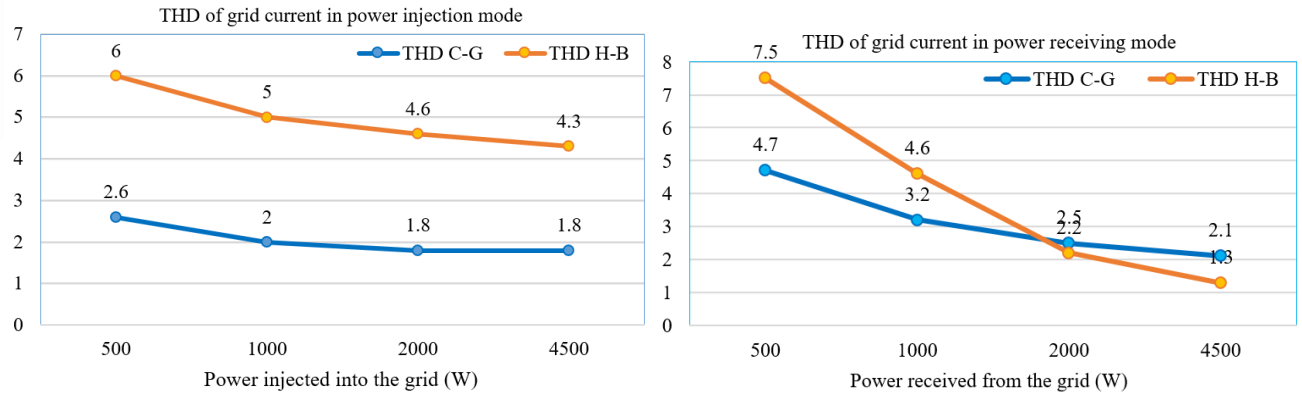

Fig. 3.1.12. Comparison of THD of grid current in the mode of power injection by using H-bridge inverters (H-B) and common-ground inverters (C-G) (a), Comparison of THD of grid current in the mode of the power receiving by using H-bridge inverters (H-B) and common-ground inverters (C-G) (b).

To summarize, it should be mentioned that using the common-ground inverters in the general structure of ER can be a potential option. Solving problems caused by leakage current and safety and on the other hand, the flexibility of these inverters in the circuit structure, and voltage increase/decrease are among their features. Of course, other matters related to the design, size of passive elements, implementation, and general control of these converters should be carefully examined

Conclusion for Back-to-Back Energy Router based on common-ground inverters

By using common-ground inverters in a B2B structure of ER, the negative port of the dc link was connected to the neutral wires of the inverters to avoid the problems caused by leakage current and ensure safety. The results obtained from the simulation in different operating conditions, the correctness of the structure's performance in conditions including changing the output power, receiving or injecting power into the grid, and bidirectional operation were checked. The THD of the grid current was compared in both cases of using the H-bridge and the common-ground inverters, and the results confirmed the valid performance of the structure based on the common-ground inverters. These results confirm the good potential of this structure in cases of using non-isolated systems for the future of ER structure.

3.1.3. Contribution to the WP objectives

As it was already mentioned, the work of ESR05 were focused on the achievement of the Objective 3.2 "*To design converters and strategies to control microgrids (as optimal operational parts of distribution grids) to manage energy flows and minimize transportation losses*" by means of Task 3.2 "*Development of an Active Bidirectional Energy Charger for providing Ancillary Services*". All results that were obtained during the first reporting period (1 year of employment in Beneficiary institution – Chernihiv Polytechnic National University - CNTU), can be summarized as follows:

1. The general structure of the energy router was defined and operation modes were examined, including the control methods of each part: the grid-connected inverter, the load-side inverter, the PV controller, and the battery controller. A new modified structure with an isolated dc link was proposed. This research result contributes to the achievement of the Objective 3.2; in particular, the new modified structure is aimed to be used in a design of new power converter – energy router - for microgrid applications.
2. Several isolated dc structures that can be used in energy router were investigated and simulated from different aspects in PLECS software for the comparison of the quality of dc link and ac main/load voltages. Results are published in the conference paper "Comparative Evaluation of Isolated dc-dc Converters for Low Power Applications" at the 2022 IEEE 20th International Power Electronics and Motion Control Conference (PEMC). This research result and dissemination activity also contributes to the same Objective 3.2, because analysed topologies of power electronics converters is a part of the energy router structure, and comparison provides the information of the most beneficial structures, that can used in energy router "to minimize energy loses", as it is pointed out in the Objective 3.2.
3. Detailed analysis of Parallel and Redundant operation of two inverters in energy router, working at the "back-to-back" principle that reduces the load of inverters was done. The issue of balancing performance was observed that proposed to be overcome by the modification of the control method by means of the so-called

"virtual impedance" block in the control structure. This work also contributes to Objective 3.2, in particular, it is aimed to develop "strategies to control microgrids … to manage energy flows".

4. Analysis of existing grounding standards for dc systems integrated with the ac system and topologies of power converters using common ground in the Energy Router structure was done. All types of common-ground inverters were investigated and simulated under different working conditions, with the aim of using them in the energy router structure and eliminating the problems caused by the leakage current. Results are published in the conference paper "Back-to-Back Energy Router Based on Common-Ground Inverters" at the 2023 IEEE Conference (CPE-POWERENG). Earth protection and protection structures were studied in dc and hybrid microgrids, and all types of isolated and non-isolated structures and grounding conditions were investigated to check protection in hybrid nanogrids. This research result and dissemination activity also contributes to the same Objective 3.2, because analysed common-grounded inverters is an ac conversion part of the energy router structure. The carried out work is related with protection, safety and reliability issues of energy routers: "To design converters … to manage energy flows", as it is pointed out in the Objective 3.2.

3.1.4. Scientific achievements

Publications

#	Title, incl. citation information	Type (Conference, journal, book chapter)	Status (Submitted, accepted, published)	DOI
1	M. Azizi, O. Husev, D. Vinnikov, O. Veligorskyi, "Comparative Evaluation of Isolated dc-dc Converters for Low Power Applications," 2022 IEEE 20th International Power Electronics and Motion Control Conference (PEMC), Brasov, Romania, 25-28 September 2022	Conference Paper	published	10.1109/PEMC51159.2022.9962944
2	M Azizi, S Rahimpour, O Husev, O Veligorskyi, "Back-to-Back Energy Router Based on Common-Ground Inverters," 2023 IEEE 17th International Conference on Compatibility, Power Electronics and Power Engineering (CPE-POWERENG), Tallinn, Estonia, 14-16 June 2023	Conference Paper	published	10.1109/CPE-POWERENG58103.2023.10227480
3	M. Azizi, O. Husev, O. Veligorskyi, S. Rahimpour, C. Roncero Clemente, "Grounding and isolation requirements in dc microgrids: overview and critical analysis", Energies	Journal Paper	submitted	

3.2. Task 3.2 – IRP6 "EV chargers, developing an active bidirectional charger able to provide ancillary services"

3.2.1. Introduction

The scientific work was mostly conducted at the Gdańsk University of Technology (Department of Electrical and Control Engineering) under the supervision of Professor Ryszard Strzelecki. Additionally, during the first secondment, which lasted for two months, research was carried out at the University of Extremadura (Department of Electrical, Electronic, and Control Engineering) under the guidance of Professor Enrique Romero-Cadaval. During the work at both institutions, communication and collaboration between them were established, resulting in shared scientific outcomes.

3.2.2. Scientific outcomes

Research motivation

The number of electric cars sold, including both battery electric vehicles (BEVs) and plug-in hybrid electric vehicles (PHEVs), almost doubled in one year, reaching 6.6 million in 2021. This brought the total number of PEVs on the roads to 16.5 million. Most of this increase came from BEVs, accounting for around 70%. Fully electric vehicles (EV), at its turn, make up 9% of the global automotive market, which is four times more than in 2019. Moreover, according to forecasts, the number of electric cars could reach 120 million by 2030, potentially having a positive impact on air quality and CO2 levels in densely populated regions such as large cities.

It is worth mentioning that most electric vehicles nowadays are charged from the central power grid, which is primarily powered by non-renewable power plants. In the European Union, coal and gas generated 33% of electricity in 2021, and in Poland, in particular, up to 80% of electricity came from coal and gas. Obviously, this reduces the positive impact of electric transportation development, as it merely shifts the source of pollution from the car to the power plant. As a result, in order to fully eliminate pollution, the energy for electric vehicle charging should come from 100% non-carbon renewable energy sources.

The main factor that affects the development and performance of EVs is their battery capacity. Unfortunately, even today, a crucial problem of recycling old batteries, which contain toxic elements, remains unsolved. The primary reason for this is that recycling is not economically viable. It is more cost-effective to build new batteries from scratch than to recycle them. Hence, interest in various solutions that can reduce the use of toxic elements is growing. One possible solution is to reduce the size of batteries while simultaneously expanding the charging network to allow for more frequent charging. However, this would complicate long-range journeys and make them less convenient. Therefore, the most rational option appears to be a combination of reducing the size of batteries (or increasing their capacity), improving the density of stored energy while maintaining (or increasing) the maximum travel distance using new technologies. This should be accompanied by the simultaneous construction of battery recycling infrastructure. Nevertheless, in any scenario, the issue of charging stations remains a top priority. The lack of a charging infrastructure, coupled with the rapid growth in the number of EVs, could lead to significant inconveniences for electric car owners. According to statistics, the number of public EV charging stations reached 1.8 million worldwide in 2021, with about 1.2 million being slow chargers and 0.6 million being fast chargers, which is twice as many as in 2019. Such rapid growth in a new industry branch is associated with several problems. Primarily, EV charging stations require the installation of additional infrastructure, including transformers, converters, protection devices, and charging spots. Installing such infrastructure is not always possible, especially in densely populated urban areas, not to mention rural areas that are sometimes still without electrification. Additionally, connecting a large number of hardly predictable consumers (EVs) to already existing networks poses several difficulties. The power delivery of modern EV chargers is increasing and can reach up to 350 kW for ultra-fast chargers for one car. At the same time, a whole car park, even with slow chargers with power up to 22 kW, places a significant burden on the network. This undoubtedly strains the existing grid, which was not designed to handle such loads. As a result, uncontrolled charging might reduce power quality, shorten the lifespan of grid transformers, and challenge the adequacy of electricity generation. A possible solution could involve the use of smart charging algorithms, which allow for intelligent EV charging while monitoring peak grid power load.

Furthermore, the use of EVs as an element of a smart grid could be beneficial and stimulate their development. When connected to the smart grid, car batteries can potentially store generated electricity excess, for example, from renewable sources, and supply it to the grid when there is a lack of generation. Realization of functions like vehicle-to-grid (V2G), vehicle-to-home (V2H), vehicle-to-load (V2L), and vehicle-to-industry (V2I) could positively impact grid power quality. Moreover, such solutions may be especially relevant for areas that are not connected to a centralized power network or that have serious problems with network stability.

In consideration of the above, it should be stated that further EV development requires:

1. Using renewable energy as the primary power source for EV battery charging.
2. Establishing recycling stations for old EV batteries.
3. Selecting appropriate locations for connecting charging stations, taking into account space limitations and the load on the grid.
4. Utilizing EV chargers with smart charging algorithms to control the charging profile depending on the network load.
5. Connecting and using car batteries as elements of the microgrid to enable V2G, V2H, V2L services.

EV charging technologies

The massive proliferation of electric vehicles in urban and rural areas entails the need for rational installing charging stations to ensure coverage, convenience and practicality. To provide such criteria, there are different types of charging stations that can be applied in each specific system, depending on the requirements.

According to power levels, EV chargers can be divided into two categories – slow charging and fast charging. Beside, ultra-fast chargers can be distinguished as part of fast chargers. Such categorization dictated by the standards that regulate EVs charging speed, power levels and voltages. Most common standards are international electrotechnical commission IEC 61 851-1, society of automotive engineers SAE J1772 and charge de move (CHAdeMO).

As can be seen from the table 3.2.1, each standard has different power levels that are additionally separated for AC and DC charging types. Thus, AC Level 1, 2 describes slow charging modes with on-board type chargers and upper power limit of 22 kW for IEC and 19 kW for SAE. Such levels are specified due to maximum household power levels, which can be reached for the Europe and USA correspondingly. Among the AC chargers, only SAE Level 3 supports fast charging and is off-board type with power level more than 50 kW. All DC standards either SAE, IEC or CHAdeMO are designed for a fast charging. It is worth highlighting that all fast charges with a power levels up to 240kW, specified as off-board, due to an EV space and weight constraints. Chargers with a power higher than that value usually called ultra-fast chargers. For example, the EVTEC TERRA HP 350 is designed for a charging power of 350 kW. Characteristics of on-board and off-board EV chargers with different power ratings described in Table 3.2.2.

An increase in the number of fast charging stations is necessary to stimulate the growth of electric vehicles and increase their competitiveness with internal combustion vehicles on long journeys. At the same time according to statistics, most of the time, cars are charged from personal charging stations at home or at work. That makes slow on-board chargers more advantageous in terms of price, since does not require the installation of extra off-board AC-DC chargers at home and at work and allows charging directly from an LV AC city network. According to the Society of Automotive Engineers (SAE), AC on-board chargers (especially AC level 2 charging infrastructure) are the most suitable for V2G applications due to available input power and compatibility that allow users to control charging. To get the benefits of the two approaches, electric cars come with two inlets, for the possibility to charge battery from fast off-board DC charger and slow on-board AC charger depending on the needs. Most popular inlet standards are CHAdeMO, GB/T-DC and Tesla for DC fast charging; J1772 Type 1, Type 2, GB/T-AC and Tesla for AC slow charging; CCS1, CCS2, ChaoJi – combined inlets for both DC and AC.

Table 3.2.1. Comparison of different charging standards [22].

Charger Type	Level	Charger location		Time to charge 300 km	Specification		
		On-board	Off-board		Voltage (V)	Current (A)	Power (kW)
AC	SAE AC charging Standards						
	Level 1	+	–	7 - 17	120	12 - 16	≤ 1.92
	Level 2	+	–	0.4 - 1.2	240	80	1.92-19.2
	Level 3	–	+	0.5 - 1	480	≥ 100	≥ 50
	IEC AC charging Standards						
	Level 1	+	–	2 - 3	250 - 450	16	4-7
	Level 2	+	–	1 - 2		63	22
DC	SAE DC charging Standards						
	Level 1	–	+	0.4 - 1.2	200 - 600	80	36
	Level 2	–	+	0.2 - 0.4		200	90
	Level 3	–	+	0.2		400	240
	CHAdeMO DC charging Standards						
	Fast Charging	–	+	≥ 0.5	≤ 480	200	≥ 135

Table 3.2.2. Comparison of market EV chargers.

Manufacturer	Model	Power (kW)	Input Voltage (V)	Output Voltage (V)	Max output current (A)	η	Time to charge 300 km
On-board Chargers							
Kia	e-soul 64 kWh	7.4	1 x 230 AC	360 DC	20	-	8 h 30m
BMW	BMW-i3 38kWh	11	3 x 230 AC	360 DC	30	-	5h 30m
Reno	Zoe 52 kWh	22	3 x 230 AC	400 DC	55	-	2h 45m
Off-Board Chargers							
ABB	DC Wallbox	22	1 x 230 AC	150-920 DC	60	95%	2h 45m
Ekoenergetyka	Wallbox DC	30	3 x 400 AC	150-1000 DC	100	94%	2h
Charge point	Express 250	62.5	3 x 400 AC	200-1000 DC	156	95%	1h
Tesla	Supercharger	135	3 x 380-480 AC	50-410 DC	330	91%	30m
EVTEC ABB	TERRA HP 350	350	3 x 400 AC	150-920 DC	500	95%	10m

Bidirectional vs unidirectional charging

At the moment, most EV chargers are unidirectional. However, due to the development of distributed alternative energy sources (private renewable sources), as well as the increase in EVs connected to the grid, the benefits of using bidirectional EV chargers are growing. For example, a car battery can be used as an energy storage unit for accumulating solar energy in a private houses and as a backup power source during blackouts. Additionally, in the case of a grid-connected EVs grouping, the total battery capacity may be sufficient to directly impact the performance of the grid network.

Comparing specific characteristics, unidirectional chargers are less expensive. Bidirectional chargers, however, have more components, more complex control algorithms and lower power density (which is a problem only for on-board charger). Besides, bidirectional power transfer accompanied by additional battery charging and discharging cycles, which negatively affect battery lifespan. Researches show, that uncontrollable EV battery charge and discharge entails significant economical expenses connected with electric energy prices fluctuations along the day, as well as battery replacement expenses, related to battery aging. However, the negative impact on a battery can be mitigated by receiving economic benefits through the provision of ancillary services together with applying smart charging algorithms. For example, special depth of discharge limits may be implemented during charging and discharging to prolong battery life, or energy price discounts may be obtained from a centralized supplier for providing services like grid stabilization. Moreover, unlike unidirectional charging, that has limited impact on the electric grid, only be able to regulate time and rate of consumed power via smart charging, bidirectional power flow can provide more services like:

- Power quality control;
- Voltage control;
- Peak shaving and load smoothing;
- Frequency control;
- Energy arbitrage;

As a result, due to ability to participate in energy exchange in smart grids, provide ancillary services and solvability of problems connected with battery aging, high part of EV chargers in the future likely will be bidirectional. Currently, the only charging standard that allows bidirectional power flow is CHAdeMO DC fast charger. In CCS2, bi-directional power transmission is planned to be standardized by 2025.

The aforementioned services are possible by assuming that an EV is connected to a home or urban grid for a significant portion of the day. Otherwise, due to the short connection times, such as in fast charging, which typically lasts only 10-15 minutes, the electric car's battery cannot be considered a reliable element of a smart grid. Conversely, fast charging has a negative impact, as it worsens power quality due to its high charging power, predominantly occurring during the daytime.

According to statistical research based on drivers travel patterns captured by the National Household Travel Survey (NHTS), the probability of a light-duty EV being parked during the day depends on various factors, including the time,

weekday, and location (see Fig. 3.2.1). Thus, during weekends, the probability of a vehicle being parked anywhere is between 0.92 and 0.95 from 10 to 18 hours, and it remains above 0.95 for the rest of the day. On weekdays, the probability drops around 8 and 18 hours as people commute to and from work but still stays above 0.92. From this can be concluded that most cars are parked somewhere during the day, driving only a relatively small amount of time. Therefore, the potential time for charging a car exceeds 20 hours a day. The same can be said for the potential time for providing V2G operation.
Additionally, when examining the probability graphs of cars being parked, it can be concluded that most cars are parked at home at night. During the daytime, the probability decreases to 0.8 on weekends and 0.6 on weekdays. Thus, following the general parking schedule, it can be stated that those cars, that are not parked at home during the day are parked elsewhere, for example in public parking lots near offices, shopping malls, or along the road.

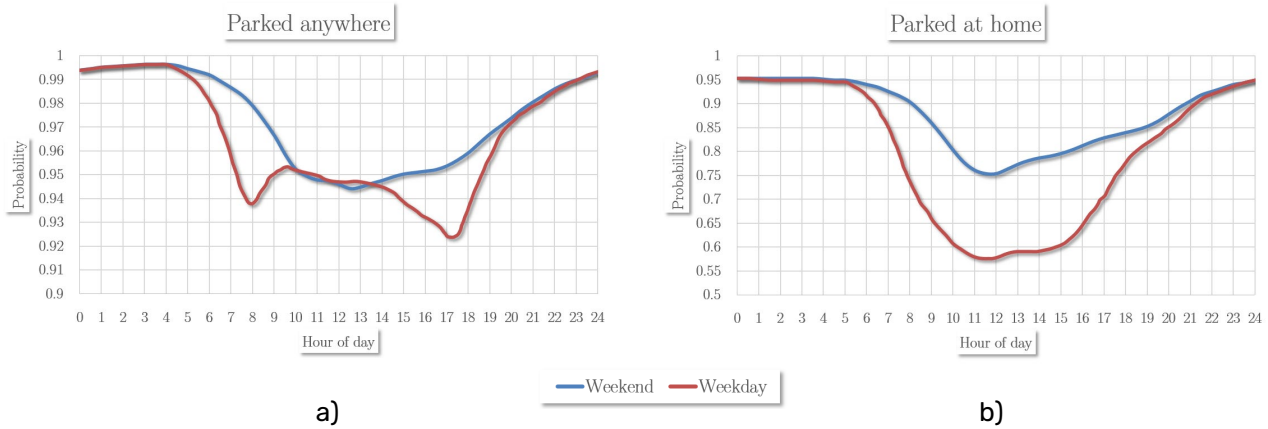

a) b)

Fig. 3.2.1: Probability of a random light vehicle to be parked (a), and EV energy consumption profiles (b).

V2X limitations and regulations

Currently, the primary limiting factor in the widespread adoption of V2G services is the absence of standards for bidirectional power transfer, along with a lack of requirements and standardization for various levels of EV integration (see Table 3.2.3). Although numerous studies explore potential reward options for utilizing a car battery as part of a smart network for V2G services, most of these remain theoretical and are seldom put into practice. Consequently, EV owners capable of offering such services often encounter difficulties in reaping any benefits, which hinders the advancement of V2G services. As shown in Table 3.2.3, standards have been well-developed only for specific levels, with cooperative smart charging being the highest. Cooperative smart charging enables the charging of groups of vehicles based on monetary and grid constraints. Conversely, bidirectional charging and aggregated bidirectional charging lack standardization and are still in the development phase.

Table 3.2.3: Grid integration levels.

	Grid compliant charging	Level 1 – V1G Smart Charging	Level 2 – V1G/H Cooperative smart charging	Level 3 – V2G/H Bidirectional charging	Level 4 – V2G Aggregated charging
Description	-Unidirectional charging -Compliant EV charging from grid to EV -Power levels are low in order to be controlled by DSO	-Unidirectional smart charging -Charging power can be regulated by EV user, home management system or DSO in automatic regime remotely according to needs	-Unidirectional charging -EV charging profiles is set according to different factors (monetary reasons, grid constrains). -EV aggregation in order to have more power (local, per charging spot)	-Bidirectional charging -Energy can be transferred from battery to customers home/load -Supports behind the meter services -Charging is motivated by economical or sustainability reasons (EV battery as a storage for local PV panels etc.)	-Bidirectional charging -EV charging goes beyond customers own needs (aggregation function, balancing market services, economic profits). -Aggregation across large area (city, country)
Requirements	-Local regulations (grid codes, IEC 61851, IEC 60364 series…)	-PWM signal -IEC 61851 -DIN-SPEC 70121 -OCPP 1.6 -Demand-response -Opt-out possibilities	-Level 1 + -ISO/IEC15118 -OCPP 1.6 -EV and Grid Telematics -Time of Use metering	-Level 2 + -ISO/IEC15118-20 -EEBus -Standards is still under development	-Level 3 + -Standards is still under development

From the above, several important conclusions can be drawn about the location and type of electric vehicle chargers:

1. Most of the time, electric vehicles (EVs) are parked either at home or in public parking areas. During these times, car batteries can potentially be used for Vehicle-to-Everything services.
2. Since predictability and reliability are key factors for bidirectional power transmission in V2G services and smart grids, the use of slow bidirectional chargers is a better option. This choice creates a smoother load on the grid during the day, promotes charging at night, and provides more opportunities to improve grid power quality.
3. Since cars move throughout the day and can park either at home or in public parking areas, using an on-board bidirectional charger is more economical. It doesn't require the installation of additional bidirectional converters at home or in public parking lots.
4. The use of fast charging stations is more expensive and negatively affects grid power quality. Due to the short charging time, it doesn't make sense to use fast charging stations for V2G services, but they can be utilized for V1G controlled charging.
5. A reward system that encourages users to use their cars for providing V2G services must be developed.

EV charger topologies

The choice of a converter topology is crucial in developing bidirectional EV charger, as it directly affects its characteristics such as cost, power density, efficiency, and therefore must be chosen carefully.
Widely used EV charger converter topologies are classified on a Fig. 3.2.2. They can be divided into frond-end AC/DC, DC/DC isolated and non-isolated, integrated with car motor windings and motor inverter, with connection directly to medium voltage, multiport and wireless. In the following sections, various converter topologies with their advantages and disadvantages are discussed.

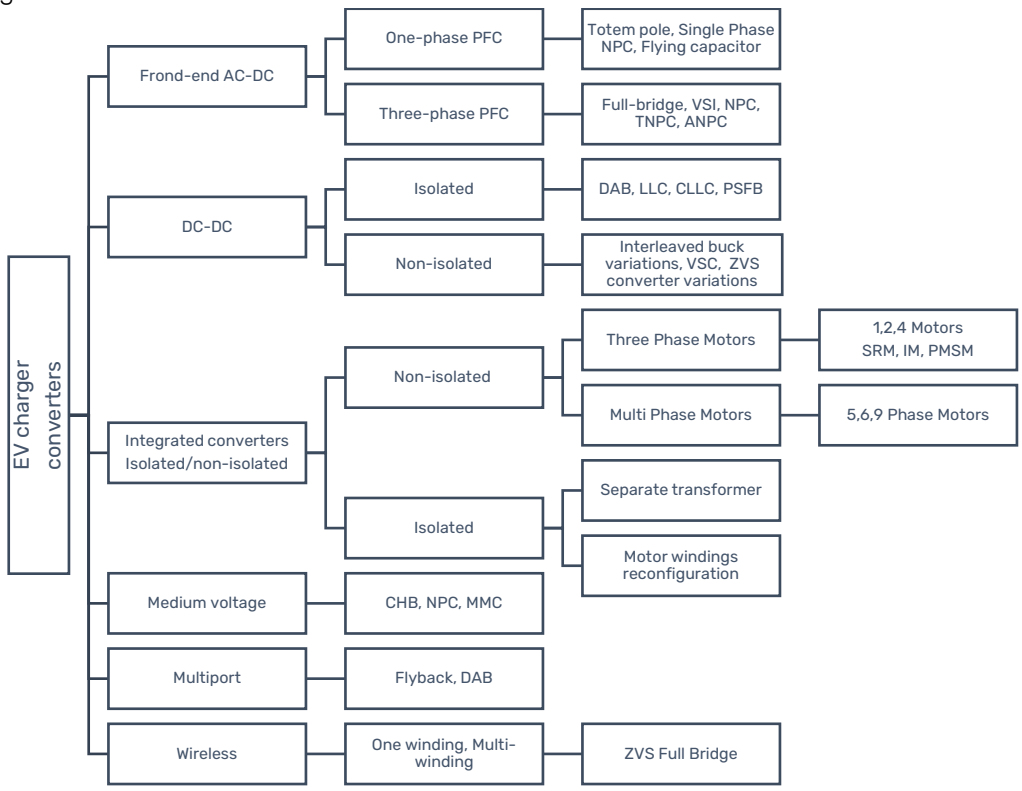

Fig. 3.2.2. EV charger topologies classification.

Front-end AC/DC converters.

A front-end (grid-interfaced) AC/DC converter is needed to connect an rectify AC power grid to comply with DC battery voltage or for further conversion with an consequent DC/DC stage in two-stage charger topologies. Depending on the direction of the current, the input converter operates as an AC/DC rectifier with PFC function (G2V operation), or as a DC/AC inverter in the case V2G operation. The main parameters of AC/DC converter in EV chargers are power density, bidirectional power flow, total harmonic distortion and efficiency. Table 3.2.4 shows the basic characteristics of the most common grid-interfaced AC/DC converters used in EV chargers with their advantages and disadvantages.

Table 3.2.4. Comparison of different front-end AC/DC converter topologies.

Topology	Bidirectional power flow	Power density	№ of switching devices	THD	Efficiency	Advantages	Disadvantages
Single-phase Totem Pole PFC a)	Yes	Low	4 switches	Highest	Lowest	-Easy to implement and control	-Low efficiency with MOSFETs due to lower body diode reverse recovery losses
Three-phase Two-level PFC b)	Yes	Low	6 switches	High	Low	-Easy to implement and control -Simplified structure and control scheme -Continuous input current -High output DC voltage -Low current stress -Low THD -High efficiency -Soft-switching	-Bulky input filter inductor -Full voltage at switches -High voltage stress on switches affects reliability -Low EMI compatibility -Harmonics appear at the DC-link voltage under unbalanced -AC input voltage -High switching losses
Single-phase Neutral Point Clamped PFC c)	Yes	High	4 switches 2 diodes	Very low	Very High at high frequency	-Reduced dv/dt stresses with lower voltage across the power switches -Reduced EMI problems -Medium control complexity	-Severe unbalancing problem caused by uncertainties (e.g., various battery technologies and random arrival of vehicles -Limited switching frequency -Limited maximum phase current -Complex control -No soft-switching
Three-phase TNPC Three-level PFC d)	Yes	High	12 switches	Very low	High	-Suitable for high power applications -Simple structure and control method -High power Density and efficiency -Low THD -Neutral connection-free structure -Low voltage stresses on the switches -Consistent with bipolar DC bus -Soft-switching operating at unity power factor -Medium control complexity	-The need for dc-link capacitors -Limited switching frequency for a better trade-off between high efficiency and high-power density
Three-phase ANPC/NPC Three-level PFC e)	Yes	High	18 switches	Very low	Very High	-Improved power density and efficiency than classic NPC -Medium control complexity	-Harder to control -Increased number of switch drivers
Multilevel flying capacitor f)	Yes	-	8 switches per level	Very low	Very High	-High-frequency operation -Smaller passive components -High power delivery capability (in three-phase)	-High cost -Challenges in PFC -No soft-switching
Cascaded half-bridge g)	Yes	High	8 switches per level	Low	Medium	-Several switching states -Modularity -Capability to isolate the faulty cells without any interruption in operations -Low current ripple -Robustness -Easy implementation	-Capacitors voltage balancing -Inadequacy of delivering maximum modulation index -Vulnerability to potential failure -Reliability -No soft-switching
Three-phase Three-level NPC h)	Yes	High	12 switches	Very low	High	-Less distortion in output voltage waveforms -Decreased stresses on switches -Low THD -Low switching losses -Improved reliability -Consistent with bipolar -DC bus structure	-Severe unbalancing problem caused by uncertainties (e.g., various battery technologies and random arrival of vehicles -Limited switching frequency -Limited maximum phase current -Complex control -No soft-switching

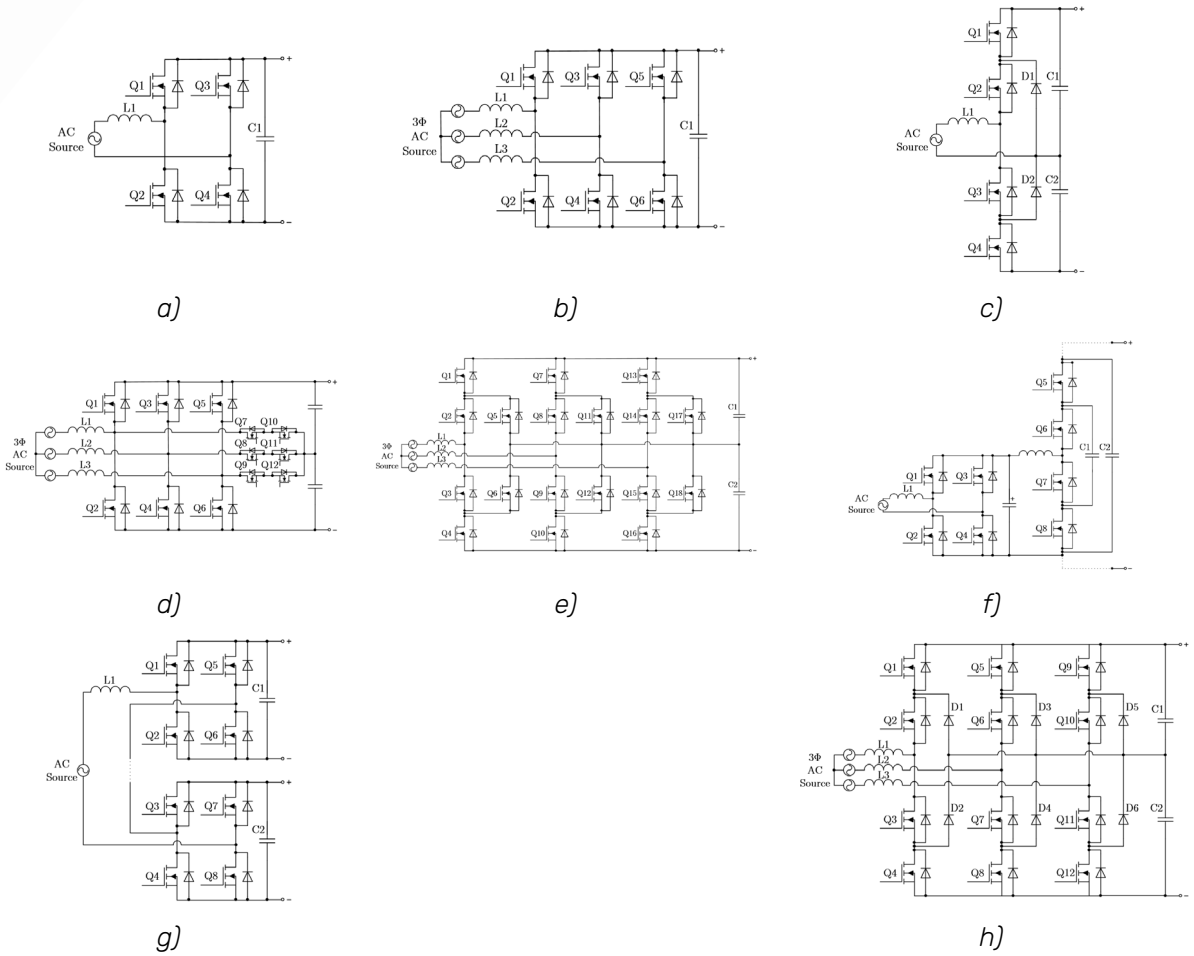

Fig. 3.2.3. Front-end AC/DC converters: a) Single-phase Totem Pole PFC ; b) Three-phase Two-level PFC ; c) Single-phase Neutral Point Clamped PFC ; d) Three-phase TNPC Three-level PFC ; e) Three-phase ANPC/NPC Three-level PFC; f) Multilevel flying capacitor; g) Cascaded half-bridge; h) Three-phase Three-level NPC.

DC/DC converter topologies

Usually the DC/DC converter used in EV chargers as a second stage after AC/DC converter to increase voltage regulation range, increase overall efficiency or to provide galvanic isolation. In addition, different DC sources and multiple EVs can be connected using multiport DC/DC converter topology. Main requirements for DC/DC converter used in EV charger are high reliability, bidirectional power transfer, high efficiency and, in the case of on-board charging, high power density. DC/DC converters used in EV chargers can be isolated or non-isolated. The presence of galvanic isolation between power sources and EV is a necessary requirement to comply with safety standards (IEC62955, IEC61851), as well as to prevent the propagation of EMI noise. There are two options for providing galvanic isolation in EV chargers - using a low-frequency transformer on the AC side (used for off-board chargers) or using a DC/DC converter with galvanic isolation. The low frequency transformer has a large size and cost, while the high frequency transformer in a DC/DC converter has a smaller size, cost, and is more preferable. The main topologies of isolated and non-isolated converters that are commonly used in EV charging stations are discussed further.

Non-isolated

Among the popular non-isolated DC/DC topologies currently used in car charging stations, interleaved converters can be distinguished. Due to a modular structure and distributed power among phases, they have relatively high efficiency, simple control, high power density and low cost. Another big group of converter used in EV chargers is three-level topologies such as 3-level voltage source converter, 3-level buck converter, 3-level zero voltage switching converter. Three level structure allows reducing the size of passive components, achieve high power density and low EMI level. To reduce switching losses, topologies with soft-switching are widely used. The main advantages and disadvantages of selected non-isolated DC/DC converters are described below (Table 3.2.5).

Table 3.2.5. Comparison of non-isolated DC/DC converters used in EV chargers.

Topology	Bidirectional power flow	Number of switches	Advantages	Disadvantages
3 phase interleaved buck a)	Yes	6 switches per module	-Low cost and simple design -Balanced power-sharing among the phases -Modularity -Low input and output current ripple -Minimized inductor size by operating in the discontinuous mode (DCM) -Soft switching -V2G support	-Different phase characteristics (such as power losses and RMS current) among the interleaved phases -Sensitivity of current equalization among the phases to duty cycle fluctuation -Soft-switching would be difficult at higher switching frequencies -Absence of isolation
3-level asymmetrical voltage source converter b)	Yes	4 switches	-Lower rated switches -High-frequency operation -Smaller inductor -Reduced price and size -Compact structure -V2G support -Lower output and inductor current ripples	-No soft-switching
Parallel 3-level buck converter c)	Yes	8 switches	-Can operate with a bipolar DC bus -Compact structure -V2G support	-High voltage ripple at the input side -High circulating current -No soft-switching
Zero voltage switching converter d)	Yes	4 switches	-High voltage conversion ratio -Compatible with different voltage ranges -Reduced voltage ripple with interleaved design -Soft-switching -V2G support	-High conduction power losses because the resonant circuit is positioned in the current path) -Absence of isolation
Half-bridge zero-voltage switching converter e)	yes	4 switches	-Capable of operating at moderate duty-cycle ratio -Lower EMI -Reduced voltage stresses on switches -Compact structure -Relatively simple control -Soft-switching -V2G support	-Limited soft-switching range -Increased losses when operating at high switching frequencies -More components in the current path -Longer conduction path -Low efficiency
3-level zero voltage switching converter f)	yes	6 switches	-Reduced voltage stresses on semiconductor devices, so suitable for medium and very high-power applications -Soft-switching -V2G support	-More resonant circuits -Increased probability of losing soft-switching -High losses at light loads -Large size and the volume of the circuit -High control complexity

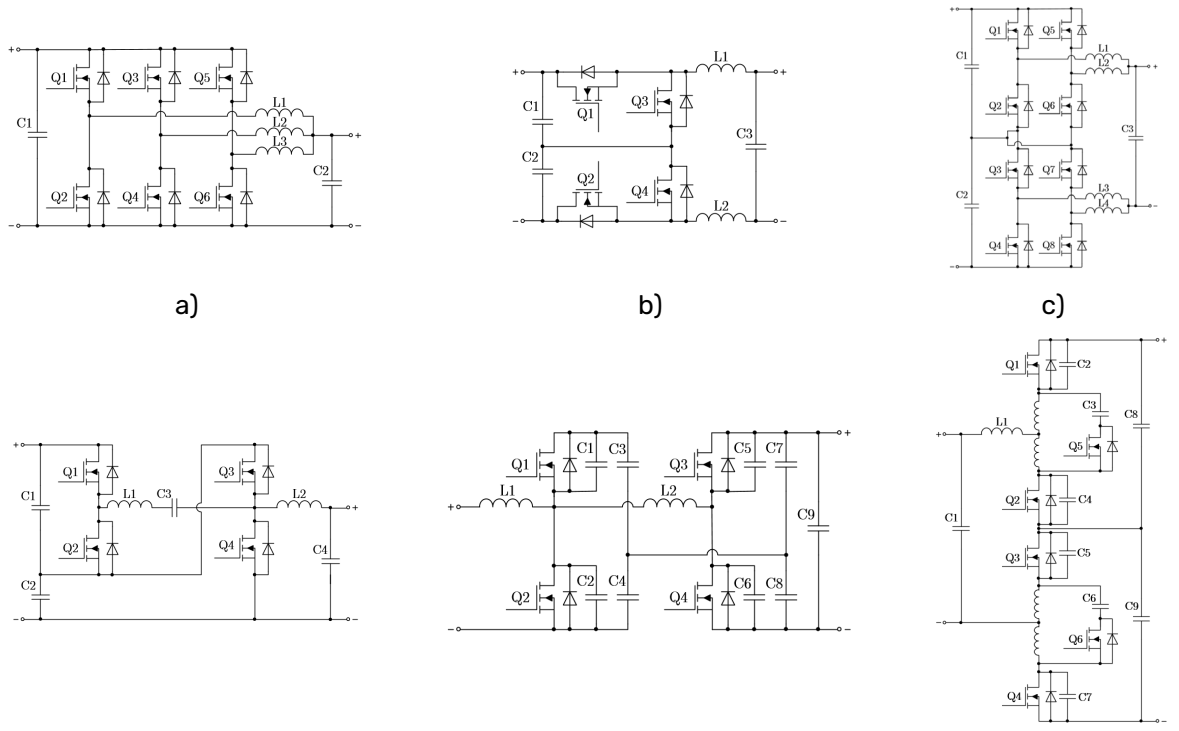

Fig. 3.2.4. Non-isolated DC/DC converter topologies: a) 3 phase interleaved buck; b) 3-level asymmetrical voltage source converter; c) Parallel 3-level buck converter; d) Zero voltage switching converter; e) Half-bridge zero-voltage switching converter; f) 3-level zero voltage switching converter.

Isolated

The most popular isolated topologies currently used in EV chargers are variations of bridge circuits - LLC converter, Phase-Shifted Full Bridge (PSFB), Dual Active Bridge (DAB), CLLC Dual Active Bridge. Their comparative analysis are listed below.

Table 3.2.6. Comparison of isolated DC/DC converters used in EV chargers.

Topology	Bidirectional power flow	№ of switches	Efficiency	Voltage regulation range	Advantages	Disadvantages
LLC Converter (a)	No	4 switches 4 diodes	High	Wide range	-Good voltage regulation -High power density -Soft-switching across wide range -High efficiency -Moderate control complexity -Low EMI	-Unidirectional power flow -Complex design procedure -Switching and resonant frequencies are close -No V2G support
Phase-shifted Full Bridge(PSFB) (b)	No	8 switches	Medium	With reduced efficiency	-Reduced current stresses on semiconductor devices -Low EMI -No circulating current on primary and secondary sides -Soft-switching -Simple control	-Hard switching for secondary side diodes -Low efficiency -Severe voltage overshoot across the full-bridge rectifier due to high-voltage EV charging -Reverse recovery problems of the diodes for high power flow -No V2G support
Dual Active Bridge (DAB) (c)	Yes	8 switches	High	With reduced efficiency	-High efficiency -High power density -Soft-switching -V2G support -Modular design -Wide range of voltage transfer ratio -Control simple to complex	-Soft-switching is challenging at light to medium loads (low EV battery voltage) -High losses for light loads -Transformer's saturation problems -Current overshoot -High-frequency current ripple leads to reduced battery lifetime
CLLC DAB (d)	Yes	8 switches	High	Limited range	-High efficiency -Soft-switching -V2G support -Transformer saturation is avoidable	-High power scaling is hard due to need of a highly symmetrical tank structure and modules synchronization -Relatively hard control -Power density is decreased

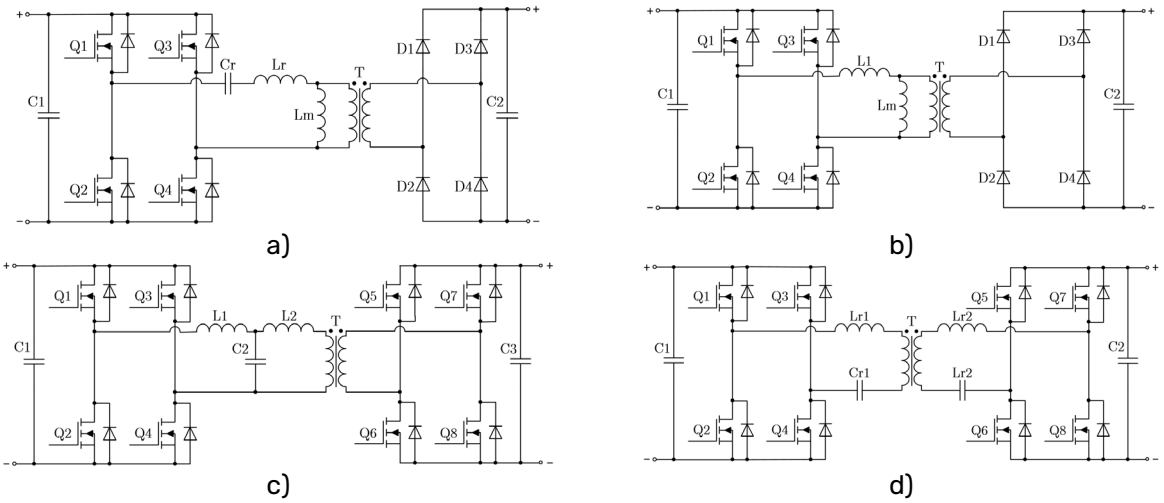

Fig. 3.2.5. Isolated DC/DC converter topologies: a) LLC converter; b) Phase-shifted Full Bridge; c) LCL Dual Active Bridge; d) CLLC Dual Active Bridge.

As can be seen, each topology has its own advantages and disadvantages, however, LLC converter and PSFB do not allow bidirectional power transfer and are not applicable for V2G systems. Thus, DAB variations remain, which is the most often used isolated topology in modern car chargers. This is due to their its high efficiency, high power density, soft-switching and wide range of voltage transfer ratio. However, due to the described shortcomings, DAB must be carefully designed.

Medium voltage and multiport EV chargers.

As was mentioned earlier, connecting EV charger to medium voltage networks is most often done through a low frequency step-down transformer. However, it is also possible to use medium voltage converter topologies, most popular of which are neutral point clamped (NPC) and modular multilevel converter (MMC). A comparison of different NPC topologies and CHB has been done earlier. Thus, in this section, EV chargers integrated into hybrid distribution transformer (HDT) and solid state transformer (SST) DC-links, modular multilevel converters (MMC) are discussed.

Connecting an EV charging station to the DC link of an SST (Fig.. 3.2.6 (a)) can be advantageous as it allows omit usage of a dedicated MV to LV charging station transformer. For this purpose, simple DC/DC converter can be used to connect charger to the SST DC link. However, the SST transformer has significant disadvantages such as lower efficiency and lower reliability in comparison with LF transformer, which limits its use in most applications.
An alternative could be usage of a HDT (Fig.. 3.2.6 (b)), which consists of a low frequency transformer and an additional power converters connected in series with a primary or secondary transformer windings. Although HDT has a smaller control range then SST, usually 10-15% regulation in AC grid is enough. Moreover, it has lower cost, higher efficiency, and in case of failure of the converter, the low frequency transformer continues to power the load, which makes it a reliable solution for distribution grids. The EV charger is connected to the converter DC-link. Such connection allows exchange of energy between grid, EV battery and other sources/loads connected to the same DC-link. The disadvantage of EV charger integration into HDT is the limited power of charging stations due to the additional load created on the power converter.

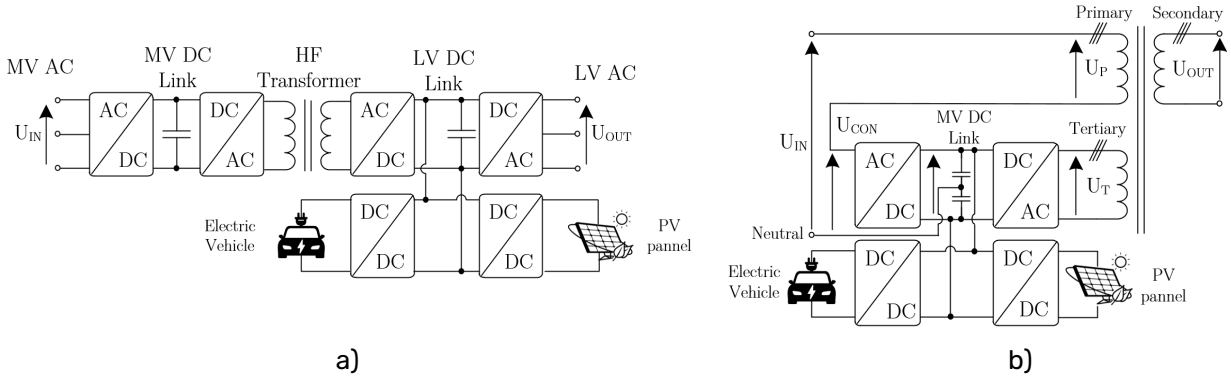

Fig. 3.2.6. EV chargers connection to SST (a) and HDT DC Links (b).

Modular multi-level converters (MMC) with integrated batteries (Fig. 3.2.7(a)) are a good solution for large-scale battery storage/EV chargers applications. In general, MMC converters have a low power density, which its drawback. However, since this is a solution for off-board EV charger, it is not essential. Additionally, MMC converters have a large number of semiconductor elements, and as a result, more complex control. Fig. 3.2.7 (b) shows possible topologies for submodules. In the SM1 and SM2 variants, the batteries are integrated into the submodules, directly replacing the capacitors or connected in parallel to them to increase efficiency and reduce cost. However, this leads to the appearance of low-frequency ripples on the batteries, which negatively affects batteries lifetime. In case of SM3, an additional DC/DC converter is installed, and in case of SM4, an additional DC/DC isolated converter is installed. However, as before, the problem of MMC converters is significant ripples on the capacitance of the submodule. To reduce it, the installation of large capacitors is required, which is costly and leads to an increase in size. In turn, the uneven connection of cars to different links leads to an uneven distribution of the state of charge of intermediate batteries and leads to the emergence of circulating main currents and an increased capacitor ripples.

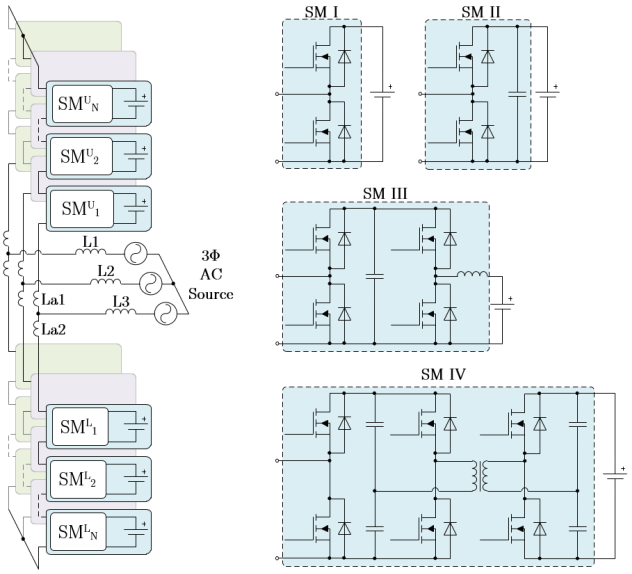

Fig. 3.2.7. Modular Multilevel Converter structure and submodule variations; Parallel MMC connection (b).

Another solution that can be used in high power fast charging stations with submodules in parallel proposed in (Fig. 3.2.8). One submodule consists of a CHB, a permanently connected battery, and a DC/DC isolated converter. The intermediate battery acts as a buffer, reducing the instantaneous load on the network. At such solution, main task of the control system is to minimize the difference in SOC of various modules. Advantage of parallel connection is that due to a parallel connection, modules are loaded equally and it is much easier to balance batteries SOC.

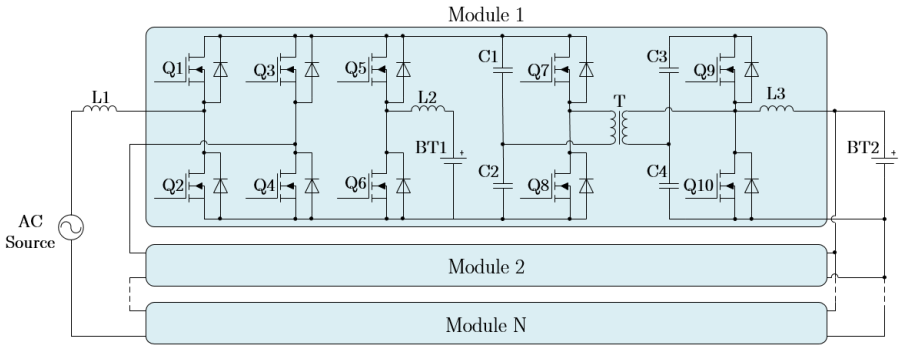

Fig. 3.2.8. Cascaded Half Bridge based MV converter.

For integrating PV panels and energy storage systems to EV charger, multiport topologies are used. The use of a multiport converter instead of separate converters, makes the system overall more economical, efficient, reduce its total size and increase system efficiency. One possible solution for a multiport converter could be usage of a Triple Active Bridge (TAB) (Fig. 3.2.9(a)). Various sources and loads, such as solar panels, EV chargers and battery storages, are connected through bidirectional DC/DC converters to the converter DC-link. Drawback of such solution is that DC/DC converters work with hard switching, which can be a problem in high power applications, however, the number of transformer windings as well as DC/DC converters can be increased and thus, power can be distributed.

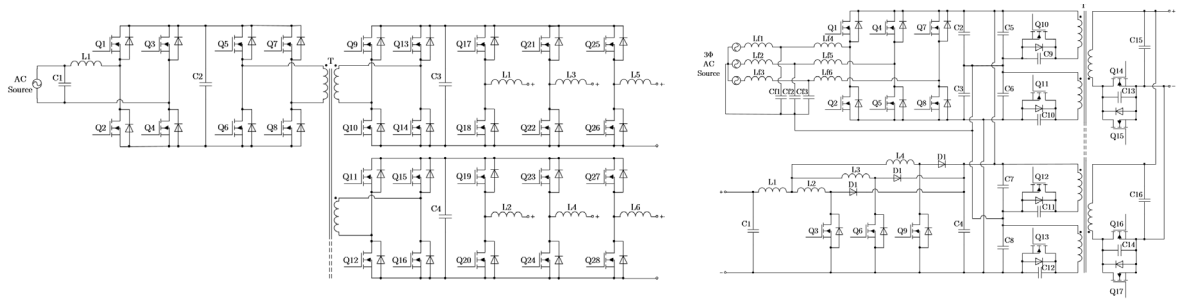

a) b)

Fig. 3.2.9. Triple Active Bridge (TAB) topology (a); Interleaved bidirectional flyback converter (b).

An alternative to the TAB converter can be interleaved flyback converter with multiple inputs and outputs (Fig. 3.2.9 (b)). Flyback topology is used due to the lower number of switches in comparison to the dual active bridge (4 versus 8 for DAB for one phase). In addition, an interleaved flyback topology with 4 phases has higher efficiency and lower volume then DAB with the similar parameter.

Bidirectional EV charger connection to existing grids

To avoid overloading of the low-voltage network, public EV charging stations are usually connected to the medium-voltage (MV) network through a low-frequency distribution transformer. Formed low voltage (LV) link can be either AC or DC based. Despite AC charger connection has been studied and used more widely, it requires additional AC-DC conversion stage for each DC load and source. Thus, AC LV link utilization in EV charger stations leads to an increased installation cost, reduced efficiency and increased size. On the contrary, DC LV bus network provides simpler structure and requires less conversion stages as it utilizes centralized AC-DC converter. Thus, DC sources and loads can be connected to the intermediate DC bus using only one DC-DC converter. Such solution allows reducing charging station size and is more beneficial for connecting car charging stations, solar panels and battery storage systems.

In modern cities, possible LV connection option is DC public traction lines (tram, trolleybus, metro). Except benefits described earlier, such connection can potentially provide range of mutual advantages for EVs and DC grids, in particular:

— DC grid voltage stabilization and energy recuperation.

At the moment of braking, traction transport creates voltage spikes at the line. To stabilize the voltage and accumulate braking energy, on-board energy batteries are actively used. They help increasing grid stability and reduce energy consumption. In case of bidirectional EV chargers connected to such a line, size of on-board batteries can be reduced since EV batteries can provide same services.

— Reactive power compensation.

In power lines for supplying electric traction transport, there is a problem of reactive power compensation, especially at night, when the active power consumed from the line is minimal. To solve the problem, various reactive power compensators are actively used. However, it is also possible to reduce $tg\varphi$ by loading the line with EV charging stations. Though it cannot fully replace compensators, their size and cost can be reduced.

— Reduced charger installation cost.

It is possible to choose the car charging moment, when public traction transport runs at reduced intervals (day and night) and does not create full load on the network. At that moments, using smart charging, EVs can be charged using existing grid, without overloading it.

As a result, traction grid connection might be beneficial both for the grid and for the EV chargers development.

A typical structure of a substation, feeding a catenary section is shown in Fig. 3.2.10, which consists of a MV to LV transformer with a consequent 12-pulse rectifier. In a default case, when no additional equipment is installed, power consumption from the substation and voltage at the catenary directly depends on the tram movement profile (Fig. 3.2.11 (a)). Two particular moments are worth mentioning. The first one is the beginning of the movement with a high acceleration speed. It results in peak power consumption from the substation, which increases stress on the equipment and requires the installation of components with redundancy to withstand peak power loads. The second one is a vehicle deceleration, which is accompanied by the release of vehicle braking energy to the LV DC line with a resulting voltage increase (Fig. 3.2.11 (b)). Usually, braking energy is dissipated in resistors, using braking choppers that are installed on the trams. However, it is associated with unwanted power loses and reduces transport efficiency by up to 30%. One possible solution that allows transferring braking energy from the DC line back to the AC grid is an Active Rectifier (AR), installed in parallel with the substation diode bridge (Fig. 3.2.10). Using such a reversible DC/AC converter allows to stabilize the voltage at the LV DC line as well as increases the efficiency of all traction vehicles in proximity to the substation. However, conventional AR has several problems:

1. Low utilization;

   The functions of AR are limited to braking energy recuperation, which occurs only for some time during the day. All other times, when there is no public transport nearby (which is the case at night) AR does not provide any significant functions.

2. Due to the absence of energy accumulators, AR cannot provide peak power shaving.

   As a result, this article proposes and analyses power converter interface structures and their functionality, which provides energy exchange between LV DC grid, AC grid and connected EVs. Proposed PCI: increases AR functionality and utilization; provides DC line voltage stabilization and transport braking energy recuperation (PREC in Fig. 3.2.11); reduces substation peak power load during traction transport rapid acceleration by providing peak power shaving (PSHAVE in Fig. 3.2.11).

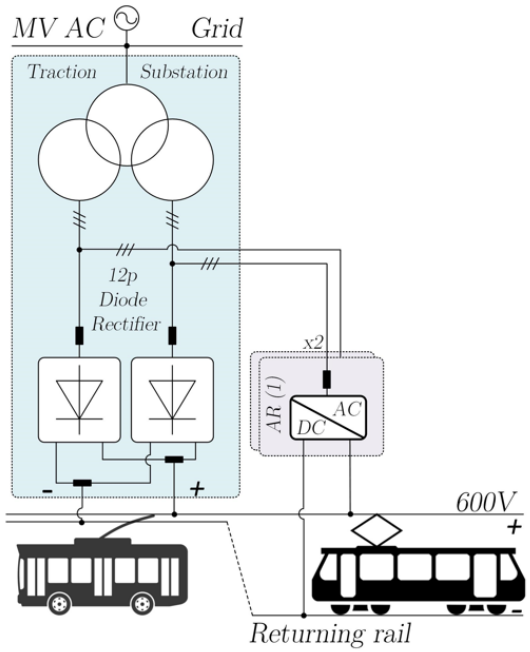

Fig. 3.2.10. Typical substation reversible converter connection scheme.

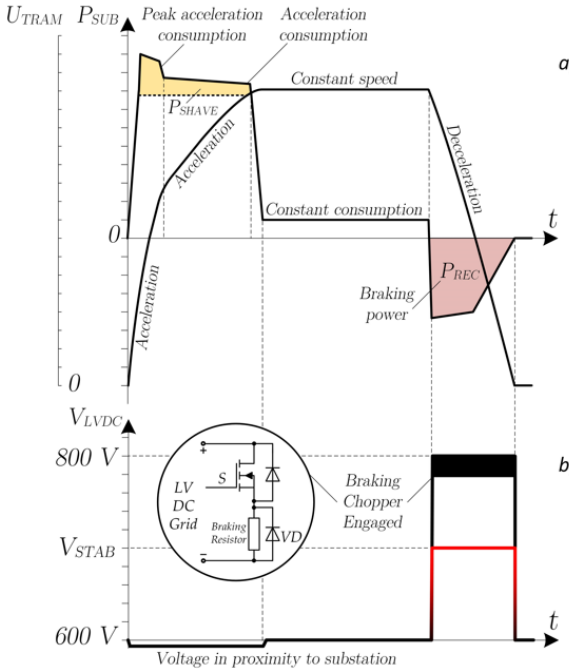

Fig. 3.2.11. Power consumed by tram from substation PSUB, which depends on its speed profile UTRAM a); and voltage at LV DC catenary in proximity to the substation VLVDC b).

Proposed PCI structure

In order to expand AR converter functions without introducing changes to its structure, it is possible to use it as an AC port in a power converter interface (Fig. 3.2.12). PCI is required in order to ensure all the requirements needed for normal system operation, such as:

- Isolated DC port for the EVs connection;

EV charging station standards require galvanic isolation from energy sources. Thus, isolation must be provided both from the MV AC network and from the LV DC grid.

- Galvanic isolation between AR and LV DC grid;

Usually, AR does not have galvanic isolation. Thus, in a conventional connection (Fig. 3.2.10) its operation is possible only when the voltage at the LV DC line is higher than at the AC side (during transport braking), i.e., when a diode bridge is not in a conductive state. Galvanic isolation allows it to operate independently from a 12-pulse rectifier.

- AR DC side voltage must be constantly higher than AC side voltage for active rectifier operation;

Procuring the abovementioned functions is possible by applying various connection schemes with the formation of different numbers of DC-buses, using different converter topologies. The schemes considered in this research are presented in Fig.3.2.12.

As a result, in addition to braking energy recuperation, usage of one of the proposed PCI structures allows AR to provide next functions:

- Work regardless of the voltage on the LV DC line;
- Active power filtering (APF) functions that improve the quality of electricity consumed from the AC network. (From this point of the research AR is going to be called APF);

Provide energy exchange between the AC network and the DC loads/sources (during day and night) that are connected to the DC-bus (bidirectional EVs, renewable energy sources, storage batteries etc.), which is particularly important in V2G applications;

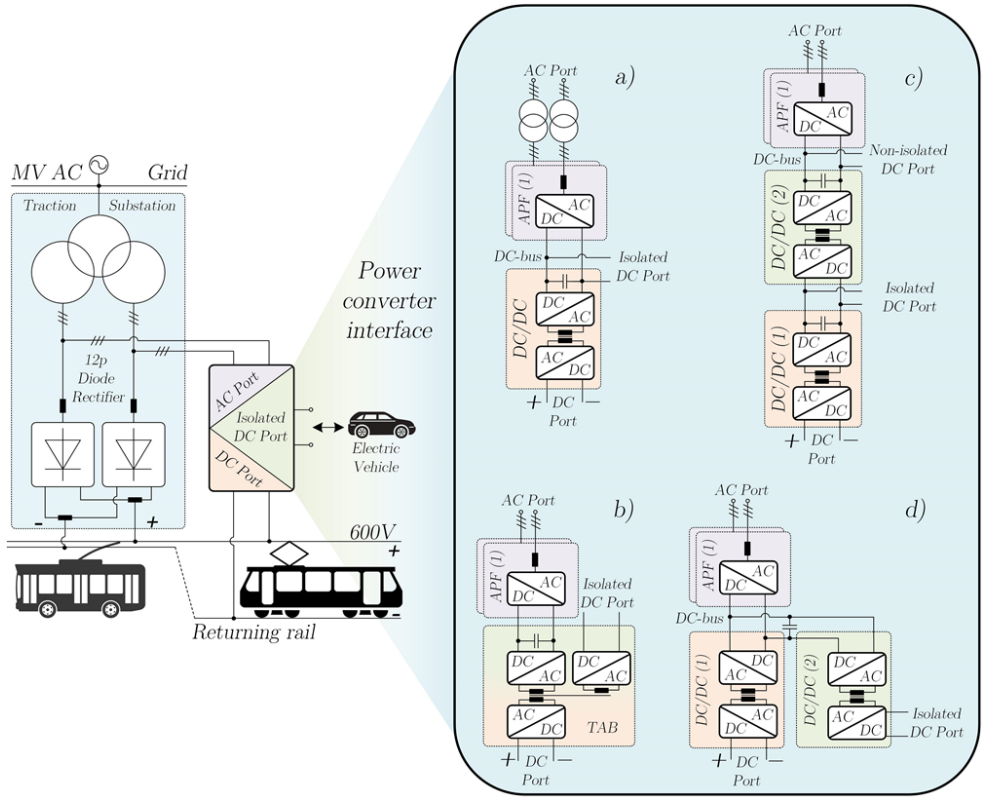

Fig.3.2.12. Possible connection schemes of power converter interface, connected to LV DC traction grid.

Table 3.2.7. Connection scheme comparison.

Name	Description
a. DC/DC converter with isolated APF	- Single isolated DC bus for EV chargers, PV generation and batteries connection; - Transformer has high efficiency and relatively low price; - 3-phase low-frequency transformer has low power density;
b. Triple Active Bridge converter (TAB)	- Single magnetic core used to connect all sources; - Two DC busses - non-isolated DC bus and isolated DC/AC output for EV chargers, PV generation and batteries connection; - Complicated control;
c. Two series DC/DC converters	- Two DC busses - non-isolated DC bus and isolated DC/AC output for EV chargers, PV generation and batteries connection; - Voltage of DC busses can have different values, which adds versatility to the circuit; - Two DC buses require more DC-bus capacitors installed.
d. Two isolated DC/DC converters	- Two DC buses - non-isolated DC bus and isolated DC/AC output for EV chargers, PV generation and batteries connection;

Additionally, the abovementioned PCI schemes, due to the presence of bidirectional EV chargers, connected to the system DC-bus, provide substation peak power shaving. A comparison of described solutions together with their main characteristics is provided in Table 3.2.7.

PCI power flow

Power flow management plays a crucial role in a PCI operation. Due to the existence of different elements of a system like MV grid, LV DC grids and EV chargers (Fig. 3.213), optimal control of such system is a separate research task and widely discussed in the literature. Nevertheless, the authors of different researches in similar systems do not take into account renewable energy sources. In contrary, this section discusses the basic power exchange principle between all system elements - MV AC grid, LV DC traction grid, EV batteries and renewables. The integration of renewable sources into such a system seems reasonable, as it follows the green energy development trend and potentially reduces the load on a substation by partially powering the line. In addition, when there is no transport operating on the traction line, generated energy is stored in EV batteries or transmitted back to the AC grid, which creates different options for renewables management.

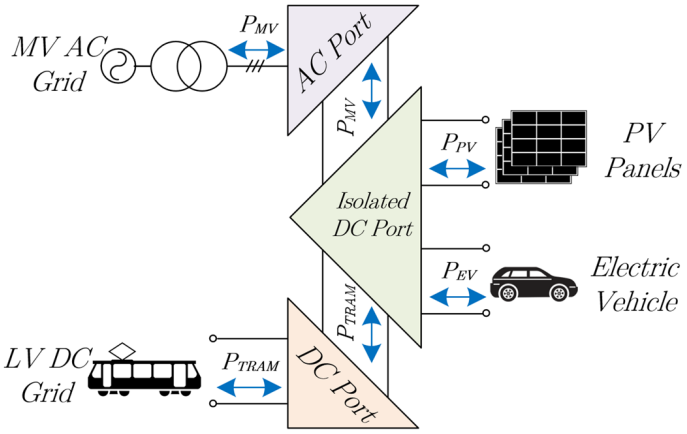

Fig. 3.2.13. Power converter interface power flow.

PCI system power flow in a simplified form is described using formula (1). **Positive power** flows are considered **in the direction of the isolated DC port**.

$$\pm P_{TRAM} \pm P_{MV} \pm P_{EV}^{mode} + P_{PV} = 0 \quad (1)$$
$$P_{PV} = f(Irradiance, Temperature)$$

where: P_{TRAM} – tram power consumption/recuperation, P_{MV} – power consumed from grid/transferred back to grid, P_{EV}^{mode} – EV charger power depending on mode, P_{PV} – PV panels generation power.

In formula (1) "±" means bidirectional power flow possibility. Thus, when the energy generated by solar panels and consumed by EVs are both equal to zero ($P_{PV}=0$, $P^{mode}_{EV}=0$), power consumed from the MV grid during tram movement and recuperated during tram braking entirely depends on tram consumption and generation ($P_{MV}=P_{TRAM}$). In the case of non-zero EVs and PV powers, the AC port manages only the mismatch between P^{mode}_{EV} and P_{PV}. That means, that when all generated by PV energy is used to charge EVs ($P_{PV}=P^{mode}_{EV}$), the same $P_{MV}=P_{TRAM}$ relation takes place. In addition, it means that when EV chargers are consuming power from the DC port, but PV generation does not fully satisfy this demand ($P_{PV}<P^{mode}_{EV}$), EV chargers consume missing power from the MV grid, creating additional load on an AC port and, consequently, on the substation. In particular, this is important during tram acceleration, when the substation is already significantly loaded. As a result, to reduce overload on an AC port and substation during peak load events, EV chargers should operate in smart charging mode.

Overall, there are several EV charger modes, which result in a different system behavior:

— Mode 1. Non-intelligent unidirectional charging:

$$Mode\ 1: \quad P_{EV}^{unidirectional} = P_{EV}^{\max},$$

where $P_{EV}^{unidirectional}$ – power consumption during non-intelligent charging, P^{max}_{EV} – maximal power consumption of installed EV chargers.

Non-intelligent EV charging is a simple EV charging method that does not consider the substation load. This mode results in an increased load on a substation, which leads to faster equipment aging. Applying such mode with a high-power charging stations is not recommended.

— Mode 2. Intelligent unidirectional charging:

$$Mode\ 2: \quad P_{EV}^{smart} = \pm P_{MV}^{\max} \pm P_{TRAM} + P_{PV},$$
$$[0 \le P_{EV}^{smart} \le P_{EV}^{\max}]$$

where P_{EV}^{smart} – power during smart EV charging, P^{max}_{MV} – power limit, overcoming which, EV chargers reduce power.

Intelligent charging is an EV charging that is controlled correspondingly to the substation load. During peak consumption from the substation, EV chargers decrease charging power to reduce peak load. However, there is no peak shaving due to unidirectional power flow. That means that when power consumed by tram is higher than substation power limit ($P_{TRAM} > P^{max}_{MV}$) it is impossible to limit substation power at level of P^{max}_{MV} using unidirectional smart charging.

— Mode 3. Intelligent bidirectional charging:

$$Mode\ 3: \quad P_{EV}^{bidirectional} = \pm P_{MV}^{\max} \pm P_{TRAM} + P_{PV},$$
$$[-P_{EV}^{\max} \le P_{EV}^{bidirectional} \le P_{EV}^{\max}]$$

where $P_{EV}^{bidirectional}$ – power during bidirectional EV charging.

Bidirectional intelligent EV charging allows providing peak shaving to reduce maximum substation load, when $P_{TRAM} > P^{max}_{MV}$. Power deficit is supplied from EV batteries (if enough cars with bidirectional power flow are present).

Simulation results

The next stage of PCI development involves simulating its operation using modern simulation systems to study the modes of EV bidirectional charging and the potential benefits it can bring to the system (what additional services bidirectional charging can offer). For the simulation, Matlab Simulink was chosen due to its comprehensive functionality and the presence of all the necessary functions for this research.

One of the key elements of PCI is the traction transport, which has relatively low dynamics. For example, the acceleration and deceleration of a tram together can take up to a minute, depending on the route. Additionally, there are modes of uniform motion that also need to be investigated. As a result, the full route of traction transport for real-time research takes minutes. Due to the presence of several converters in the system, simulating such a long time using full converter models would take a significant amount of time and, as a result, is not practical. Therefore, an averaged model of the system was developed, in which real converter models are replaced by their equivalent circuits (Fig. 3.2.14). Such a model allows for reducing the simulation time to a mere ten seconds, enabling various system tests, some of which will be presented later.

As can be seen, the DAB (DC-DC Converter) models for car charging and LVDC (Low Voltage Direct Current) network connection are based on dependent current sources. The active filter model and diode rectifier model are based on controlled voltage sources and current sources. The solar panel model is taken from a ready-made Simulink library and allows for changing panel parameters and irridiance to alter power output. The converter connecting the solar panels and the DC link is also built using controlled voltage sources and current sources and operates in maximum power point tracking mode. Full model in the Matlab Simulink can be seen in Fig. 3.2.15.

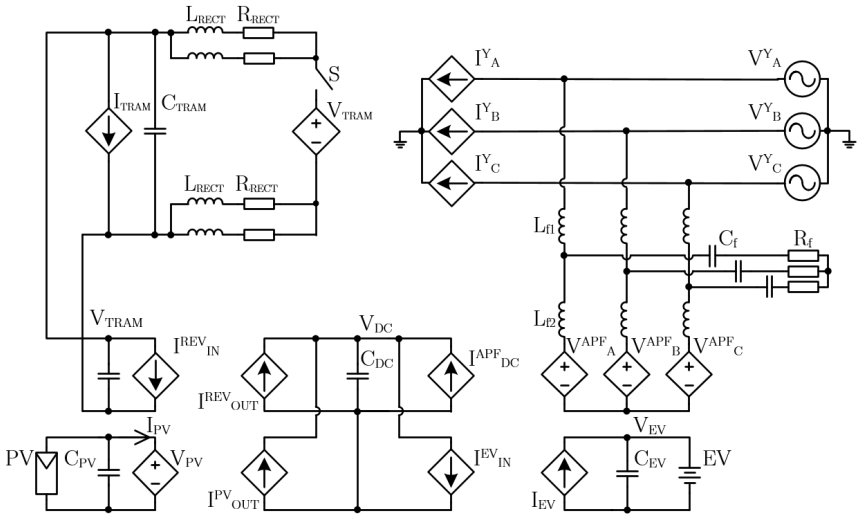

Fig. 3.2.14. Power converter interface averaged model used for simulation.

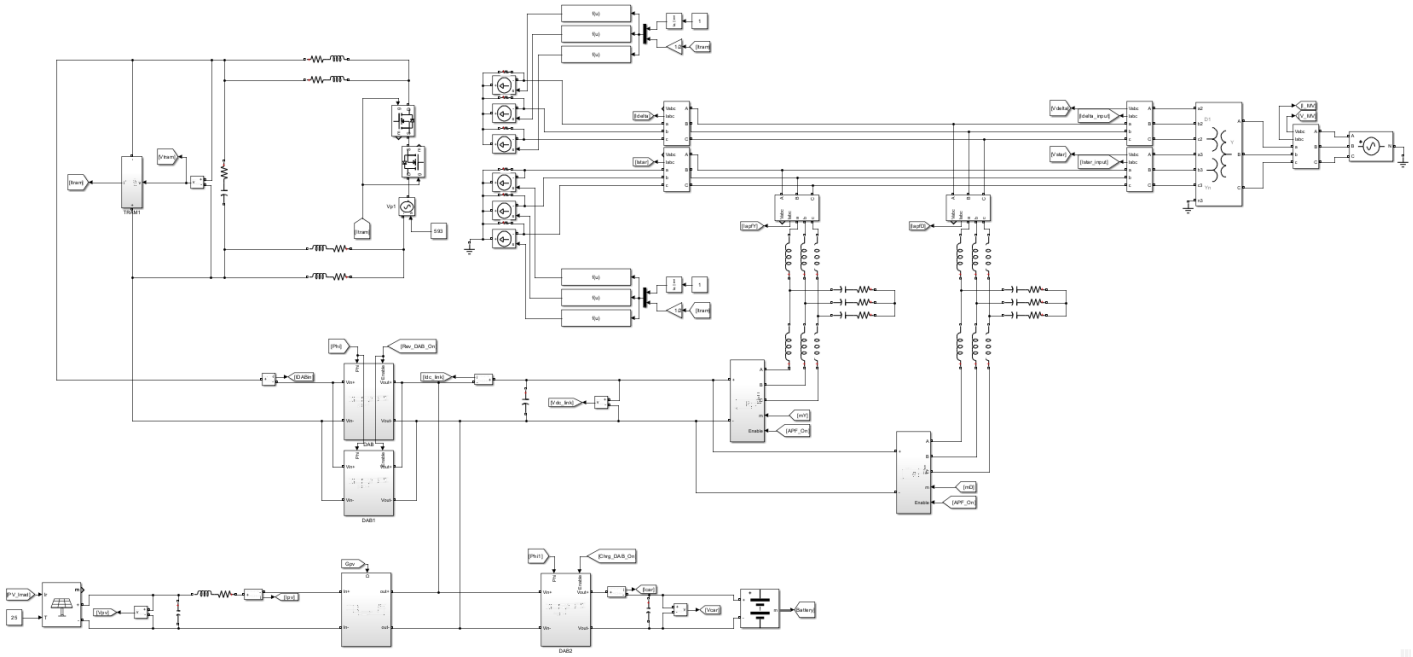

Fig. 3.2.15. PCI model in Matlab Simulink.

The control system for the converters in PCI is primarily built in the PLECS environment (Fig. 3.2.16). PLECS is a software tool for system-level simulations of electrical circuits developed by Plexim, which allows for simulating converters at the component level with a sufficiently high speed, using the actual switching frequency of the switches. Initially, there was an attempt to simulate the entire system in PLECS. However, the simulation speed was insufficient. Therefore, the decision was made to create an averaged model. Nevertheless, implementing the control system for individual converters in the PLECS environment will allow for more detailed simulation of the studied converters (particularly bidirectional vehicle charging) in the future, which will be the next stage of the research. The mode switching system for vehicle charging is built in the Simulink environment and represents an implementation of the formulas described earlier.

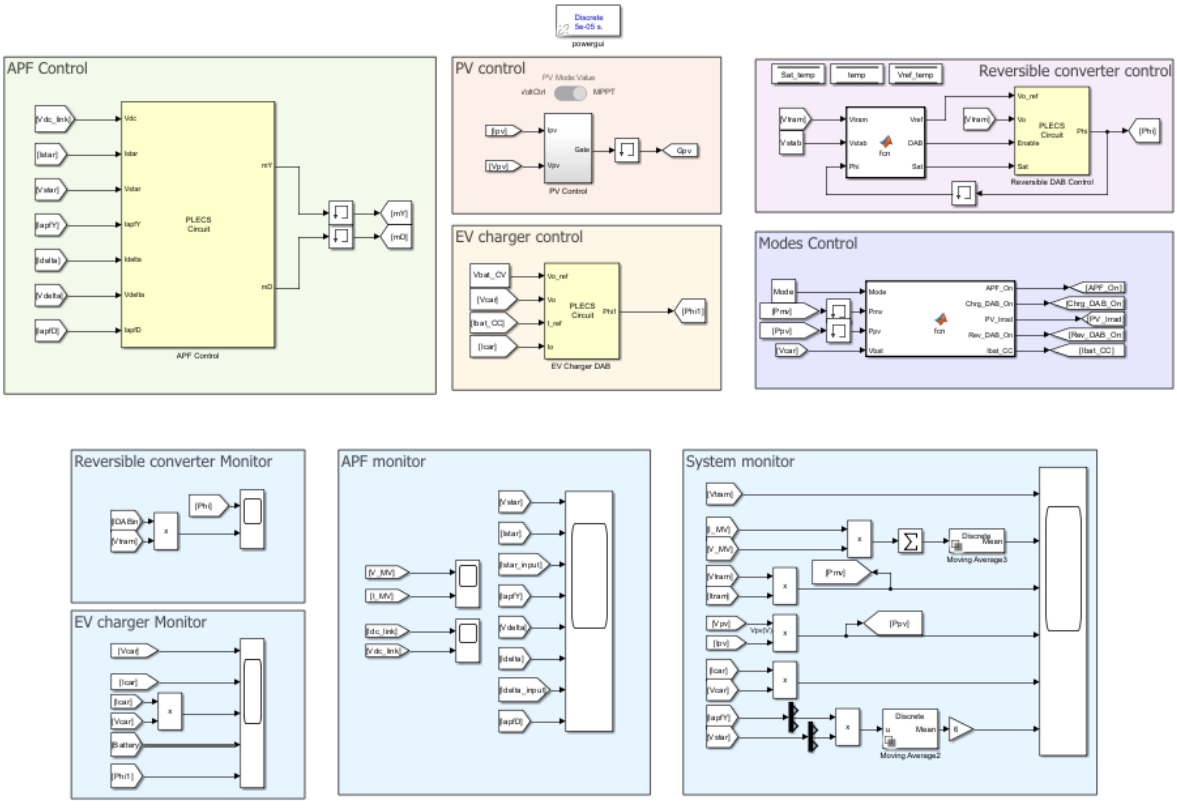

Fig. 3.2.16. PCI control system in Matlab Simulink.

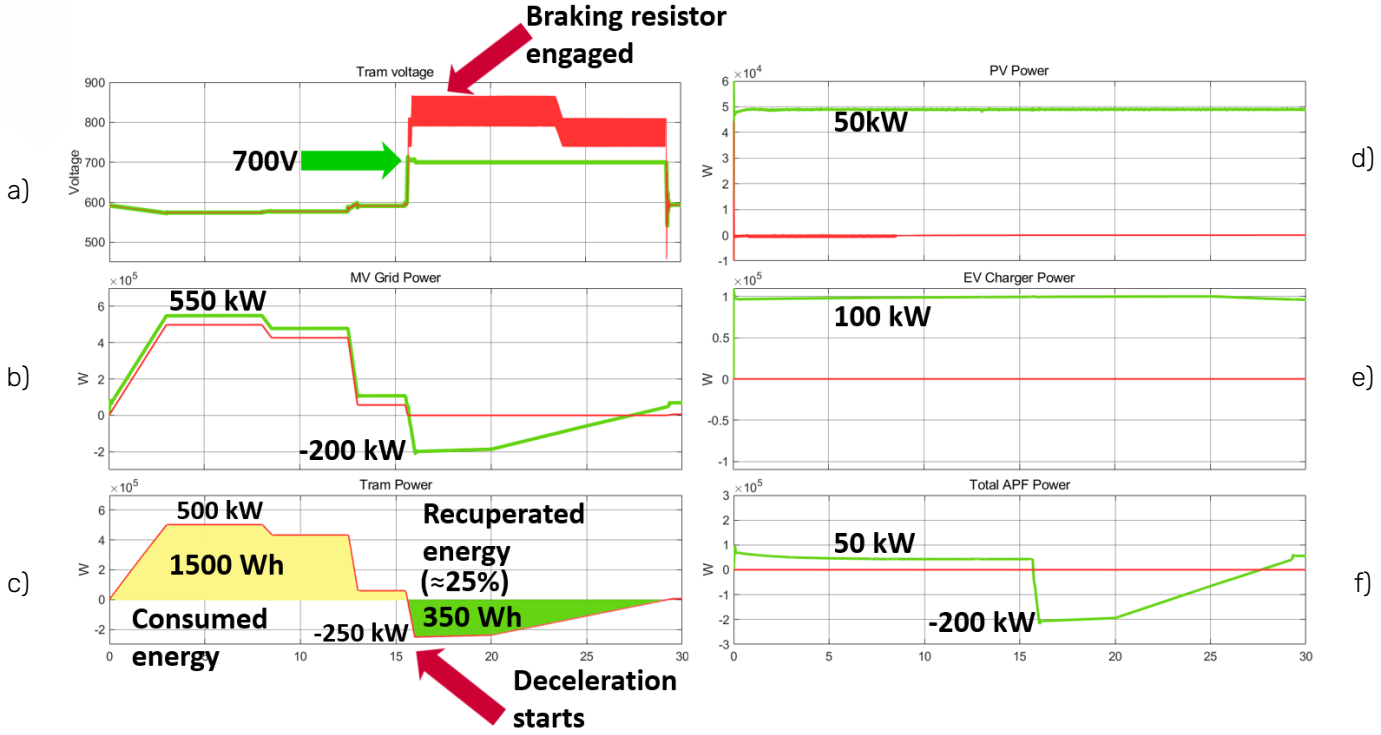

Fig. 3.2.17. PCI working diagrams during Mode 1 EV charging (Red lines – PCI interface is turned off. Green lines – PCI interface is turned on): a) Voltage at LV DC catenary line; b) Power consumed\Recuperated to MV grid; c) Power consumed\Recuperated by tram; d) PV panels power; e) EV charger power; d) APF power.

In Fig. 3.2.17, the simulation results of the system's operation is presented, when PCI is not enabled (red line) and when all PCI components are operating (green line), including vehicles in mode 1 (uncontrolled charging). From time 0 to 12.5 seconds, the tram's acceleration, accompanied by a peak power consumption of approximately 500 kW (Fig. 3.2.17 e) can be observed. The voltage on the line changes insignificantly (Fig. 3.2.17 a) because the measurement is taken near the substation, and the wire resistance is minimal. The solar station generates 50 kW of power, while the vehicle chargers consume 100 kW. The difference between the vehicle consumption and the solar panel generation of 50 kW is drawn from the MV grid through the APF (Fig. 3.2.17f), explaining the total consumption of 550 kW (500 kW tram + 50 kW vehicle charging). During this time, the energy spent on acceleration reaches 1500 Wh.

From 12.5 seconds to 16 seconds, the tram moves uniformly without acceleration with a consumption of about 100 kW. Network consumption accordingly decreases.

From 16 seconds to 30 seconds, the tram begins to decelerate, which accompanied by energy recuperation. The peak recuperation power is 250 kW, and the total energy recovered during the entire recuperation cycle is 350 Wh, which represents approximately 25% of the energy spent on acceleration (situation may vary depending on the tram's power, track slope, passenger count, etc.). In the case of the PCI system being turned off, the recuperated energy dissipates in braking resistors, often installed on the tram's roof. In Fig. 3.2.17 a, can be seen that when braking resistors are used, the voltage on the line increases to 850 V. As a result, all the recuperation energy is simply dissipated and lost. However, when the PCI system is in operation, the energy is redirected for vehicle charging (if they are present) or sent back to the AC grid. In this case, it is accompanied by a reduction in voltage on the LV DC line to a level of 700 V (700 V is chosen as an intermediate value between the nominal 600 V and 800 V, which are typically used for systems with braking resistors). When the system operates this way, recuperation energy is utilized effectively, resulting in increased efficiency of the traction transport near the substation. It should also be noted that at the peak of recuperation, when the power is 250 kW, vehicles can only accept 50 kW (since an additional 50 kW is coming from the solar panels). The remaining 200 kW is sent back to the grid through the APF, as can be seen in Fig. 3.2.17 (b, f).

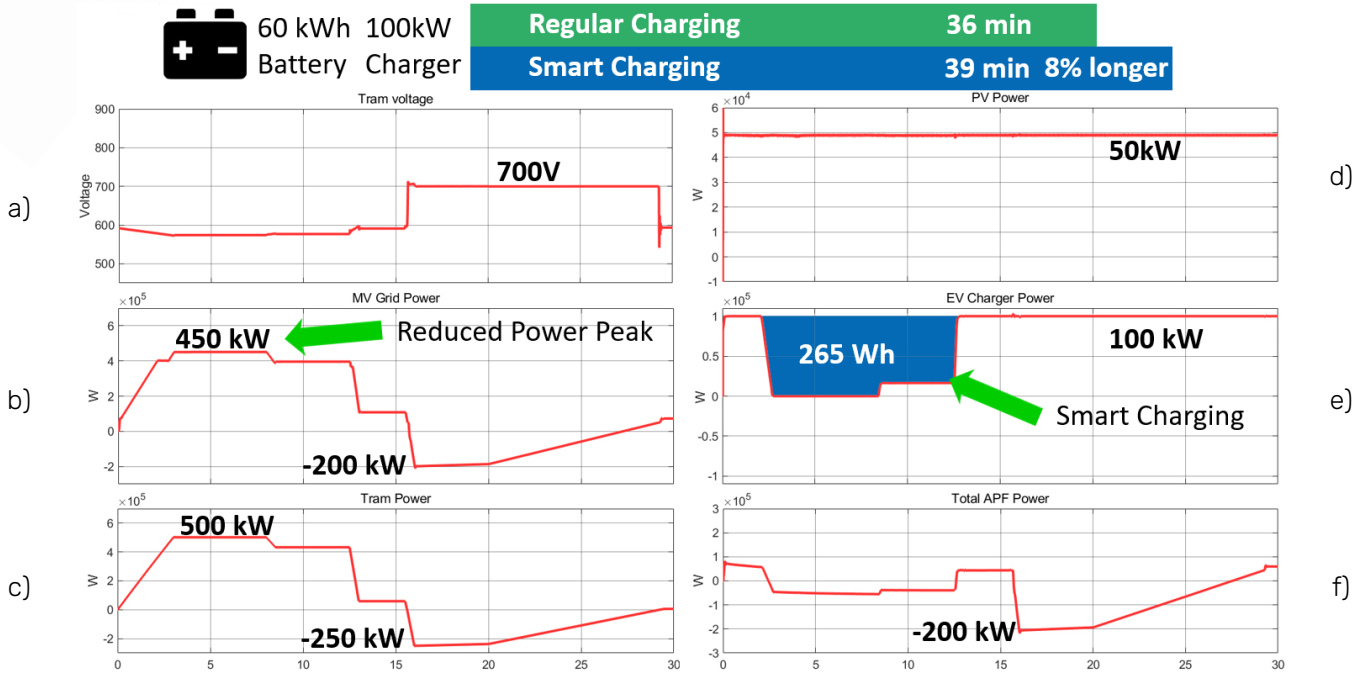

Fig. 3.2.18. PCI working diagrams during Mode 2 EV charging: a) Voltage at LV DC catenary line; b) Power consumed\Recuperated to MV grid; c) Power consumed\Recuperated by tram; d) PV panels power; e) EV charger power; d) APF power.

In Fig. 3.2.18, the operation of PCI and EVs in mode 2 is shown, where the charging station operates in smart charging mode. As can be seen in Fig. 3.2.18 (e), the power of the car charging station varies from the nominal 100 kW to zero, depending on the peak load on the traction substation. For example, when the load on the substation is at its maximum and reaches 500 kW (tram peak consumption), the power of the charging station is reduced to zero to reduce the peak load on the substation. As a result, compared to standard charging (Fig. 3.2.17 (b) Green), the peak power is reduced by 100 kW (Fig. 3.2.18 (b)). It should be noted that a drawback of this charging method is longer charging times compared to regular charging. As can be seen, the charging duration has increased by 8%. However, the change in charging duration directly depends on the frequency of tram acceleration near the substation, its power, and the desired level of peak power reduction. In the research case, it was assumed that trams depart from the station every 2 minutes, which was characterized by a potential loss of 265 Wh every two minutes and, in the case of charging with a standard 60 kW battery, leads to an increase in charging time by 3 minutes.

The criterion for smart charging in this specific case was not to exceed the substation power level of 400 kW. However, as can be seen from Fig. 3.2.18 (b), the power still exceeded the desired 400 kW and reached 450 kW regardless of the smart charging algorithm. This is because the power of the charging station had already been reduced to 0 kW, and further reduction in the peak power of the substation is only possible with an additional source of energy. The car's battery can serve as such a source, but bidirectional charging of the car in mode 3 should be applied in such case.

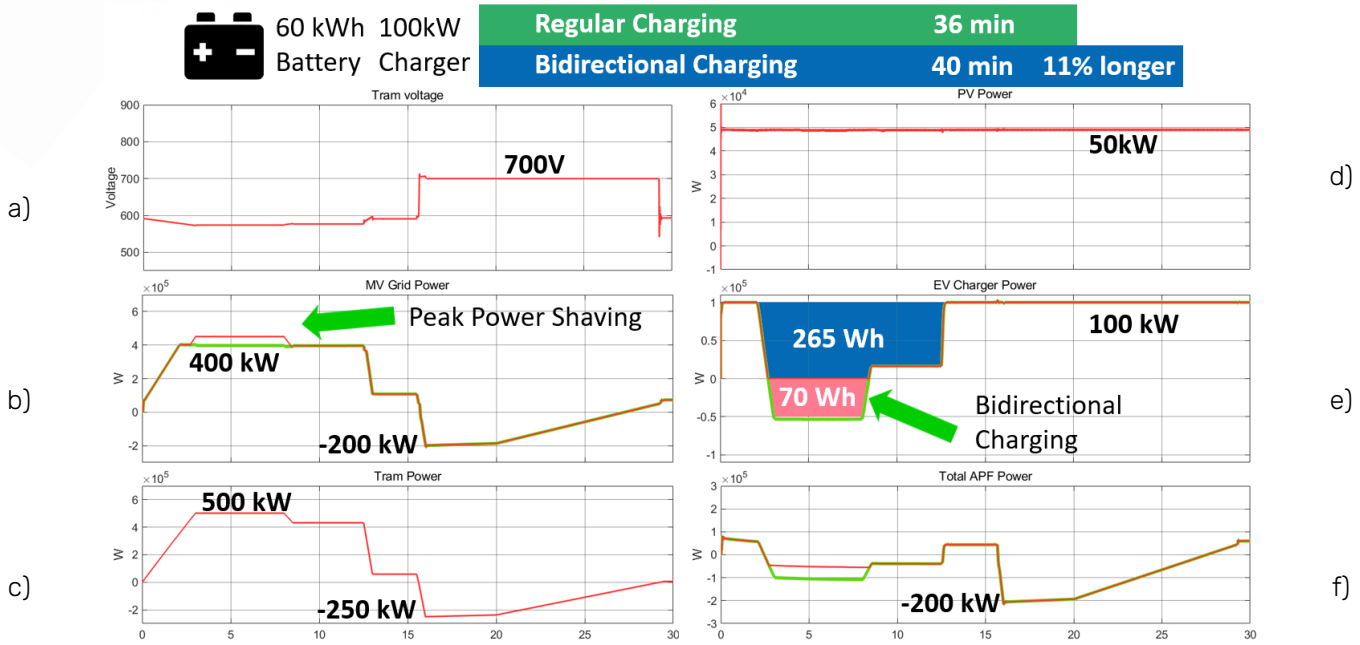

Fig. 3.2.19. PCI working diagrams during Mode 3 EV charging (Red – unidirectional mode 2 charging; Green – bidirectional mode 3 charging): a) Voltage at LV DC catenary line; b) Power consumed\Recuperated to MV grid; c) Power consumed\Recuperated by tram; d) PV panels power; e) EV charger power; d) APF power.

Fig. 3.2.19 depicts the third mode of car charging in which charging stations have the capability for bidirectional charging (green). In the case of bidirectional charging of the car, it is possible to achieve the desired reduction in the substation's peak power to the level of 400 kW while retaining all other system functions. However, when compared to one-way charging, an even greater overall reduction in charging time is observed. As a result, a 60 kW battery charges for 4 minutes longer (11%) compared to regular charging. The battery discharge energy in this case was 70 Wh.

As a result, the following conclusions can be drawn:

1. The integration of electric vehicle charging stations into low-voltage traction networks does not impose a significant load on the substation when smart charging algorithms are applied.
2. Smart and bidirectional charging only slightly increase the charging time of the car.

3.2.3.Contribution to the WP objectives

Main results of a research is a proposed connection scheme together with a control algorithm, which complies with the working package objectives 2, 3 and 4. In particular:

Proposed converter connection scheme allows optimizing power distribution between systems components, reducing losses, improving AC and DC grid power quality. The developed power converter interface structure, along with its control algorithm, enables the utilization of EV charger batteries through bidirectional EV chargers as a flexible component of a smart grid. The system enhances the power quality of a low-voltage DC grid, provides ancillary services, facilitates the exchange between AC and DC grids, and optimizes power flow among system participants. In particular, it allows using recuperated energy from traction transport for EV batteries charging, rather than dissipating it in braking resistors or returning it to the grid. This reduction of the current path results in decreased losses. The same principle applies to PV panels connected to the PCI DC-link. Connecting PV panels in close proximity to consumers like EVs and the traction grid, while implementing the proposed control methods, helps reduce ohmic losses in the system.

Additionally, implementation of the active power filter in the power converter interface allows to reduce THD of the current consumed from the AC grid from 30% to 5%, which positively affects energy distribution losses. Connection of the EV chargers to the traction grids reduces reactive power consumption from the grid (EV charging during night makes tg(phi) < 0.4), removing penalties for reactive power consumption. Moreover, installation of the proposed PCI system improves traction transport efficiency by up to 30% thanks to the braking energy recuperation. In the studied

in the simulation model case, with a real tram power profile, voltage peak at the line during tram braking was reduced from 850-900V to 700V, which shows that LV DC power quality is improved. In its case, implementation of the bidirectional EV charging during peak power consumption from the substation, allowed to reduce peak substation load from 550kW (no intelligent charging) to 400kW (bidirectional charging). Reduced peak power consumption shows that EVs can be connected to the existing infrastructure, creating no excessive load only in case of intelligent charging. However, it is worth mentioning, that intelligent and bidirectional EV charging leads to an increased charging time, which is undesirable for fast chargers. Thus, in the studied case, unidirectional smart charging led to an 8% longer charging time and bidirectional charging to an 11% longer charging time.

3.2.4.Scientific achievements

Publication

#	Title, incl. citation information	Type (Conference, journal, book chapter)	Status (Submitted, accepted, published)	DOI
1	Power Converter Solutions for Industrial PV Applications—A Review	Journal	Published	10.3390/en15093295
2	Power converter interface for urban DC traction substations - solutions and functionality	Journal	Accepted (Publication is expected in November 2023)	http://pe.org.pl/
3	Key activities to improve energy management in DC microgrids connected by urban traction	Journal	Accepted (Publication is expected in November 2023)	http://pe.org.pl/
4	Feature of Solar Radiation Forecast Services Use for Solar Plants	Conference	Published	10.1109/ESS57819.2022.9969258
5	Bidirectional EV charger integration into LV DC traction grid	Conference	Published	10.1109/CPE-POWERENG58103.2023.10227489
6	An Overview of Bidirectional EV Chargers: Empowering Traction Grid-Powered Chargers	Book Chapter	Accepted (Publication is expected in November 2023)	https://link.springer.com/book/9783031447716

Others

Dissemination activities

#	Title	Conference	REFERENCE
1	Hybrid distribution transformer with MV side control and DC bus for	The 15th Conference Control in Power Electronics and Electric Drives - "SENE 2022", Łódź,	https://www.sene.p.lodz.pl/index.php?www=artykuly_2022.html https://smartgysum.eu/Home/Outcomes

	connecting an EV charger	November 23-25th 2022	
2	LV DC traction substation with connected bidirectional EV chargers and improved functionality	XI Konferencja Naukowo-Techniczna –I-MITEL-2023, Sulęcin, kwiecień 12-14, 2023	https://imitel.zut.edu.pl/?id=10502&L=0 https://smartgysum.eu/Home/Outcomes

3.3. Task 3.3 – IRP7 "Reliability and Availability of Smart Transformers for Cost Effective and High Quality of Services in the Grid"

3.3.1. Introduction

The concept and architectures of the smart transformer (ST) as a link between medium and low voltage (MV and LV) ac and dc grids were thoroughly investigated. A three-stage ST architecture was selected, and a modular multilevel converter (MMC) was identified as a suitable solution for the MV AC-DC conversion stage. Therefore, the MMC was subjected to in-depth analysis. The studied materials and derived conclusions were summarized in a conference paper. In the next stage, to increase the lifetime of the MMC and make it more economically attractive, a new balancing method was suggested, in which the voltage of the capacitor, junction temperature of switches, and capacitor losses can be effectively balanced through it. These scientific outcomes have been obtained during 12 months in the facilities of the Chair of Power Electronics at the Kiel University (Christian-Albrechts-Universität zu Kiel).

3.3.2. Scientific outcomes

Solid-state transformer (SST) is a power electronic-based transformer and is considered as an alternative to the conventional power transformer (CPT). Smart transformer (ST) is an SST with control and communication capabilities. These capabilities besides its main role as an interface and isolator of medium and low-voltage (MV and LV) grids augment the functionalities of the SST by providing ancillary services to the grid to optimize its performance. One of the significant functionalities of the ST, compared to CPT, is its dc connectivity. ST can offer dc connectivity in MV and LV levels and contribute to realize the ac-dc hybrid grid.

Various architectures have been suggested for the ST, including 1) single-stage, 2) two-stage, and 3) three-stage. Each of these architectures of the ST are depicted in Fig. 3.3.1, respectively. The three-stage structure is a preferred architecture to be exploited, since it can provide MV and LV dc connectivity, input/output decoupling of voltage and current, and more degrees of freedom in terms of control than the others.

The three-stage architecture consists of MVac/MVdc, MVdc/LVdc, and LVdc/LVac stages. Among them, the MVac/MVdc stage present a quite challenges. The power converter employed in this stage should be able to handle the MV level. The modular multilevel converter (MMC) and cascaded H-bridge (CHB) are the two suitable candidates to be used in this stage. MMC and CHB can operate at MV level with LV switches. The structures of MMC and CHB are depicted in Fig. 3.3.2. A distinguishing difference between MMC and CHB is their capability in establishing the MVdc link. CHB cannot directly from a MVdc link, while MMC inherently can do it without the need for huge capacitor. Therefore, MMC can be considered as a suitable solution to employ in MV side of ST.

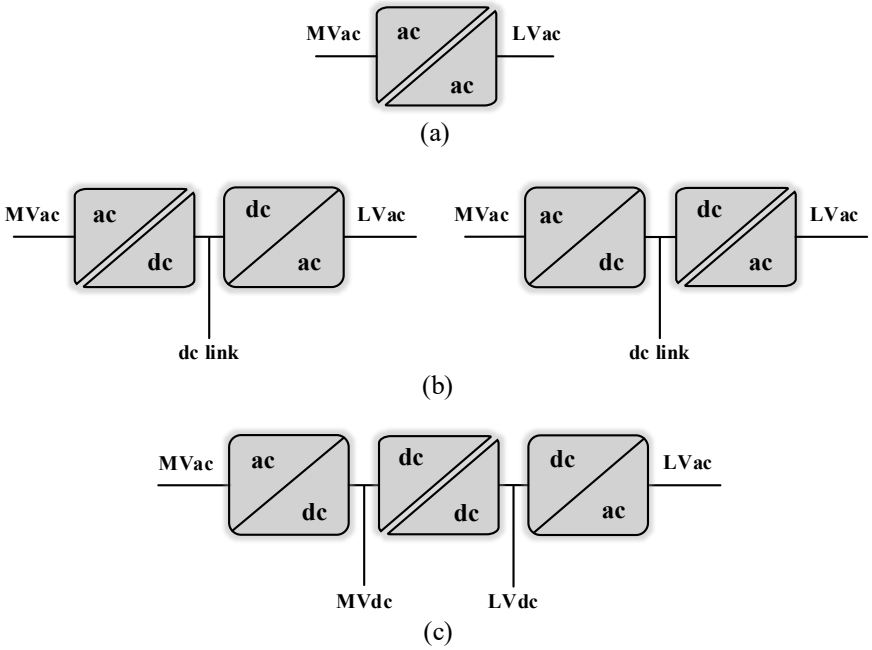

Fig. 3.3.1. ST architectures, (a) single-stage, (b) two-stage, and (c) three-stage.

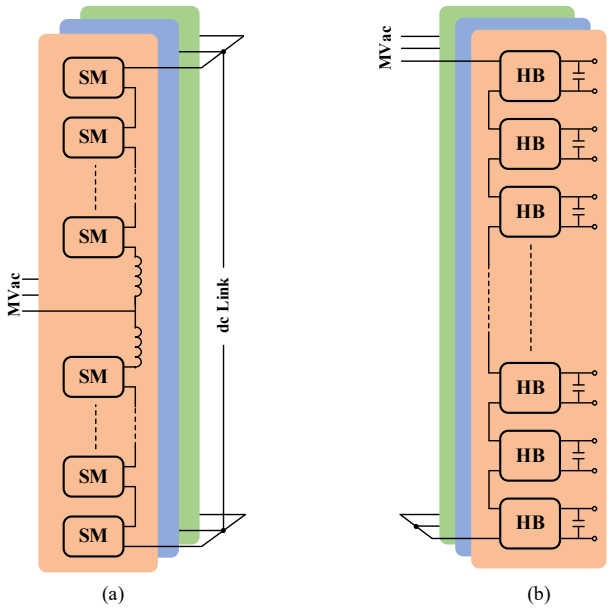

Fig. 3.3.2. Modular converters, (a) modular multilevel converter, (b) cascaded H-bridge.

The MMC consists of submodules (SMs) which are connected in series. A sequence of SMs connected in series forms an arm, and two such arms, connected to their inductors, create a leg. The inductor in each arm is referred to as the arm inductor (L_{arm}). The arm inductor limits both the circulating current and the current resulting from the instantaneous voltage differences between the arms. Various topologies can be employed for the SMs of the MMC, each offering distinct characteristics concerning capacitor voltage ripple, efficiency, and fault current blocking capability. The half-bridge (HB) represents the most fundamental topology for SM usage.

Various structures have been suggested for utilizing the MMC on the MV side of SST. The basic form of the MMC, as depicted in Fig. 3.3.3(a), can be used. In this topology, the MVdc link provided by the MMC can be advantageous in the SST architecture, where it is necessary, but the dc-dc stage of SST is necessary to connect the MVdc and generate LVdc on the other side of it.

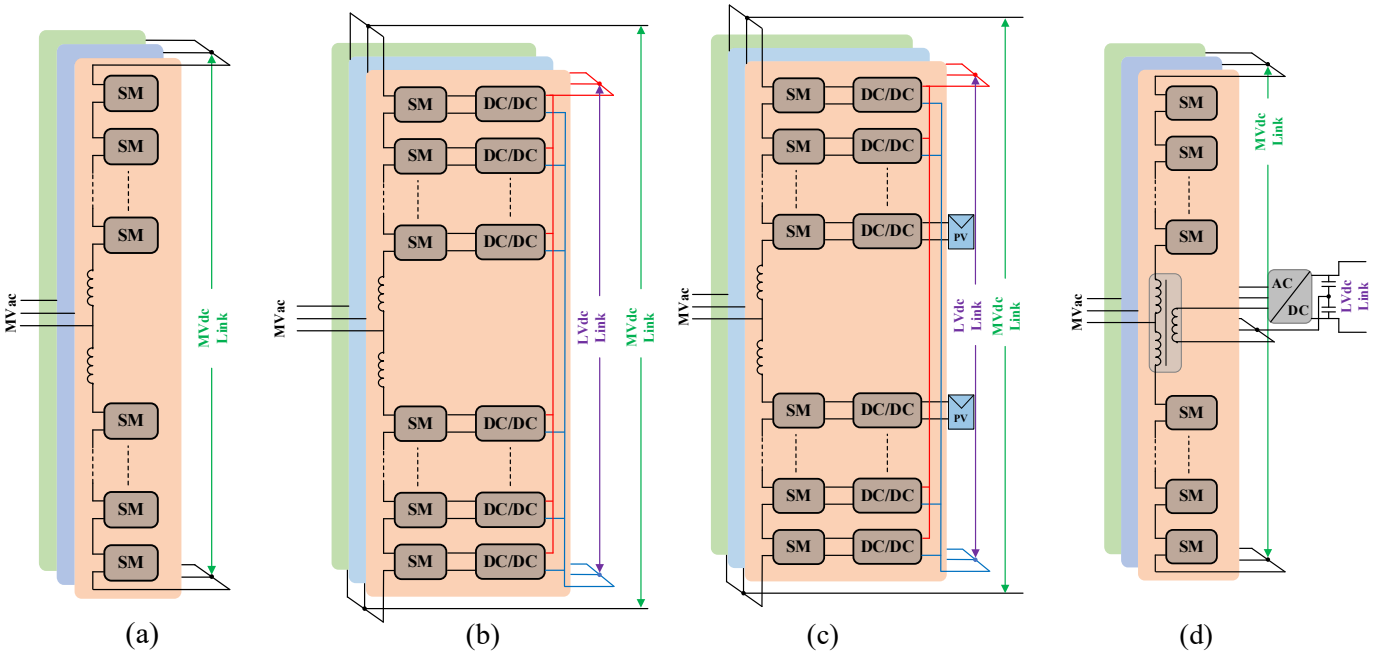

Fig. 3.3.3. MMC-based ac-dc converters, (a) Basic three-phase MMC, (b) MMC with integrated common output isolated dc-dc converters to SMs, (c) MMC with integrated isolated dc-dc converter to SMs, (d) MMC with the integrated transformer in legs.

Alternative configuration is illustrated in Fig. 3.3.3(b). In this topology, the capacitors of the submodules are linked to dc-dc converters arranged in parallel on the output side. This design still provides an MVdc link similar to the fundamental topology, shown in Fig. 3.3.3(a). Each dc-dc converter is individually controlled, allowing some to be connected to other dc sources like battery energy storage systems (BESS) or PV systems, as represented in Fig. 3.3.3(c). Given their controllability, efficiency, and isolation capabilities, dual active bridges (DAB) emerge as viable options for these intermediate dc-dc converters.

Yet another approach to employing MMC in hybrid grids involves the integration of a medium frequency (MF) transformer within the leg of MMC, as presented in Fig. 3.3.3(d). This design benefited from galvanic isolation and coupling between the grid and the low-voltage side. Nonetheless, the efficiency rates documented for this setup are not as high. Moreover, MF transformers can introduce complications in SST control, especially under abnormal conditions.

The configurations presented in Fig. 3.3.3(b)-(d) are capable of generating multiple dc buses at both MV and LV levels. A qualitative comparison of these configurations has been conducted, with results displayed in Fig. 3.3.4. The comparison shows that the basic MMC design has optimal implementation attributes, such as lower overall cost, fewer switching devices, and simpler control and implementation. However, other structures offer the advantage of allowing multiple dc links at the expense of increased system complexity and higher cost.

Given that the MMC has been recognized as a suitable solution for the MV side of the ST, emphasis on extending of the lifetime of MMC to enhance its economic viability becomes an important area of focus. The MMC is known for its scalability across varied power levels and its high controllability. It can also attain high efficiencies when utilizing low-frequency switching techniques like the nearest level modulation (NLM). However, implementing NLM requires capacitor voltage balancing algorithms. This often results in unbalanced loading for the power semiconductors and capacitors across the submodules (SMs). While NLC combined with capacitor voltage balancing achieves satisfactory thermal balance among the SMs, its performance under low power factor conditions, such as during low-voltage fault ride-through or reactive power injections, reduces the effectiveness of the standard MMC capacitor voltage balancing approach. Consequently, to maintain a similar thermal stress distribution across different SMs and to maintain equal capacitor losses within the SMs, a new balancing method is suggested. This method balances the junction temperature of switches and capacitor losses and is intended to complement the traditional capacitor voltage balancing technique.

The efficiency and lifetime of the converter are closely related to the junction temperature of the switches. However, the direct measurement of the junction temperature is not economically feasible. In addition, given the large number of switches, direct measurement of the junction temperature, even if considered feasible, is a complex and costly challenge. A more cost-effective approach to obtain the junction temperature of the switches is employing of model-based techniques, utilizing only the case temperature measurements and thermal characteristic data extracted from datasheets. For this purpose, the Foster model for the IGBT, as depicted in Fig. 3.3.5, is used.

Additionally, the power losses in the capacitor of SMs are calculated. The losses on the capacitors are determined by value of ESR of the capacitors and the current flowing through them. The number of SMs to be inserted or bypassed is obtained from the NLM and relying on the measured capacitor voltages and the current direction, decisions are made on the order of inserting or bypassing the SMs. However, in the proposed method, an additional stage has been integrated into the control system. In this improved approach, the decision of inserting or bypassing a capacitor is not merely determined by its voltage. Considerations are extended to include the semiconductor junction temperature and the losses of the capacitors. To realize the goal of balancing the voltage of capacitor, junction temperature of switches and losses of the capacitors, a cost function has been defined during the balancing stages, including the mentioned factors. Each of these elements is attributed a weight, indicating its priority in the overall assessment.

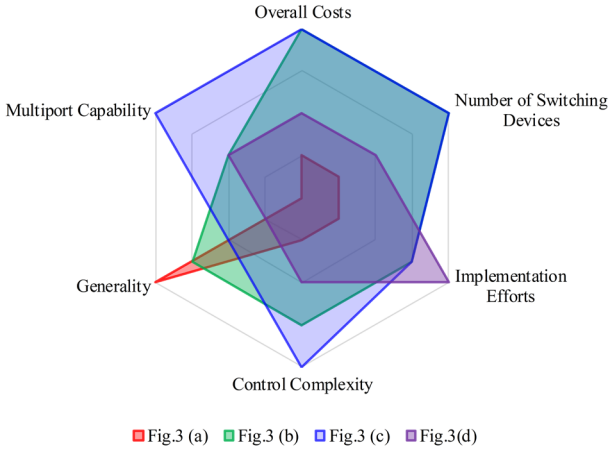

Fig. 3.3.4. Qualitative comparison of MMC-based ac-dc converters.

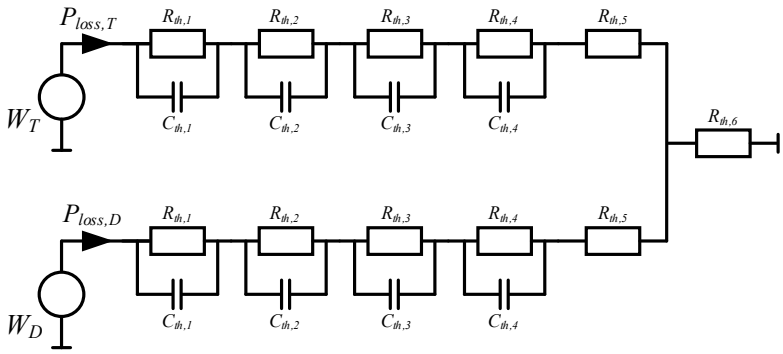

Fig. 3.3.5. Foster model for IGBT module and cooling system

To evaluate the feasibility of the suggested approach, a simulation is conducted on a three-phase MMC consisting of 20 SMs in each arm and 120 SMs in total. In this simulation model, the suggested method is integrated into the balancing stage. Then, the performance of the model and the effectiveness of the proposed balancing method are evaluated both before and after the application of this method.

The ac side voltage of the MMC is shown in Fig. 3.3.6. The capacitor voltages within an arm of the MMC are shown in Fig. 3.3.7. As can be seen in Fig. 3.3.7, a balance of capacitor voltages is maintained even when multiple factors are considered simultaneously.

In Fig. 3.3.8., the junction temperature of the switches in one arm is demonstrated. Fig. 3.3.8(a) shows the junction temperatures of the transistor and diode of upper switches (Tj,T1 and Tj,D1) and the transistor and diode of lower switches (Tj,T2 and Tj,D2) of the jth SM. In Fig. 3.3.8(b), same temperatures are demonstrated after the applying the new balancing method. Fig. 3.3.8(b) demonstrate the effectiveness of the proposed method in balancing the junction temperature and reducing the maximum temperature of the switches. Both can contribute to increasing the lifetime of the switches.

In addition, the suggested method is helpful in balancing the losses of the capacitor, which is helpful in reducing the temperature and increasing the lifetime of the capacitors. The normalized capacitor losses before and after the balancing method for one leg are presented in Fig. 3.3.9(a) and (b), respectively.

The final step is to validate the obtained simulation results with an experimental prototype. The testing of a power converter with a large number of semiconductors is significantly expensive and complex. In order to solve this problem, a test bench can be used to evaluate the effects of the proposed method. Since the temperature of a switch is fundamentally linked to the switching and conduction losses, it is anticipated that maintaining a similar switching profile and current flow through the switches would result in the same thermal behavior of the switch as in a full converter. Within the test bench setup, the switching commands derived from the simulation module of the entire MMC are applied to a half-bridge designated as the Device Under Test (DUT). Simultaneously, the current flowing through the IGBT is regulated by the other side of the test bench acting as current controller (CC). Currently, the test bench is in a critical evaluation phase. Utilizing the knowledge gained in the FPGA, which is instrumental in monitoring and controlling the operation of both the DUT and the CC, the test bench has reached operational status. Moving forward, it is imperative to examine various scenarios under different conditions and carefully observe their respective thermal behaviors. This process is critical to fostering a comprehensive understanding and facilitating further advancements in the study.

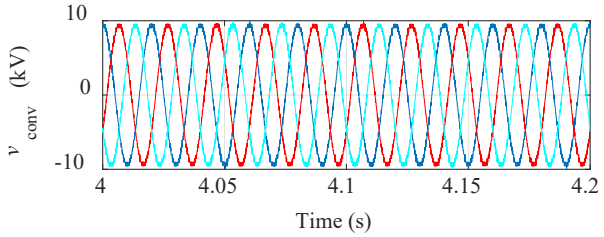

Fig. 3.3.6. Generated voltages in the ac side of the MMC

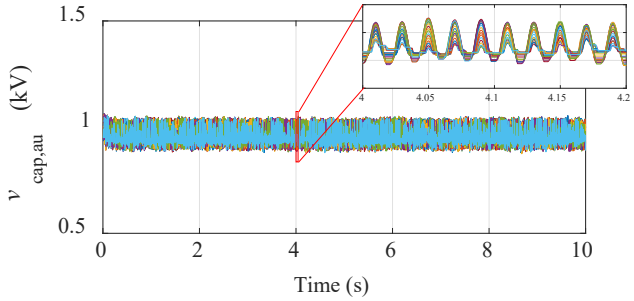

Fig. 3.3.7. Voltages of capacitors in the upper arm of phase a

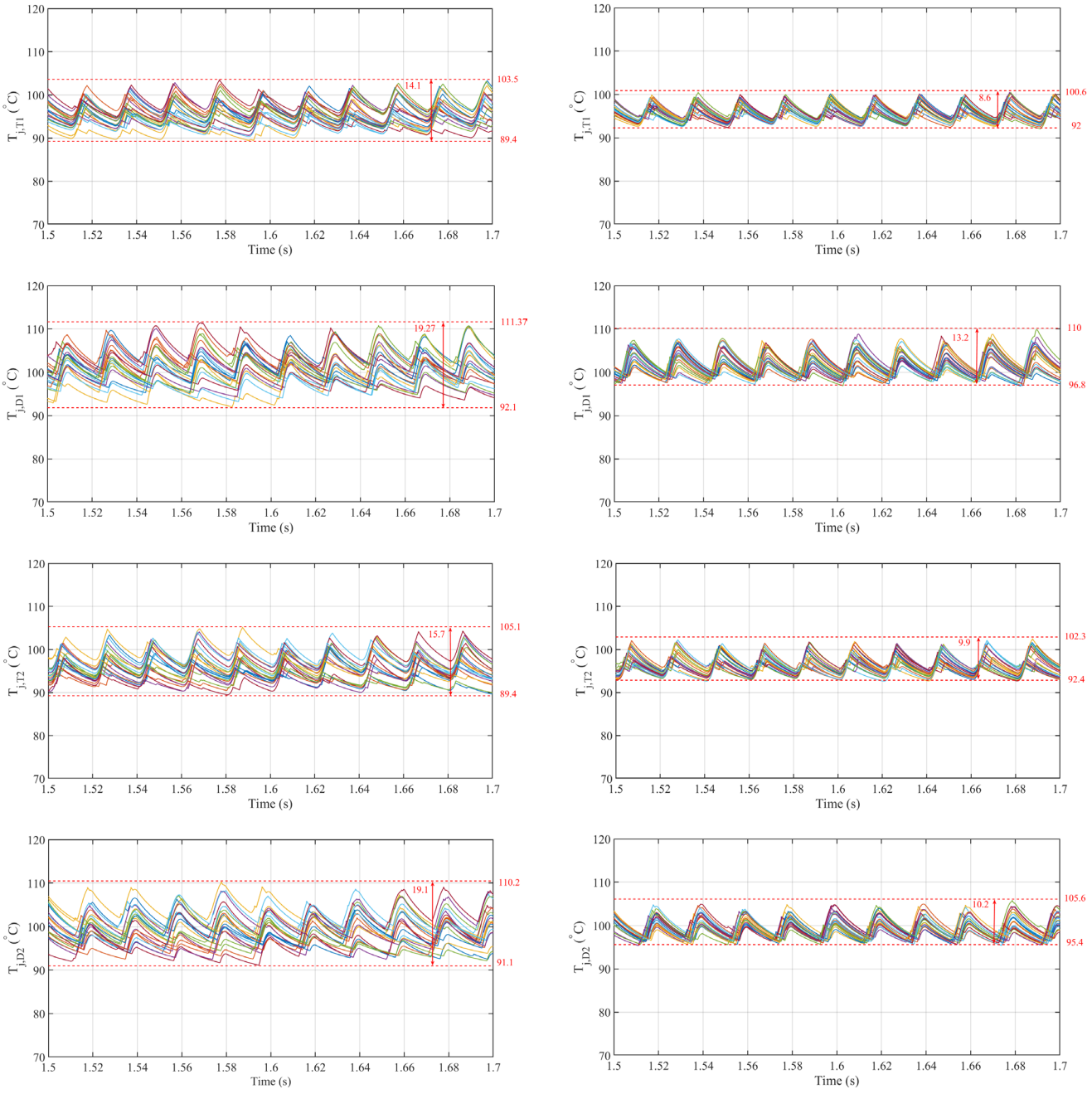

(a) (b)

Fig. 3.3.8. Junction temperatures of the switches in the (a) conventional balancing method, and (b) proposed balancing method

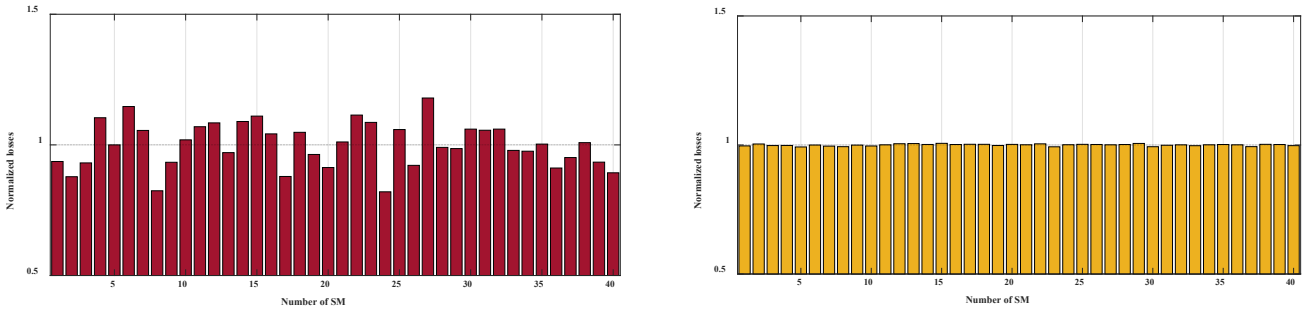

(a) (b)

Fig. 3.3.9. The normalized capacitor losses in (a) conventional balancing method and (b) new balancing approach

3.3.3.Contribution to the WP objectives

So far, the project has been on target. Literature reviews, theoretical studies and simulations were conducted to understand the concept of smart transformer and modular multilevel converter (MMC) as an important part of the topology. ST can act as a system to control the hybrid grids. Also, it can provide the infrastructure to integrate new loads and sources.

As for the contribution to the WP objectives, it should be mentioned, that work that was done in the framework of the IRP are corresponds with the acheivements of the following WP objectives:

i. To design converters and strategies to control microgrids (as optimal operational parts of distribution grids) to manage energy flows and minimize transportation losses.
ii. To coordinate the production of different generators with the consumption of different consumers to match generation and consumption in a safety and optimize way.

3.3.4. Scientific achievements

Experimental prototypes

#	Name	Description	Status (designed, assembled, tested)	Photo
1	Interface of the ZYNQ board	This board is used as an interface between ZYNQ board and the converter.	Redesigned	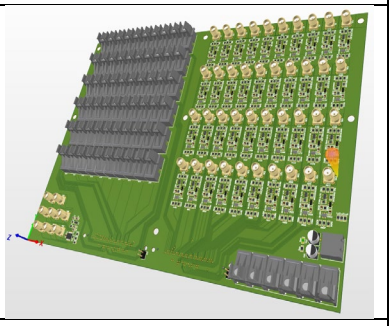

Publication

#	Title, incl. citation information	Type (Conference, journal, book chapter)	Status (Submitted, accepted, published)	DOI
1	Modular Multilevel Converters Enabling Multibus DC Distribution	Conference paper	published	10.1109/CPE-POWERENG58103.2023.10227452

3.4. Task 3.4 – IRP8 "Real-time modelling and validation of Distributed Energy Storage Systems and Integration strategies"

3.4.1. Introduction

The research work has been conducted in the Energy Lab 2.0 at the Institute for Technical Physics at the Karlsruhe Institute of Technology during the period from April 2022 to August 2023. The research has been focused on DC networks to underline their main features and their potential to be one of the main actors of the future energy transformation. In particular, some different aspect has been dealt with in this first period. First of all, the comparison between an isolated and a non-isolated topology in terms of efficiency and short circuit behaviour [1]. Moreover, the modeling of a dual active bridge converter through different integration techniques has been done to understand their impact on the accuracy of power electronic simulations [2]. Finally, a comprehensive review of DC fast charging stations as been done, considering standards, isolation, kind of microgrid architecture, voltage and power levels, battery energy storage systems and power converters [3].

3.4.2.Scientific outcomes

In former years environmental impact of fossil fuels brought to an increasing use of renewable energy resources (RES). However, directly connection of RESs and distributed generators (DGs) in general can bring to problems in terms of voltage deviation and protection issues, congestion of transmission lines and reduction of generators used to keep the desired grid frequency [1], [2], [3], [4].
In order to find a solution to these issues the concept of microgrid was invented [5]. The increasing spread of power electronics in the electrical domain leads to consider DC for microgrids. In fact, DC microgrids have a series of advantages compared to AC microgrids. First of all, they have a less number of conversion stages, which makes them less complex and more efficient compared to AC microgrids. An AC microgrid does not require a rectification stage from the upper grid, but it needs an AC/DC conversion stage for every load and DG connected to it. On the other side, DC microgrids have an initial rectification stage from the upper grid but they do not require extra AC/DC conversion stages. Moreover, they are more suitable to interface DGs, such as photovoltaic panels, fuel cells, wind turbine and microgas turbines. DC microgrids do not even have any frequency issue and skin effects does not appear in DC, which allows to make the cables smaller and to reduce the costs. In order to prove the higher efficiency and reliability, the first experimental DC microgrid was developed by Ito *et al*. in 2004, with a power of 10 kW [6].

Despite these advantages, DC microgrids also present some challenges that researchers have been facing during the last years. The most important problem is related to the protections. In fact, whenever a fault occurs in DC microgrids, the fault current can reach up to 100 times the nominal current of the system in few milliseconds and protection devices cannot be developed based on the natural zero crossing point like in AC microgrids, because it does not exist in DC microgrids. For this reason, protection devices are more complex and expensive in DC rather than in AC microgrids. A second problem is related to the transition from AC to DC infrastructure, which could take some years and large investments. Finally, power quality is another problem that must be faced in DC microgrids. Even though theoretically in DC there is no reactive power, the grid to which the DC microgrid is connected and the power converters inside the DC microgrid itself can introduce harmonic issues [1], [3].

An example of DC microgrids is represented by telecom networks. Initially developed with a 48 V DC bus, research is studying how to improve their efficiency increasing the DC bus voltage up to 380 or 400 V [7], [8]. Other examples of DC microgrids are DC buildings and data centers [9], [10], [11], industrial and ship networks [12], more electric aircrafts [13], electrification of rural areas [14], [15] and DC fast charging stations. In particular, research and development has grown in the last years in the area of DC fast charging stations. The reason behind this technology is the necessity to reduce the charging time of electric vehicles, making them comparable to combustion engine cars, in such a way to reduce the fear of costumers in the event of a long trip [16], [17]. For this reason, DC fast charging stations have be taken as test case of this research.

This chapter has been made by putting together the conference papers done during the first reporting period [18], [19], [20] into an homogeneous structure. To start with, this section covers DC fast charging stations, considering their standards, features, architecture, and power conversion technology [18]. Then, a comparison between an isolated DC-DC converter, the dual active bridge (DAB), and non-isolated one, the four-switch buck-boost (FSBB) is reported [19]. These two converters have been developed for an AC charging application, but they can be easily extended to DC fast charging. Finally, the modelling of a DAB converter has been reported [20] since modelling is an

important part of power electronic simulations. The modelling of such a converter has been taken under different integration methods to compare their accuracy and computational time.

DC Fast Charging of Electric Vehicles: Main Standards and Architectural Features

The need for reduction of the pollution generated by internal combustion engines (ICEs) has brought to an expansion of the EV market and, as consequence, also to an increased number of charging stations and to the development of new technologies for fast charging. The latter is meant to face the problem of many customers who do not have charging stations at home or relatively close to their home, and that cannot wait for hours to recharge their vehicles. DC fast charging stations can make in this way EVs more appealing for a larger number of customers. Moreover, they can also allow long distance trips, which are not possible without a solid network of fast charging stations [21], [17], [22].

EV charging standards are different and have different classifications based on the country and/or continent. To simplify the explanation EV charging standards will be divided in AC charging standards and DC charging standards. Understanding the AC charging standards allows to understand the reason of the need of DC fast charging. To start with, the SAE J1172 standard is adopted in North America, Japan, and South Korea. It has two level of AC charging, respectively level 1, with a maximum charging power of 1.9 kW, and level 2, which a maximum charging power of 19.2 kW. IEC 61851 is instead the AC charging standard adopted in Europe. It is divided in 3 modes: mode 1 enables a maximum charging power of 13.3 kW, whereas mode 2 and 3 enables up top 22 kW of charging power. GB/T is the AC charging standard adopted in China and India, which provides up to 12.8 kW of charging power. The charging standard developed by Tesla and now open to all the other companies is known as north American charging standard (NACS) and it allows up to 11.5 kW of charging power [23].

Now that the overview about AC charging standards has been provided, it results clear that it is not possible to reach power ratings higher than 22 kW with AC charging. For this reason, DC charging is needed to provide charging power in the range of 50-400 kW. To start with, CHAdeMO provides is spread all over the world with a charging power of 400 kW. GB/T standard also offer DC fast charging with a maximum power transfer of 237.5 kW. CCS Type 1 is adopted in North America and South Korea and it offers a maximum power transfer of 350 kW. CCS Type 2 also offers a maximum power transfer of 350 kW but it is used in Europe and Australia. Finally, NACS is also adopted for DC charging and it reaches a maximum power of 350 kW [17]. Furthermore, ChaoJi is a new standard resulting from the collaboration between the CHAdeMO association and the China Electricity Council. It is compatible with CHAdeMO, GB/T and maybe in future with CSS. It can reach a maximum charging power of 900 kW [24].

DC fast charging stations are typically connected into an AC microgrid, with a bus of 250-480 V line-to-line AC. This means that the MV uppergrid is connected to the AC microgrid with a MV/LV transformer. Such AC microgrid has the advantage to have well established technology, measurment and protection standards. However, the main drawback of AC microgrids is that they require a further AC/DC stage in every charging station, which decreases the efficiency of the overall system. Moreover, control in AC microgrids is complex, because it needs to keep the power factor into regulation levels. On the other side, DC microgrids just need a first rectification stage from the MV upper grid, removing the need for further AC/DC conversion stages per each charging station, which increases the efficiency of the overall system. Furthermore, control in DC microgrids is easier than in AC microgrids, because it does not have to deal with reactive power. Despite these advantages, the main drawback of DC microgrids is that there is no protection coordination standard, even though DC protection devices already exist. Another disadvantage is that there is no standard about accuracy and calibration of DC meters. Hence, DC protections and meters are challenges that companies and research institutes need to face in order to widespread the use of DC microgrids for DC fast charging station systems [17], [21], [24]. The difference between AC connected fast charging systems and DC connected fast charging systems is shown in Fig. 3.4.1.

DC fast charging stations are currently available on the market with a power range from 30 to 400 kW. The output voltage is instead between 50 and 950 V, whereas the output current varies between 31.5 and 500 A. Due to the lack of protection and metering standards, most of them have been designed to be connected to the AC grid. Tritium PKM150 is instead an example of DC fast charging station designed to be connected to a DC microgrid. Its augmented efficiency compared to most of the other DC fast charging stations proves that the DC microgrid concept will play a key role in the future of EVs charging.

Due to their high power transfer, DC fast charging stations might require an upgrade of the existing grid infrastructure. This might happen especially in the countryside and highways, where DC fast charging stations are demanded for long-distance trips. In order to reduce grid reinforcement costs, it is possible to use energy storage systems (ESSs). ESSs can also help to reduce operational costs due to demand charges because they can be charged at low power compared to the power of DC fast charging stations. Moreover, ESS can be used to connect RESs with EV fast charging stations, which is a step forward toward the green energy transition [25].

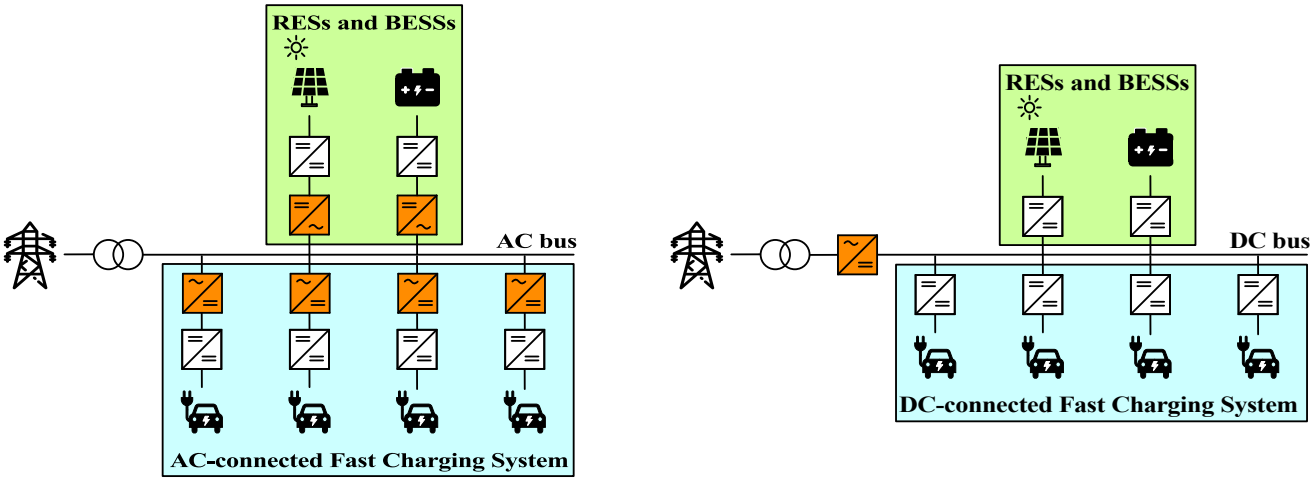

(a) (b)

Fig. 3.4.1: DC fast charging infrastructure. (a) AC-connected fast charging system. (b) DC-connected fast charging system.

An important point to consider when designing DC fast charging stations is to provide isolation from the AC grid, in such a way as to avoid the propagation of a fault. The alternatives to reach this goal are to use a low-frequency transformer before the rectification stage or to use isolated DC-DC converters made of high-frequency transformers. The advantage of high-frequency transformers is that they are smaller and cheaper compared to low-frequency ones. Moreover, a low-frequency transformer can be seen as a single point of failure for the system and if it is damaged it is not possible to use any charging station connected to it. Furthermore, an architecture with a low-frequency transformer limits the operating switching frequency and makes the size and costs of the passive filters higher. On the other hand, high-frequency transformers influence soft-switching conditions and particular attention must be taken in their design [26].

DC Fast Charging of Electric Vehicles: Power Conversion Technology

Power electronics is the technology that enables the power transfer capability of EV charging stations. In particular, DC fast charging stations are made of two power conversion stages, respectively AC-DC and DC-DC. For this reason, this section aims to review the main AC-DC and DC-DC converters used in DC fast charging applications.

AC-DC converters

The three-phase PWM rectifier is a boost-type bidirectional topology made of three half-bridges, each of them with two switching devices, typically IGBTs or MOSFETs [27]. This topology enables unity power factor and low total harmonic distortion (THD) thanks to its high controllability and capability to decouple active and reactive power. This topology is commonly preferred over the traditional diode rectifier, which is not considered a suitable choice for DC fast charging stations because of its high input harmonic content. So, the diode rectifier absorbs reactive power from the grid, which cannot be mitigated due to the lack of controllable switches. This phenomenon reduces the efficiency and deteriorates the grid voltage, which would represent a big issue because of the increasing spread of EVs and EV charging stations [28]. The three-phase PWM rectifier is shown in Fig. 3.4.2a.

The neutral-point-clamped (NPC) rectifier is another boost-type AC-DC converter suitable for DC fast charging stations. In comparison to the three-phase PWM rectifier, it has two additional switches and two diodes per each leg, used to clamp the output voltage to the neutral point voltage. This topology has some advantages compared to the three-phase PWM rectifier. To start with, the voltage on the switching devices is only half of the DC-bus voltage. This

means that there is less stress on the switching devices and that this topology has a double power rating than a three-phase PWM rectifier. Moreover, the THD of the NPC topology is lower than the one of the three-phase PWM rectifier. Yet, this topology allows the creation of a bipolar DC-bus. However, the presence of a bipolar DC-bus implies the need to balance the voltage of the neutral point through a proper control technique and/or additional balancing circuitry in case of load differences. So, the need for voltage balancing and the increased number of switches make the NPC rectifier control more complex than the three-phase PWM rectifier one [29], [30]. The NPC rectifier is shown in Fig. 3.4.2b.

The Vienna rectifier is a unidirectional topology made of a diode rectifier and three bidirectional switches. This topology provides very low THD, high power density, and high efficiency. Moreover, the switching devices are affected only by half the blocking voltage stress, because of the neutral point as in the NPC converter [31], [32], [33]. The bidirectional version of this topology is the t-type converter, which substitutes the diode bridge with a three-phase PWM rectifier. The t-type converter keeps the advantages of the Vienna rectifier and allows the vehicle-to-x (V2X) operation mode, making it a suitable candidate for DC fast chargers of EVs [34]. The Vienna rectifier and t-type converter are shown respectively in Fig. 3.4.2c and Fig. 3.4.2d.

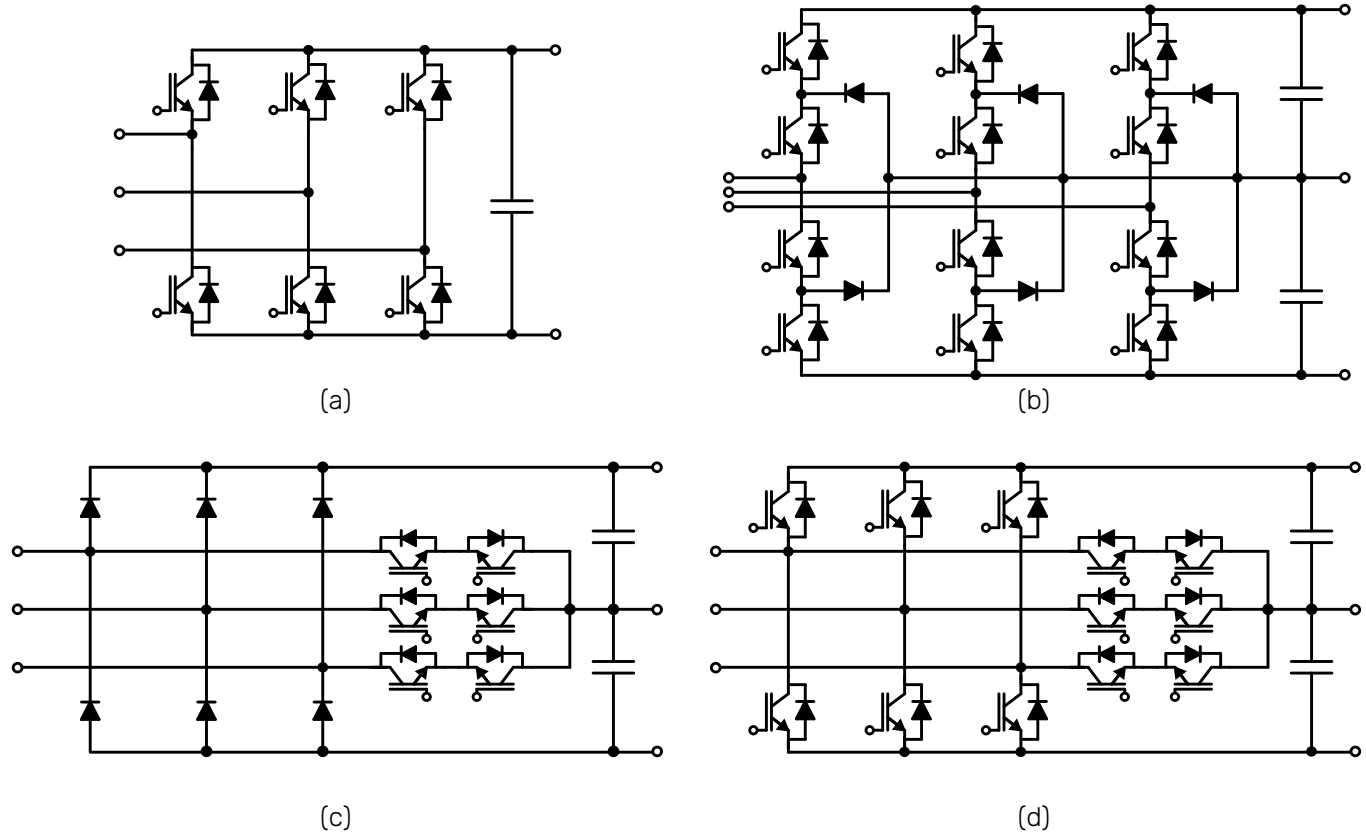

Fig. 3.4.2: AC-DC power converters. (a) Three-phase PWM rectifier. (b) Neutral-point-clamped rectifier. (c) Vienna rectifier. (d) T-type converter.

DC-DC Converters

The phase-shift full-bridge (PSFB) is a unidirectional topology suitable for high-power and high-voltage applications such as DC fast charging stations [35], [36]. This converter is an isolated topology, and it is made of a high-frequency transformer, a full bridge on the first side, and a diode bridge on the second side. The leakage inductance of the transformer enables the zero-voltage switching (ZVS) condition on the turn-on state of the switching devices. However, ZVS cannot be reached for low load currents because the ZVS condition of this topology is that the energy stored in the leakage inductance must be greater than the one stored in the output capacitance \cite{sabate1990design}. The PSFB is shown in Fig. 3.4.3a.

The dual active bridge (DAB) is a well-known bidirectional topology, used in many applications, such as microgrids, aerospace, battery interface, and automotive, especially as on/off-board battery charger for EVs. In addition to its bidirectional power flow, this topology is appealing because of its galvanic isolation, high power density, high voltage

gain, and capability to perform soft-switching through proper modulation techniques. The DAB is made of two full bridges, connected through an isolation transformer. The series inductance of the transformer is designed to establish the power transfer of the converter itself [37], [38], [39]. The DAB is shown in Fig. 3.4.3b.

Series resonant converters (SRCs) are a family of converters identified by a high-frequency transformer to guarantee galvanic isolation, and a series resonant tank made of an inductor and a capacitor. The first side can be a half-bridge, full-bridge, or even a multilevel half/full-bridge. The second side is a diode bridge in case of unidirectional topologies or typically equal to the first side in case of bidirectional topologies [40]. The switching frequency of these converters can be chosen as the same, higher, or lower than the resonant frequency. However, it is recommended to choose the switching frequency equal to, or slightly above the resonant frequency to reach the soft-switching conditions [40]. In addition to their soft-switching capability, SRCs are also chosen for their fault-tolerance feature [41]. These features make these converters appealing for DC fast charging applications [42]. A unidirectional SRC and a bidirectional one are shown respectively in Fig. 3.4.3c and Fig. 3.4.3d.

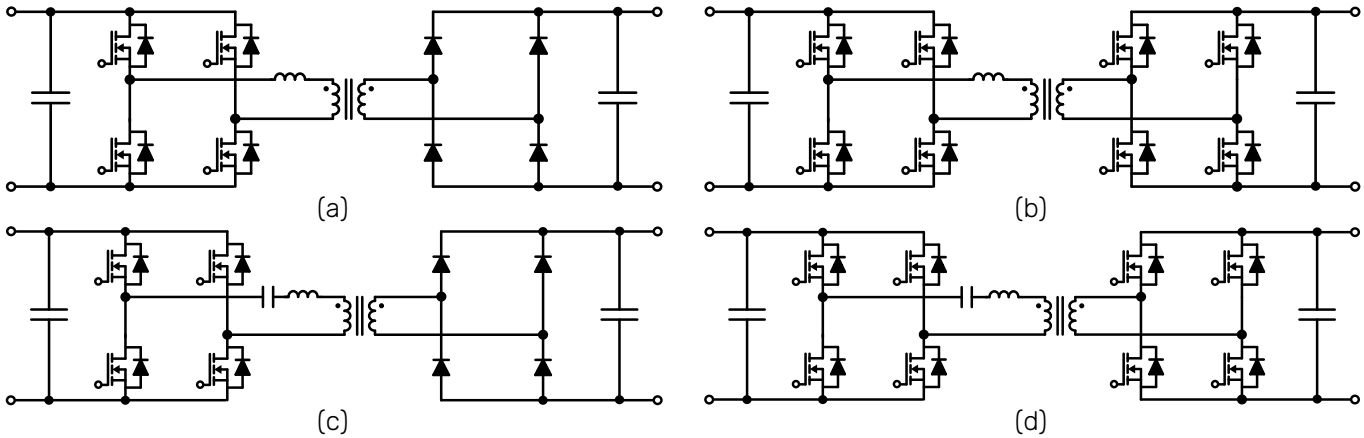

Fig. 3.4.3: DC-DC power converters. (a) Phase-shift full-bridge. (b) Dual active bridge. (c) Unidirectional series resonant converter. (d) Bidirectional series resonant converter.

Examples of DC Fast Charging Systems

Now that the main converter topologies used in DC fast charging stations have been discussed, it is possible to introduce some DC fast charging systems that have been proposed in literature.

A 50 kW DC fast charger made of a three-phase PWM rectifier and a three-phase DAB has been proposed in [43]. The fast charger is connected to a 400 V three-phase grid, which is converted by the three-phase PWM rectifier in 700 V DC. The battery voltage is expected instead to be between 250 V and 400 V. This system reaches a power density of 50~kW/L and an efficiency of 95 %, which is quite good compared to the commercial solutions.

[44] has proposed a 150 kW DC fast charger based on modular three-phase interleaved converters. Both AC-DC and DC-DC power stages are made of three modules of three-phase PWM converters and each of them is rated at 50 kW. The difference between the AC-DC and DC-DC stages is that in the AC-DC stage, each module is connected to a grid phase, whereas in the DC-DC stage, the modules are connected in parallel. Moreover, the charger is connected to a 400 V three-phase grid and the DC-link voltage is rated at 700 V. Furthermore, the authors have implemented a control strategy able to significantly reduce the output current ripple. Finally, an experimental prototype of the DC-DC stage has been developed, with a reduced DC-link of 150-200 V and a maximum current of 30 A.

[45] has proposed a DC-connected fast charging system with NPC converter and three-level non-isolated DC-DC converters, in which the isolation is provided by a low-frequency transformer. The NPC converter has been chosen because of its high voltage and power ratings, very low THD, and bipolar DC-bus. Moreover, the three-level non-isolated DC-DC converter has been chosen because of its bipolar input, which allows a direct connection with the bipolar bus generated by the NPC. Since this DC-DC topology is non-isolated, a low-frequency transformer has been chosen to isolate the grid from the DC-connected fast charging system. The drawback of this architecture is the voltage balance of the DC-bus. For this reason, the authors propose a comparison between the voltage balance control of the NPC and the coordinated voltage balance control of the three-level DC-DC converters. The results

have been verified in simulation on a 240 kW system with a total 1600 V DC-bus and on a 1.2 kW prototype composed by an NPC and a three-level non-isolated DC-DC converter with a total 110 V DC-bus.

[34] has implemented a fast charger with a split storage battery to decrease the stress on the switching devices and increase the efficiency of the DC-DC converter interfacing with the vehicle battery. In this case, the grid interface is made of a t-type inverter and a three-port DAB, which is connected to two batteries of 400 V and 200 V respectively, and total power of 20 kWh. Moreover, the grid interface is connected to a 400 V three-phase grid. Since the split storage battery does not need a high charging rate, the grid interface is rated at 20 kW, whereas its estimated efficiency is 98.1 %.
Finally, a multi-phase interleaved converter of 6 modules has been chosen as the DC-DC power stage connected to the vehicle battery because of its low losses, high efficiency, soft-switching capability, and small output current ripple. Its power rating is 220 kW, and its estimated efficiency is 99.57 %. The drawback of this architecture is that it leads to an unequally stressed storage system, because of their different connection with the vehicle battery.

[46] has proposed a DC-connected fast charging system of 6 DC fast chargers, each rated at 350 kW. A cascaded H-bridge (CHB) and a DAB-based solid-state transformer (SST) configuration have been used as an interface with an MV grid, whereas phase-shift full-bridge-based partial power converters have been used as DC-DC stages. Moreover, a battery energy storage system is connected to the DC-bus in the proposed configuration. Partial power converters process only part of the power, whereas a direct infeed path transfers the bulk power to the EV battery. For this reason, they enable increased system efficiency and can be rated just for part of the full power. Furthermore, the authors implemented a partial power converter showing a 0.6 % efficiency increase at the full-load condition and 1.6 % efficiency increase at 50 % load condition compared to a full power converter. Moreover, this converter has been designed just for 27 % of the rated power, which is 3.2 kW. This means that not only is the partial power converter able to increase efficiency but also to reduce design costs. The DC-link of this setup is 300 V, whereas the EV battery voltage is between 360 V and 400 V.

[47] has analyzed an infrastructure of DC fast charging stations based on the modular multilevel converter (MMC) and connected to the MV grid. An SST connected to the charging poles has been compared to a direct connection of an MMC. Moreover, half-bridge and full-bridge submodules have been compared. The authors suggest the use of the DAB converter as the DC-DC submodule, for both SST-based connection and direct connection. Hence, DAB submodules are connected in an input-series-output-parallel configuration.
In order to evaluate this infrastructure, a 400 kW prototype of MMC connected to a 3 kV grid has been developed, showing a 98.2 % efficiency with half-bridge submodules and 97.4 % efficiency with full-bridge submodules. However, authors suggest full-bridge submodules as the best choice because they also consider simplicity, reliability, and compactness as decisional parameters. In particular, the authors suggest a full-bridge-based direct connection in case of a low number of charging poles and a full-bridge-based SST solution in case of a high number of charging poles. Furthermore, a DC-DC stage based on DAB submodules has been implemented, reaching an efficiency close to 99 %.

Table 3.4.1 summarizes the comparison between the discussed examples of architecture.

TABLE 3.4.1: Comparison of different DC Fast Charging Systems.

Reference	Grid voltage	Bus type	DC-link voltage	Type of isolation	AC interface stages	Power rating	BESS
[62]	400 V ph-ph	-	700 V	High-frequency transformer	1	50 kW	No
[63]	400 V ph-ph	-	700 V	-	1	150 kW	No
[64]	-	DC bipolar	1600 V	Low-frequency transformer	1	240 kW	Yes
[52]	400 V ph-ph	DC bipolar	600 V	High-frequency transformer	2	220 kW	Yes
[65]	-	DC unipolar	650 V	High-frequency transformer	2	350 kW	Yes
[66]	10 kV ph-ph	None or DC unipolar	6 kV	High-frequency transformer	1 or 2	400 kW	No

Four-Switch Buck-Boost and Dual Active Bridge Converters.

The working principle of the four-switch buck-boost and dual active bridge converters will be explained in this paragraph to have a comparison between an isolated and a non-isolated topology. The comparison was originally made for an AC charging application but the converter topologies can be rated for higher power to match DC fast charging applications.

Four-Switch Buck-Boost

The idealized circuit diagram of a Four-Switch bidirectional Buck-Boost converter is shown in Fig. 3.4.4a. It is a non-isolated converter which benefits from a low number of switching elements and a simple design and control.
With D_1 as the duty cycle of S_1 (while $S_2 = \overline{S_1}$) and D_2 as the duty cycle of S_4 (while $S_3 = \overline{S_4}$) the voltage gain of the FSBB can be expressed with [48]:

$$\frac{V_{DC2}}{V_{DC1}} = \frac{D_1}{1 - D_2} \tag{1}$$

The FSBB can be used in buck, boost, or buck-boost mode. From the ratio (1) it can be derived that if D_2 tends to zero the FSBB gets Buck property, whereas it gets Boost property for D_1 tending to zero. In this paper, the FSBB is used in Buck and boost modes by respectively setting $\mathrm{D}_2 = 0$ and $\mathrm{D}_1 = 1$.
It allows also a current flow directly from one side to the other by simultaneously setting $\mathrm{D}_1 = 1$ and $\mathrm{D}_2 = 0$.

Dual Active Bridge

DAB is one of the most widespread converters in DC microgrids and automotive applications. Even though it was firstly proposed in the early 1990s [49], losses due to old technologies of power devices resulted in low efficiency. However, it gained popularity after the development of silicon carbide (SiC) and gallium-nitride (GaN) switching devices [38], making it appealing for power grid applications. The features that make this converter so appealing are the galvanic isolation, wide voltage gain range, and capability to perform soft-switching through proper modulation techniques [38], [37], [50].

As shown in Fig. 3.4.4b, the Dual Active Bridge is composed of two full bridges, connected to two voltage sources. This is a typical case of a ESSs connected to a DC grid through a medium or high frequency transformer to guarantee the galvanic isolation.
The inductor L is modeled in series to the transformer and represents the sum of the leakage inductance of the transformer and an external inductor, which is designed to achieve a certain power transfer.
The phase shift angle between the gate control signals of the two full bridges is used to regulate the power transfer of this converter, which can be described by:

$$P_{DAB} = \frac{n\, V_{DC1} V_{DC2}\, \varphi(\pi - |\varphi|))}{2\, f_s\, \pi^2 L}, \quad \forall -\pi \le \varphi \le \pi \tag{2}$$

where n is the turn ratio $\mathrm{N}_1/\mathrm{N}_2$ and f_s is the switching frequency.
The total inductance of the converter can be designed from (2) by imposing a maximum power transfer and a maximum phase shift angle.

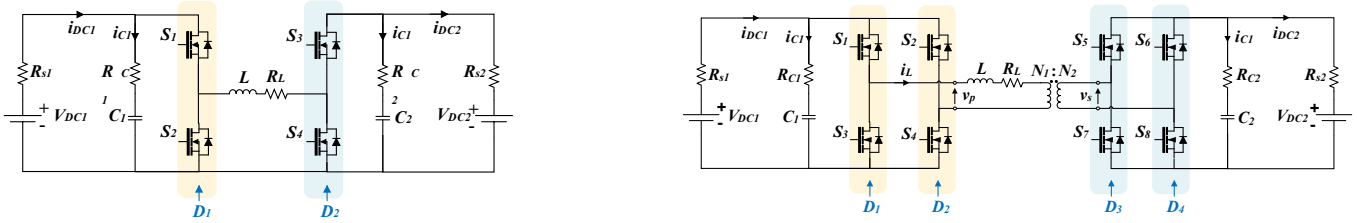

(a) (b)

Fig. 3.4.4: Converter Topology: (a) four-switch buck-boost, (b) dual active bridge

Converter Losses

In this section, the loss analysis for both converters is performed.

During the switching process of a SiC-MOSFET, energy losses occur due to the simultaneous presence of drain-source voltage and drain current. These losses are called switching losses. Due to the approximately triangular rise and fall of the drain-source voltage, the switch energy losses can be approximated by:

$$P_s = \frac{1}{2} V_{DS} I_D (t_r + t_f) f_s \tag{3}$$

where V_{DS} is the drain-source voltage and I_D is the RMS value of the drain current.
Conduction losses in switching components can be modeled with an equivalent series resistance R_{on}. Hence, the conduction losses can be calculated with:

$$P_{cond,on} = R_{on} I_D^2 \tag{4}$$

where R_{on} is the equivalent series resistance of semiconductor.
To prevent a short circuit of two series SiC-MOSFETs, a dead time t_{Dead} is used between the turn-on and the turn-off of the two switches respectively of the same leg. During this time the current forced by the inductance flows through the body diode of the low-side SiC-MOSFET. The dead time losses P_{Dead} is calculated as:

$$P_{dead} = V_{diode} I_{diode} t_{dead} f_s \tag{5}$$

where V_{diode} is the forward voltage of the diode and I_D is the RMS value of the diode current.
The inductor contributes essentially with conduction losses, converting electrical energy into heat due to the inductor resistive behavior. To represent these losses, a series DC resistance R_L has been modeled and hence calculated with:

$$P_L = R_L I_L^2 \tag{6}$$

where I_L is the RMS value of the inductor current. The capacitor losses, caused by leakage and dielectric loss, can also be modeled with an equivalent series resistance R_C and calculated in the same way as for inductor conduction loss in (6). Finally, the transformer losses for the DAB can also be modeled with a series resistance R_T, neglecting the magnetic losses. The total power loss will be modeled as a superposition of the aforementioned losses. The efficiency can thus be described according to the equation (7).

$$\eta = \frac{P_{out}}{P_{In}} = \frac{P_{out}}{P_{out} + \sum (P_s + P_{cond,on} + P_{dead}) + P_R} \tag{7}$$

where P_R is the sum of the resistor losses related to inductors, capacitors and transformer.

Short-Circuit Analysis of the Four-Switch Buck-Boost and Dual Active Bridge Converters

Four-Switch Buck-Boost

Depending on the converter type and mode, there are multiple different impacts on the DC fault characteristic. In boost mode three causes contribute to the short circuit current. The natural discharging response occurring from the capacitors, inductor forced current through the freewheeling diodes, and the input source feeding through the diodes [4].
The capacitor discharge current occurs through the RC circuit and can be written as:

$$R_{fault} \frac{di_{fault,C}(t)}{dt} + \frac{1}{C} i_{fault,C}(t) = 0 \tag{8}$$

The equation (8) can be used for Boost as well as for buck mode and also for short circuit analysis on each side.
While the boost mode has a natural response coming from the capacitors, the freewheeling diodes, and the input source feeding, the buck mode has an intrinsic immunity to the input source impacts [4], [51]. Consequently, a FSBB has the ability to prevent input source influence in case of a high voltage side short circuit.
The freewheeling current differs depending on the short circuit side. In both cases, the current can be calculated with the discharge function of a RL-circuit.

$$L\frac{di_{fault,L}(t)}{dt} + (R_L + R_{fault})i_{fault,L}(t) = 0 \quad (9)$$

Without an additional safety mechanism in boost mode operation, the fault current will increase to the system limits [4], [51]. Since a short circuit on the high voltage side will cause the voltage to zero, the FSBB will change to buck mode and consequently, it will be able to suppress the current through the converter. The short circuit behavior after switching to buck mode will also depend on the control algorithm. The investigation of control effects to short circuit behavior is not part of this paper.

Dual Active Bridge

The short circuit dynamic of the DAB has been already discussed in [52]. It can be carried on by neglecting the dynamic of the capacitor on the first side of the DAB and considering a fault resistance $\mathrm{R_{fault}}$. This results in two differential equations, of which the first one describes the inductor's current behavior:

$$\frac{di_L(t)}{dt} = \frac{V_{dc1}}{L}M_1(t) - \frac{N_1}{N_2}\frac{v_2(t)}{L}M_2(t) - \frac{R_L}{L}i_L(t). \quad (10)$$

The second one rather describes the voltage of the capacitor on the second side of the converter:

$$\frac{dv_2(t)}{dt} = \frac{N_1}{N_2}\frac{i_L(t)}{C_o}M_2(t) - \frac{v_2(t)}{R_{fault}C_o}, \quad (11)$$

where $\mathrm{M_1(t)}$ and $\mathrm{M_2(t)}$ are the modulation functions, obtained as:

$$M_1(t) = D_1(t) - D_2(t) \quad (12)$$

$$M_2(t) = D_3(t) - D_4(t) \quad (13)$$

An equivalent simplified model of DAB for first side faults can be obtained by neglecting the second side capacitor and inserting R_{fault} on the first side instead

Moreover, the steady state behaviour of this converter in the phasor domain has been investigated in [19]. Here, it is supposed that the switching devices can tolerate up to two times their rated current and after a mathematical analysis it was obtained that the inductor must be designed for a phase shift $28.96° \leq \varphi \leq 90°$.

Simulation results and Comparison

This section evaluates the short circuit performances and efficiency results for both converters by using the Matlab/Simulink environment. The specifications of the converters are reported in Tab. II and III, in which it is possible to notice that the first and secondary voltages are respectively $\mathrm{V_{DC1}} = 400$ V and $\mathrm{V_{DC2}} = 750$ V, whereas the power rating is $\mathrm{P} = 5$ kW. These power and voltage ratings are typical of home electric vehicle battery charger applications. In the following simulations, the efficiency has been evaluated from $1\,\%$ to $100\,\%$ at $1\,\%$ steps, whereas the short circuit fault has been simulated at $\mathrm{t_{fault}} = 0.1$ s.

Table 3.4.2: System specification

System Parameters			
Name	Value	Name	Value
P	$5\ kW$	C_1	$235\ \mu F$
f_{sw}	$20\ kHz$	C_2	$235\ \mu F$
V_{DC1}	$400\ V$	L_{DAB}	$177.78\ \mu H$
V_{DC2}	$750\ V$	L_{FSBB}	$5.5\ mH$

Table 3.4.3: Losses specification

Loss Parameters			
Name	Value	Name	Value
t_r	22 ns	R_{on}	$80\ m\Omega$
t_f	14 ns	R_{C1}	$0.02\ \Omega$
t_{dead}	150 ns	R_{C2}	$0.02\ \Omega$
$R_{L\ FSBB}$	$0.3\ \Omega$	$R_{L\ DAB}$	$0.03\ \Omega$

Fig. 3.4.5 shows the simulated converter efficiency as a function of output power in percentage up to 5 kW at 100 %. The FSBB achieves a peak efficiency of 98.25 % at 32 % of the maximum power considered. On the other hand, the DAB reaches a peak efficiency of 98.66 % at 73 % of the maximum power. The DAB efficiency surpasses the efficiency of the FSBB converter at
41 % of the maximum power.
A comparison of the simulated results for the converter efficiencies shows that FSBB has a higher efficiency in low power ranges, whereas DAB has a higher efficiency in high power ranges.

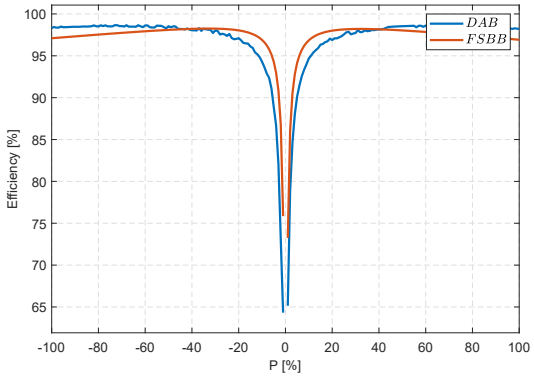

Fig. 3.4.5: Efficiency from -5 kW to $+5$ kW for DAB and FSBB

Since an FSBB converter is only meaningful in combination with a mode switching control, the following simulations are performed using a simple mode switch. Depending on the voltage level of both sides, switching between buck and boost mode is performed.
Fig. 3.4.6 shows the simulated transient behaviour of a FSBB with a short circuit fault at $t_{fault} = 0.1$ s. Fig. 3.4.6a depicts that the main contribution to the fault current is coming from the capacitor discharge current in the form of an exponential fall according to (8). In Fig. 3.4.6b a suppression of the HV side current is noticeable. For the short circuit fault on the HV side, the simulation results are illustrated in Fig. 3.4.7. It is worth highlighting that the contribution of the LV side in the case of a short circuit fault on the HV side is restricted as exposed in Fig. 3.4.7a. Unlike the conventional boost converter, the FSBB is able to suppress the fault current on the LV side in the case of a short circuit on the HV side. The short circuit fault will drop the voltage on the HV side down, which will lead to a switch of the FSBB to buck mode. The spikes in Fig. 3.4.6b and 3.4.7a result from the fact that the reference current value through the converter is 6.6 A. The control algorithm is switching the SiC-MOSFETs on to reach the reference.
The DAB converter has been designed for a maximum phase shift of $60°$ at the maximum power of 5 kW, since the maximum phase shift angle of $90°$ is usually avoided for control reasons during normal operations. The short circuit simulations have been carried out in open loop to show the ability of this converter to work during faults. The related results of LV and HV faults are shown in Fig. 3.4.8 and 3.4.9, where it is possible to notice that the main contribution of the fault current comes from the capacitor. Moreover, DAB is able to nullify its fault current contributions in milliseconds range, as shown in Fig. 3.4.8b and 3.4.9a. Further fault riding-through strategies can be used to improve DAB performances in faulty conditions, such as blocking the switching signals or adding a proper inductor on the output terminals to limit the fault current as described in [52].

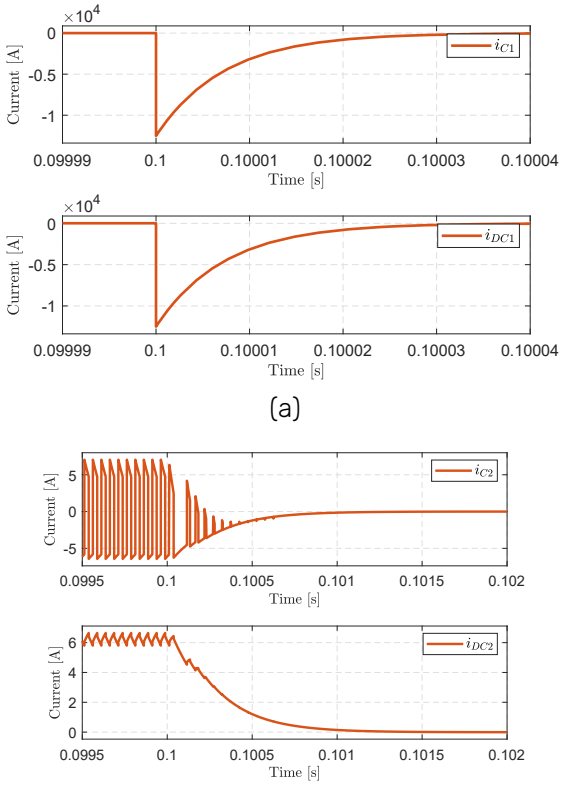

(a)

(b)

Fig. 3.4.6: Transient behavior of the FSBB during LV fault: a) LV side capacitor current and DC current, b) HV side capacitor current and DC current

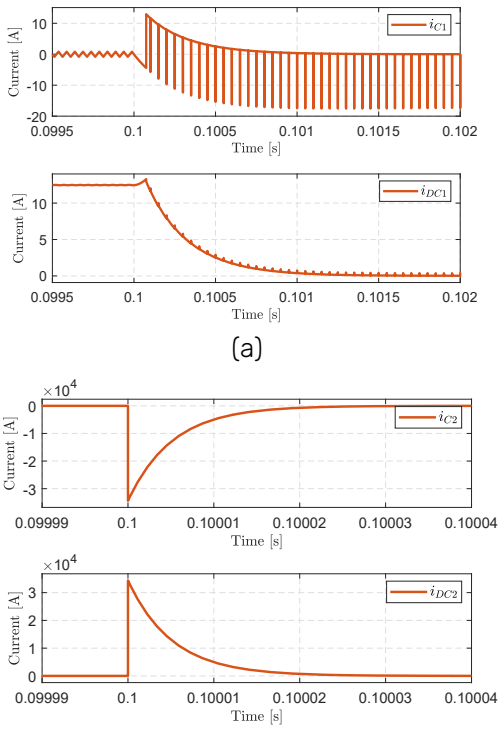

(a)

(b)

Fig. 3.4.7: Transient behavior of the FSBB during HV fault: a) LV side capacitor current and DC current, b) HV side capacitor current and DC current

Simulations show that the main contribution to the short circuit current of both converters comes from the filter capacitors. Since DC Microgrids require this kind of filters to correctly operate, it is not possible to eliminate this problem, which increases in high power applications due to the increased size of capacitors. DAB and FSBB demonstrated an inherent capability to suppress the fault current in milliseconds range for both LV and HV faults. In particular, FSBB needs a mode switch mechanism to prevent the fault current to grow exponentially, which makes this converter not robust in case of controller malfunctioning or measurement failure. On the other side, DAB is intrinsically safe even without any control strategy to bring the fault current to zero, because of the galvanic isolation provided by its transformer.

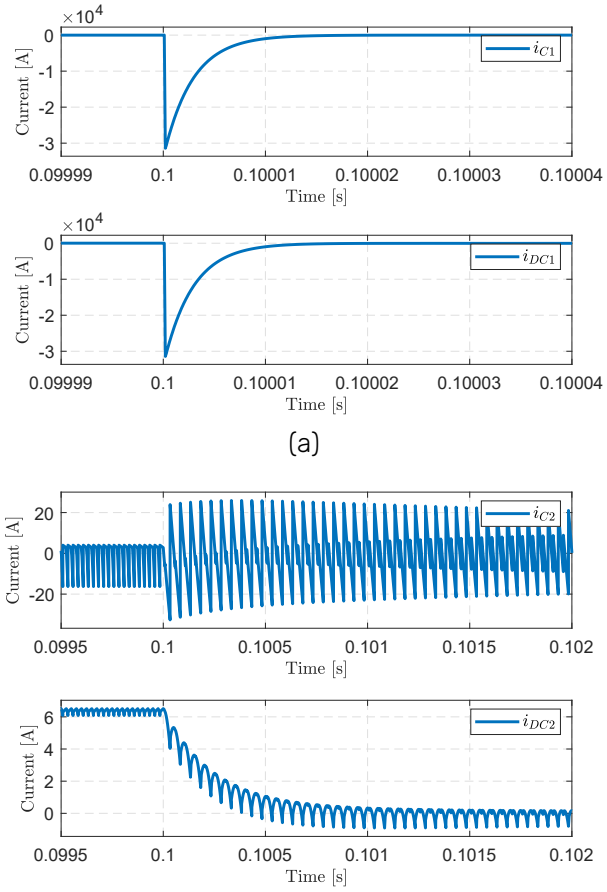

Fig. 3.4.8: Transient behavior of the DAB during LV fault: a) LV side capacitor current and DC current, b) HV side capacitor current and DC current

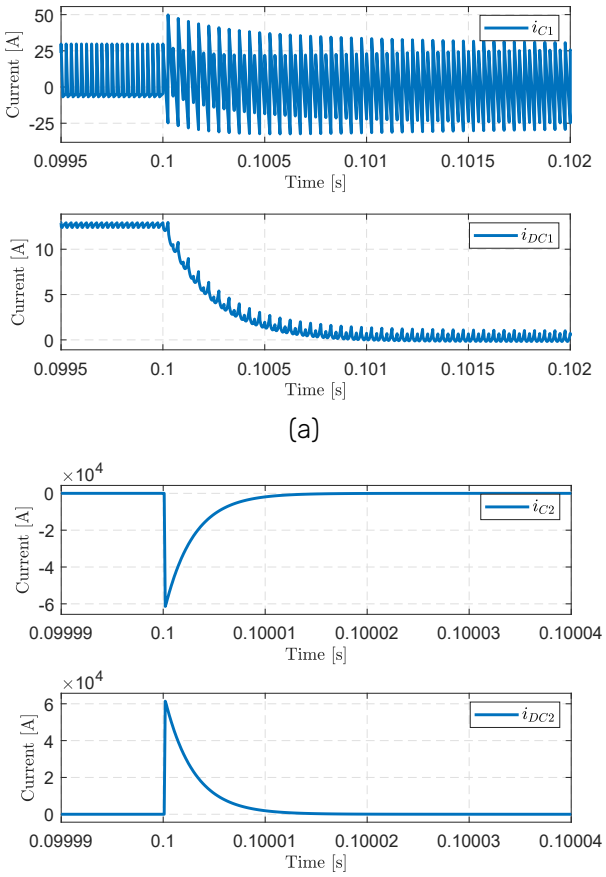

Fig. 3.4.9: Transient behavior of the DAB during HV fault: a) LV side capacitor current and DC current, b) HV side capacitor current and DC current.

Integration methods

This paragraph is about the numerical integration methods used in simulations to solve the ODE of the DAB. Only fixed step integration methods are discussed here, because in digital real-time simulators like OPAL-RT only these methods can be employed. Moreover, only explicit integration methods are considered because the implicit ones increase the computational effort, making them a worse choice for real-time simulations, even though they are more stable. The chosen integration methods range from the first to the fourth order and are respectively Euler, Heun, Bogacki-Shampine and Runge-Kutta [53], [54], [55].

Euler Method

The Euler method is a first order integration method to solve differential equations, where the local error is proportional to the square of the time step and the cumulative error is proportional to the time step. It is described by the following equation:

$$y_{n+1} = y_n + \Delta t \cdot F(t_n, y_n) + O(h^2), \tag{14}$$

where y_n and y_{n+1} are respectively the values of the state variables at the current and next time step, Δt is the time step, $F(t_n, y_n)$ is the system of differential equations to be solved and $O(h^2)$ means that this method has a first-order accuracy.

Heun's Method

The second order integration method is called Heun's method and it calculates the next value of the differential equation by calculating first an intermediate value. The Heun's integration method is given as follows:

$$\tilde{y}_{n+1} = y_n + \Delta t \cdot F(t_n, y_n) \tag{15}$$

$$y_{n+1} = y_n + \frac{\Delta t}{2}[F(t_n, y_n) + F(t_{n+1}, \tilde{y}_{n+1})] + O(h^3) \tag{16}$$

where $\tilde{y}_{n+1}$ is an intermediate value, $\mathrm{F}(\mathrm{t_n}, \tilde{y}_{n+1})$ is the differential equation calculated for $\tilde{y}_{n+1}$, and $\mathrm{O}(\mathrm{h}^3)$ means that a second order integration method has been used to integrate the differential equations.

Bogacki-Shampine method

Bogacki-Shampine method is a third order method to solve differential equations. It is given as follows:

$$\begin{cases} y_{n+1} = y_n + \frac{2}{9}\Delta t \cdot k_1 + \frac{1}{3}\Delta t \cdot k_2 + \frac{4}{9}\Delta t \cdot k_3 + O(h^4) \\ k_1 = F(t_n, y_n) \\ k_2 = F\left(t_n + \frac{1}{2}\Delta t, y_n + \frac{1}{2}\Delta t \cdot k_1\right) \\ k_3 = F\left(t_n + \frac{3}{4}\Delta t, y_n + \frac{3}{4}\Delta t \cdot k_2\right) \end{cases} \tag{17}$$

where $O(h^4)$ means that this is a third order integration method.

Runge-Kutta Method

Finally, the 4th order integration method is the Runge-Kutta method. It is defined as follows:

$$\begin{cases} y_{n+1} = y_n + \frac{\Delta t}{6} \cdot (k_1 + 2k_2 + 2k_3 + k_4) + O(h^5) \\ k_1 = F(t_n, y_n); \\ k_2 = F\left(t_n + \frac{1}{2}\Delta t, y_n + \frac{1}{2}\Delta t \cdot k_1\right); \\ k_3 = F\left(t_n + \frac{1}{2}\Delta t, y_n + \frac{1}{2}\Delta t \cdot k_2\right); \\ k_4 = F(t_n + \Delta t, y_n + \Delta t \cdot k_3); \end{cases} \tag{18}$$

where $O(h^5)$ means that the Runge-Kutta method is a fourth order integration method.
All the methods previously explained can be obtained as particular cases of the Runge-Kutta method.

Simulation results

The simulations in this chapter have been carried out by using Matlab as development environment. This chapter is divided into two paragraphs, respectively the comparison of the results of different integration methods with the ode45 Matlab solver as reference; and the analysis of the computational time required by each solver to run the simulation. Two DAB have been considered to show the different results that an integration method can achieve in terms of accuracy when the switching frequency changes. Their parameters are reported in Table 3.4.4. The only differences between these two configurations are the switching frequency, respectively 10 kHz and 1 kHz, and the inductor values, respectively 400 μF and 4 mH. The inductor value changes together with the switching frequency in order to keep the same power rating. In fact, power and voltages have been chosen according to home battery charger applications for electric vehicles, whereas the inductor value is obtained from (2) by substituting $\frac{\pi}{2}$ to φ, because this is the phase shift angle for which the maximum power transfer of the DAB is achieved.

Table 3.4.4: System specification

System Parameters			
Name	Value	Name	Value
P	5 kW	C	470 μF
V_{DC1}	400 V	R_{load}	110 Ω
N_1	8	N_2	15
f_{sw1}	10 kHz	L_1	400 μH
f_{sw2}	1 kHz	L_2	4 mH

Comparison of the results

Fig. 3.4.10 compares the output voltage of the first configuration of DAB made by the Runge-Kutta method at different time steps and the ode45 result. Fig. 3.4.11 makes the same comparison for the inductor current. In both these figures, it is possible to notice that the improvement in terms of accuracy is higher when passing from 10 μs to 1 μs time step, than when passing from 1 μs to 100 ns. So, as already expected, the more the time step decreases, the less improvement it is achieved in terms of accuracy. This means that, in specific conditions, it is possible to choose even a time step in the order of μs in power electronics simulations if the considered application does not require a high accuracy. Achieving a good compromise between accuracy and computational time is important especially when working with real time simulations, where the smaller is the time step and the higher is the risk of overruns, which compromise the validity of such simulations.

Fig. 3.4.12 and 3.4.13 compare the capacitor voltage and inductor current of the first configuration of DAB for the different integration methods proposed in this paper at a time step of 100 ns with the ode45 result. The same comparison has been made in Fig. 3.4.14 and Fig. 3.4.15 at a time step of 1 μs. From both these time steps, it is possible to notice that the Bogacki-Shampine method approximates the system better. In particular, the output voltage achieved from the Bogacki-Shampine method and from the ode45 solver are almost superimposed at both 100 ns and 1 μs.

Fig. 3.4.16 and 3.4.17 show capacitor voltage and inductor current of the second configuration of DAB for all the integration methods discussed at a time step of 100 ns and ode45. This time, not only are the Bogacki-Shampine results almost superimposed on the ode45 results, but also the Euler results are. So, while the Runge-Kutta method was better than Euler for approximating the first configuration of DAB, Euler is more suitable for the second one. This result means that different parameters, even for the same converter and differential equations, can lead to a different choice of the integration method.

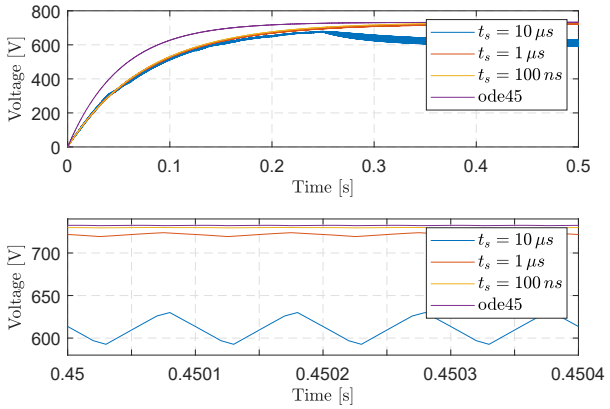

Fig. 3.4.10: Output voltage of the first configuration of DAB. Comparison between Runge-Kutta at different integration steps and ode45.

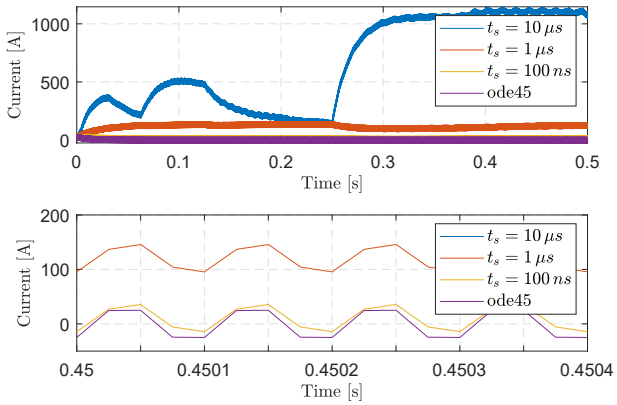

Fig. 3.4.11: Inductor current of the first configuration of DAB. Comparison between Runge-Kutta at different integration steps and ode45.

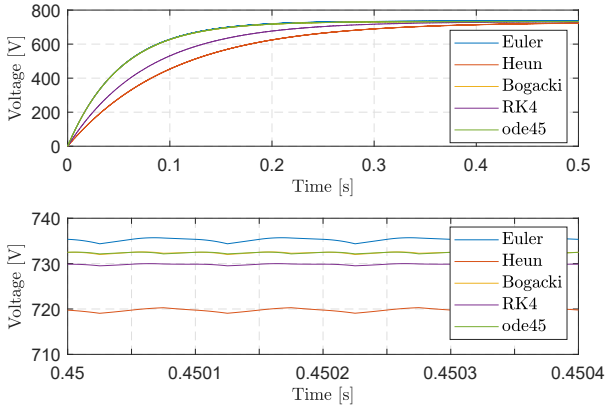

Fig. 3.4.12: Output voltage of the first configuration of DAB. Comparison between different solvers at $t_s = 100\ ns$

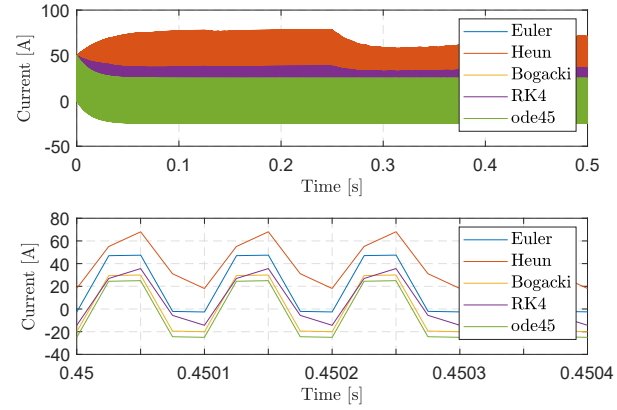

Fig. 3.4.13: Inductor current of the first configuration of DAB. Comparison between different solvers at $t_s = 100$ ns.

Computational time

The computational time has been measured on a laptop with an Intel(R) Core(TM) i7-10510U CPU with 1.80 GHz base clock frequency and 16 GB of RAM, whereas the operating system is Windows 10 Enterprise.

Tables 3.4.5 and 3.4.6 compare the minimum and maximum simulation duration of the discussed integration methods and the ode45 solver for both DAB configurations, respectively at $t_s = 100$ ns and $t_s = 1$ µs, for a simulated time of 0.5 s. These results show that the Euler method can be more appropriate when the computational time is a key factor, such as real-time simulations. However, it is always important to achieve a good compromise between the accuracy and the computational effort, because a fast but not accurate simulation can give some wrong information about the system itself. Another detail to observe is that the ode45 solver is a variable step solver. So, it is faster than the other integration methods for small time steps but slower for high time steps.

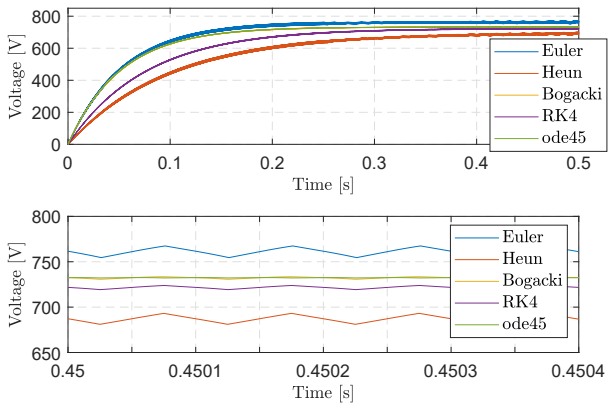

Fig. 3.4.14: Output voltage of the first configuration of DAB. Comparison between different solvers at $t_s = 1\,\mu s$.

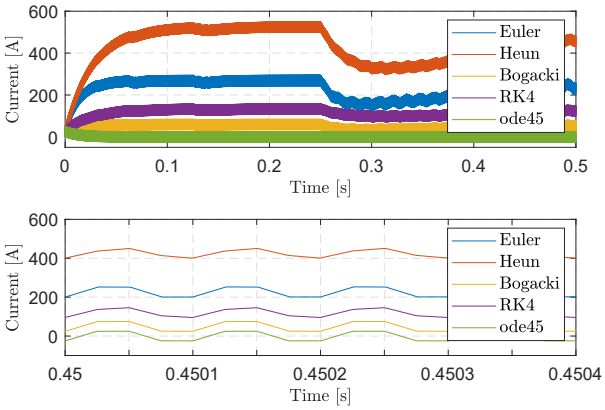

Fig. 3.4.15: Inductor current of the first configuration of DAB. Comparison between different solvers at $t_s = 1\,\mu s$.

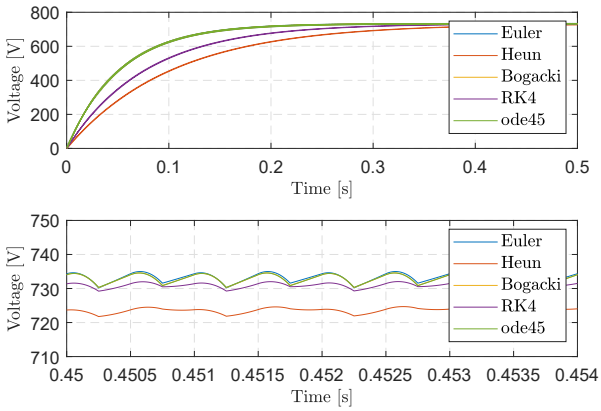

Fig. 3.4.16: Output voltage of the second configuration of DAB. Comparison between different solvers at $t_s = 100$ ns.

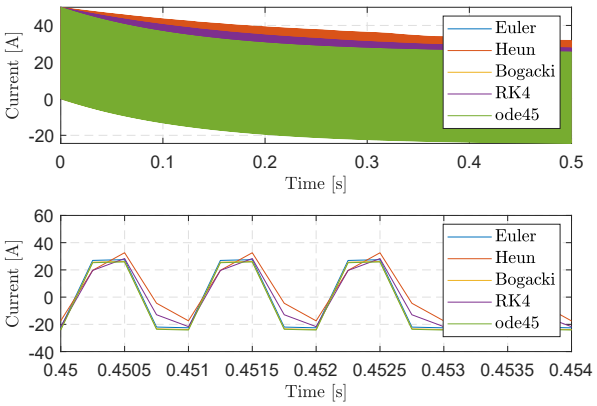

Fig. 3.4.17: Inductor current of the second configuration of DAB. Comparison between different solvers at $t_s = 100$ ns.

Table 3.4.5: Simulation duration for $t_s = 100\ ns$

Simulation duration		
Int. method	**min. sim. duration (s)**	**max. sim. Duration (s)**
Euler	7.553	8.371
Heun	21.683	22.874
Bogacki-Shampine	21.086	22.738
Runge-Kutta	27.878	30.360
ode45	12.366	17.950

Table 3.4.6: Simulation duration for $t_s = 1\,\mu s$.

Simulation duration		
Int. method	min. sim. duration (s)	max. sim. Duration (s)
Euler	0.836	0.963
Heun	2.283	2.756
Bogacki-Shampine	2.155	2.870
Runge-Kutta	2.801	3.319
ode45	12.366	17.950

Conclusion

This section has put together the results achieved in the first reporting period and published in conference papers [18], [19], and [20], giving an homogeneous structure. To start with, standards, architecture and main features of DC fast charging stations have been dealt with. The power converters adopted in DC fast charging stations have also been considered and some examples of architecture of DC fast charging stations have been given as well. Furthermore, a comparison between the FSBB and the DAB topologies has been done in terms of losses and short-circuit behaviour. It resulted that for lower power ratings the FSBB is more efficient than the DAB topology, whereas the DAB topology is more efficient for higher power ratings. It also resulted that through a simple control strategy that switches the FSBB behaviour from boost mode to buck mode this converter can be resilient again faults. Finally, the DAB converter has been modelled under different integration methods to compare their accuracy and computation times, and it has been found out that the integration method with the higher order does not give necessarily the best approximation of the converter. So, further work is needed to establish good procedures for the choice of the integration method for power electronic simulations. The future research work will focus more on DC fast charging stations, in particular a review journal is expected on this topic. Yet, the future work will also cover a benchmark of DC-DC converters with high-voltage range and optimization methods for DC fast charging stations.

3.4.3. Contribution to the WP objectives

The main results achieved during the first reporting period are related to the DC-DC converters and their modelling for DC networks. Moreover, the focus has also been to identify the main features, characteristics and power converters of DC fast charging stations for electric vehicles as a particular case of DC networks. In this sense, the main contribution of the work which has been conducted until now is the study of power converter topologies and their main features to fit the requirements of DC networks, in particular DC fast charging stations. The future work will also analyse the opportunities of energy storage systems in DC fast charging stations.

3.4.4. Scientific achievements

Experimental prototypes

#	Name	Description	Status (designed, assembled, tested)	Photo
1	8 kW Dual Active Bridge setup	An 8 kW Dual Active Bridge setup from the Imperix Company. It has different inductor values in such a way to experiment different possible configurations.	Assembled	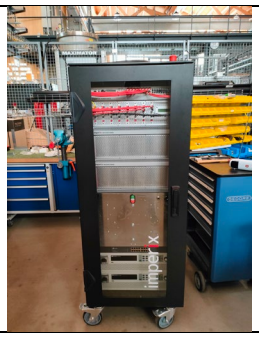

2	20 kW Dual Active Bridge	A 20 kW Dual Active Bridge setup from the Imperix Company. It has different inductor values in such a way to experiment different possible configurations.	Assembled	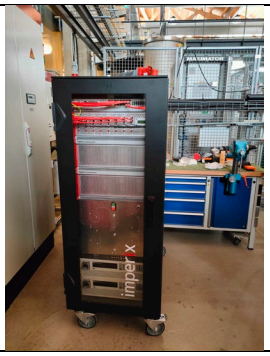

Publication

#	Title, incl. citation information	Type (Conference, journal, book chapter)	Status (Submitted, accepted, published)	DOI
1	Ö. Ekin, G. Arena, S. Waczowicz, V. Hagenmeyer and G. De Carne, "Comparison of Four-Switch Buck-Boost and Dual Active Bridge Converter for DC Microgrid Applications," 2022 IEEE 13th International Symposium on Power Electronics for Distributed Generation Systems (PEDG), Kiel, Germany, 2022, pp. 1-6, doi: 10.1109/PEDG54999.2022.9923074.	Conference	Published	doi: 10.1109/PEDG54999.2022.9923074.
2	G. Arena, D. Vinnikov, A. Chub and G. De Carne, "Accuracy Analysis of Dual Active Bridge Simulations under Different Integration Methods," *2022 AEIT International Annual Conference (AEIT)*, Rome, Italy, 2022, pp. 1-6, doi: 10.23919/AEIT56783.2022.9951711.	Conference	Published	doi: 10.23919/AEIT56783.2022.9951711.
3	G. Arena, P. Emiliani, A. Chub, D. Vinnikov and G. D. Carne, "DC Fast Charging of Electric Vehicles: a Review on Architecture and Power Conversion Technology," *2023 IEEE 17th International Conference on Compatibility, Power Electronics and Power Engineering (CPE-POWERENG)*, Tallinn, Estonia, 2023, pp. 1-6, doi: 10.1109/CPE-POWERENG58103.2023.10227492.	Conference	Published	doi: 10.1109/CPE-POWERENG58103.2023.10227492.

4	P. Emiliani, A. Blinov, G. D. Carne, G. Arena and D. Vinnikov, "Predictive Control for Isolated Matrix Rectifier Without Current Distortion at Sector Boundary," 2023 IEEE 17th International Conference on Compatibility, Power Electronics and Power Engineering (CPE-POWERENG), Tallinn, Estonia, 2023, pp. 1-6, doi: 10.1109/CPE-POWERENG58103.2023.10227405.	Conference	Published	doi: 10.1109/CPE-POWERENG58103.2023.10227405.
5	P. Emiliani, A. Blinov, G. De Carne, G. Arena and D. Vinnikov, "Three-Phase Four Wire High-Frequency Link Converter for Residential DC Grids," 2023 IEEE 17th International Conference on Compatibility, Power Electronics and Power Engineering (CPE-POWERENG), Tallinn, Estonia, 2023, pp. 1-5, doi: 10.1109/CPE-POWERENG58103.2023.10227416	Conference	Published	doi: 10.1109/CPE-POWERENG58103.2023.10227416.

4. Conclusions

All ESRs involved in WP3 started their activities with just few months of disalligmet among them. From the scientific point of view relevant tasks have been undertaken towards WP3 objectives. For each research line, ESRs performed insight scientific literature review and started with the analysis and simulation of the identified most promising architecues. In some cases the design of prototype or the definition of board to be used for experimental validation is also started.

For the ESR05 the structure of the energy router was defined, and operation modes were examined, including the control methods. Several isolated dc structures were investigated and simulated for the comparison of the quality of dc link and ac main/load voltages. Detailed analysis of Parallel and Redundant operation of two inverters in energy router, working at the "back-to-back" principle that reduces the load of inverters was done.

ESR06 proposed a converter connection scheme that allows optimizing power distribution between systems components, reducing losses, improving AC and DC grid power quality. The developed power converter interface structure, along with its control algorithm, enables the utilization of EV charger batteries through bidirectional EV chargers as a flexible component of a smart grid.

ESR07 studied architectures of the smart transformer (ST) as a link between medium and low voltage (MV and LV) ac and dc grids. Theoretical studies and simulations were conducted to understand the concept of smart transformer and modular multilevel converter (MMC) as an important part of the topology. ST can act as a system to control the hybrid grids. Also, it can provide the infrastructure to integrate new loads and sources. A new balancing method was suggested, in which the voltage of the capacitor, junction temperature of switches, and capacitor losses can be effectively balanced.

The main results achieved by ESR08 are related to the DC-DC converters and their modelling for DC networks. Moreover, the focus has also been to identify the main features, characteristics and power converters of DC fast charging stations for electric vehicles as a particular case of DC networks. The study of power converter topologies and their main features to fit the requirements of DC networks, in particular DC fast charging stations has been carried out.

Finally is worth to note that, except ESR05 who is hosted at UEX due to the war in Ukraine, the remaing ESRs already had their first secondment by reinforcing the collaboration with the other partners of this project and, in some cases, by publishing joint conference papers.

5. References

[1] D. Kumar, F. Zare and A. Ghosh, "DC microgrid technology: system architectures, AC grid interfaces, grounding schemes, power quality, communication networks, applications, and standardizations aspects," *Ieee Access,* vol. 5, p. 12230–12256, 2017.

[2] T. Dragičević, X. Lu, J. C. Vasquez and J. M. Guerrero, "DC microgrids—Part I: A review of control strategies and stabilization techniques," *IEEE Transactions on power electronics,* vol. 31, p. 4876–4891, 2015.

[3] T. Dragičević, X. Lu, J. C. Vasquez and J. M. Guerrero, "DC microgrids—Part II: A review of power architectures, applications, and standardization issues," *IEEE transactions on power electronics,* vol. 31, p. 3528–3549, 2015.

[4] S. Beheshtaein, R. M. Cuzner, M. Forouzesh, M. Savaghebi and J. M. Guerrero, "DC microgrid protection: A comprehensive review," *IEEE Journal of Emerging and Selected Topics in Power Electronics,* 2019.

[5] R. H. Lasseter, "Microgrids," in *2002 IEEE power engineering society winter meeting. Conference proceedings (Cat. No. 02CH37309)*, 2002.

[6] Y. Ito, Y. Zhongqing and H. Akagi, "DC microgrid based distribution power generation system," in *The 4th International Power Electronics and Motion Control Conference, 2004. IPEMC 2004.*, 2004.

[7] A. Pratt, P. Kumar and T. V. Aldridge, "Evaluation of 400V DC distribution in telco and data centers to improve energy efficiency," in *INTELEC 07-29th International Telecommunications Energy Conference*, 2007.

[8] J. Inamori, H. Hoshi, T. Tanaka, T. Babasaki and K. Hirose, "380-VDC power distribution system for 4-MW-scale cloud facility," in *2014 IEEE 36th International Telecommunications Energy Conference (INTELEC)*, 2014.

[9] E. Rodriguez-Diaz, J. C. Vasquez and J. M. Guerrero, "Intelligent DC homes in future sustainable energy systems: When efficiency and intelligence work together," *IEEE Consumer Electronics Magazine,* vol. 5, p. 74–80, 2015.

[10] D. J. Becker and B. J. Sonnenberg, "DC microgrids in buildings and data centers," in *2011 IEEE 33rd International Telecommunications Energy Conference (INTELEC)*, 2011.

[11] B. T. Patterson, "Dc, come home: Dc microgrids and the birth of the" enernet"," *IEEE Power and Energy Magazine,* vol. 10, p. 60–69, 2012.

[12] Z. Jin, G. Sulligoi, R. Cuzner, L. Meng, J. C. Vasquez and J. M. Guerrero, "Next-generation shipboard dc power system: Introduction smart grid and dc microgrid technologies into maritime electrical netowrks," *IEEE Electrification Magazine,* vol. 4, p. 45–57, 2016.

[13] G. Buticchi, L. Costa and M. Liserre, "Improving system efficiency for the more electric aircraft: A look at dc\backslash{}{/}{d}c converters for the avionic onboard dc microgrid," *IEEE Industrial Electronics Magazine,* vol. 11, p. 26–36, 2017.

[14] P. A. Madduri, J. Rosa, S. R. Sanders, E. A. Brewer and M. Podolsky, "Design and verification of smart and scalable DC microgrids for emerging regions," in *2013 IEEE Energy Conversion Congress and Exposition*, 2013.

[15] A. Jhunjhunwala, A. Lolla and P. Kaur, "Solar-dc microgrid for Indian homes: A transforming power scenario," *IEEE Electrification Magazine,* vol. 4, p. 10–19, 2016.

[16] S. Srdic and S. Lukic, "Toward extreme fast charging: Challenges and opportunities in directly connecting to medium-voltage line," *IEEE Electrification Magazine,* vol. 7, p. 22–31, 2019.

[17] H. Tu, H. Feng, S. Srdic and S. Lukic, "Extreme fast charging of electric vehicles: A technology overview," *IEEE Transactions on Transportation Electrification,* vol. 5, p. 861–878, 2019.

[18] G. Arena, P. Emiliani, D. Vinnikov, A. Chub and G. De Carne, "DC Fast Charging of Electric Vehicles: a Review on Architecture and Power Conversion Technology," in *2023 International Conference on Compatibility, Power Electronics and Power Engineering +(CPE-POWERENG 2023)*, 2022.

[19] Ö. Ekin, G. Arena, S. Waczowicz, V. Hagenmeyer and G. De Carne, "Comparison of Four-Switch Buck-Boost and Dual Active Bridge Converter for DC Microgrid Applications," in *2022 IEEE 13th International Symposium on Power Electronics for Distributed Generation Systems (PEDG)*, 2022.

[20] G. Arena, D. Vinnikov, A. Chub and G. De Carne, "Accuracy Analysis of Dual Active Bridge Simulations under Different Integration Methods," in *2022 AEIT International Annual Conference (AEIT)*, 2022.

[21] G. Rajendran, C. A. Vaithilingam, N. Misron, K. Naidu and M. R. Ahmed, "A comprehensive review on system architecture and international standards for electric vehicle charging stations," *Journal of Energy Storage,* vol. 42, p. 103099, 2021.

[22] M. Yilmaz and P. T. Krein, "Review of battery charger topologies, charging power levels, and infrastructure for plug-in electric and hybrid vehicles," *IEEE transactions on Power Electronics,* vol. 28, p. 2151–2169, 2012.

[23] S. Rivera, S. Kouro, S. Vazquez, S. M. Goetz, R. Lizana and E. Romero-Cadaval, "Electric vehicle charging infrastructure: From grid to battery," *IEEE Industrial Electronics Magazine,* vol. 15, p. 37–51, 2021.

[24] L. Wang, Z. Qin, T. Slangen, P. Bauer and T. Van Wijk, "Grid impact of electric vehicle fast charging stations: Trends, standards, issues and mitigation measures-an overview," *IEEE Open Journal of Power Electronics,* vol. 2, p. 56–74, 2021.

[25] M. A. H. Rafi and J. Bauman, "A comprehensive review of DC fast-charging stations with energy storage: Architectures, power converters, and analysis," *IEEE Transactions on Transportation Electrification,* vol. 7, p. 345–368, 2020.

[26] D. Aggeler, F. Canales, H. Zelaya-De La Parra, A. Coccia, N. Butcher and O. Apeldoorn, "Ultra-fast DC-charge infrastructures for EV-mobility and future smart grids," in *2010 IEEE PES Innovative Smart Grid Technologies Conference Europe (ISGT Europe)*, 2010.

[27] B. Wu, H. Chen, G. Guan, T. Ding and L. Yin, "Simulation model of three-phase PWM rectifier charging station and harmonic analysis on grid," in *2017 IEEE Innovative Smart Grid Technologies-Asia (ISGT-Asia)*, 2017.

[28] Z. Zhang, H. Xu, L. Shi, D. Li and Y. Han, "A unit power factor DC fast charger for electric vehicle charging station," in *Proceedings of The 7th International Power Electronics and Motion Control Conference*, 2012.

[29] A. Nabae, I. Takahashi and H. Akagi, "A new neutral-point-clamped PWM inverter," *IEEE Transactions on industry applications,* p. 518–523, 1981.

[30] N. Celanovic and D. Boroyevich, "A comprehensive study of neutral-point voltage balancing problem in three-level neutral-point-clamped voltage source PWM inverters," *IEEE Transactions on power electronics,* vol. 15, p. 242–249, 2000.

[31] J. W. Kolar and F. C. Zach, "A novel three-phase utility interface minimizing line current harmonics of high-power telecommunications rectifier modules," *IEEE Transactions on Industrial Electronics,* vol. 44, p. 456–467, 1997.

[32] J.-S. Lee and K.-B. Lee, "A novel carrier-based PWM method for Vienna rectifier with a variable power factor," *IEEE Transactions on Industrial Electronics,* vol. 63, p. 3–12, 2015.

[33] W. Ding, C. Zhang, F. Gao, B. Duan and H. Qiu, "A zero-sequence component injection modulation method with compensation for current harmonic mitigation of a Vienna rectifier," *IEEE Transactions on Power Electronics,* vol. 34, p. 801–814, 2018.

[34] D. Christen, F. Jauch and J. Biela, "Ultra-fast charging station for electric vehicles with integrated split grid storage," in *2015 17th European Conference on Power Electronics and Applications (EPE'15 ECCE-Europe)*, 2015.

[35] N. Hassanzadeh, F. Yazdani, S. Haghbin and T. Thiringer, "Design of a 50 kw phase-shifted full-bridge converter used for fast charging applications," in *2017 IEEE Vehicle Power and Propulsion Conference (VPPC)*, 2017.

[36] S. Rivera, J. Rojas, S. Kouro, P. W. Lehn, R. Lizana, H. Renaudineau and T. Dragičević, "Partial-power converter topology of type ii for efficient electric vehicle fast charging," *IEEE Journal of Emerging and Selected Topics in Power Electronics,* vol. 10, p. 7839–7848, 2021.

[37] F. Krismer and J. W. Kolar, "Accurate small-signal model for the digital control of an automotive bidirectional dual active bridge," *IEEE transactions on power electronics,* vol. 24, p. 2756–2768, 2009.

[38] B. Zhao, Q. Song, W. Liu and Y. Sun, "Overview of dual-active-bridge isolated bidirectional DC–DC converter for high-frequency-link power-conversion system," *IEEE Transactions on power electronics,* vol. 29, p. 4091–4106, 2013.

[39] G. Arena, G. Aiello, G. Scelba, M. Cacciato and F. Gennaro, "A Cost-Effective Hardware in the Loop Implementation of Dual Active Bridge for Fast Prototyping of Electric Vehicles Charging Controls," in *2021 23rd European Conference on Power Electronics and Applications (EPE'21 ECCE Europe)*, 2021.

[40] L. F. Costa, G. Buticchi and M. Liserre, "A family of series-resonant DC–DC converter with fault-tolerance capability," *IEEE Transactions on Industry Applications,* vol. 54, p. 335–344, 2017.

[41] L. Costa, G. Buticchi and M. Liserre, "A fault-tolerant series-resonant DC–DC converter," *IEEE transactions on power electronics,* vol. 32, p. 900–905, 2016.

[42] N. H. Kutkut, D. M. Divan, D. W. Novotny and R. H. Marion, "Design considerations and topology selection for a 120-kW IGBT converter for EV fast charging," *IEEE Transactions on Power Electronics,* vol. 13, p. 169–178, 1998.

[43] S. Haghbin, "A 50 kW Compact and Efficient Charger Prototype Utilizing SiC Power Modules and Nanocrystalline Magnetic Materials," in *2018 20th European Conference on Power Electronics and Applications (EPE'18 ECCE Europe)*, 2018.

[44] K. Drobnic, G. Grandi, M. Hammami, R. Mandrioli, M. Ricco, A. Viatkin and M. Vujacic, "An output ripple-free fast charger for electric vehicles based on grid-tied modular three-phase interleaved converters," *IEEE Transactions on Industry Applications,* vol. 55, p. 6102–6114, 2019.

[45] L. Tan, B. Wu, V. Yaramasu, S. Rivera and X. Guo, "Effective voltage balance control for bipolar-DC-bus-fed EV charging station with three-level DC–DC fast charger," *IEEE Transactions on Industrial Electronics,* vol. 63, p. 4031–4041, 2016.

[46] V. M. Iyer, S. Gulur, G. Gohil and S. Bhattacharya, "An approach towards extreme fast charging station power delivery for electric vehicles with partial power processing," *IEEE Transactions on Industrial Electronics,* vol. 67, p. 8076–8087, 2019.

[47] L. Camurca, T. Pereira, F. Hoffmann and M. Liserre, "Analysis, Limitations, and Opportunities of Modular Multilevel Converter-Based Architectures in Fast Charging Stations Infrastructures," *IEEE Transactions on Power Electronics,* vol. 37, p. 10747–10760, 2022.

[48] M. Orellana, S. Petibon, B. Estibals and C. Alonso, "Four switch buck-boost converter for photovoltaic DC-DC power applications," in *IECON 2010-36th Annual Conference on IEEE Industrial Electronics Society*, 2010.

[49] R. W. A. A. De Doncker, D. M. Divan and M. H. Kheraluwala, "A three-phase soft-switched high-power-density DC/DC converter for high-power applications," *IEEE transactions on industry applications,* vol. 27, p. 63–73, 1991.

[50] S. Shao, L. Chen, Z. Shan, F. Gao, H. Chen, D. Sha and T. Dragičević, "Modeling and advanced control of dual-active-bridge DC–DC converters: A review," *IEEE Transactions on Power Electronics,* vol. 37, p. 1524–1547, 2021.

[51] S. Liu, J. Liu, Y. Yang and J. Zhong, "Design of intrinsically safe buck DC/DC converters," in *2005 International Conference on Electrical Machines and Systems*, 2005.

[52] Y. Chen and Y. Zhang, "Fault characteristics and riding-through methods of dual active bridge converter under short-circuit of the load," *IEEE Transactions on Power Electronics,* vol. 36, p. 9578–9591, 2021.

[53] F. Li, Y. Wang, F. Wu, Y. Huang, Y. Liu, X. Zhang and M. Ma, "Review of real-time simulation of power electronics," *Journal of Modern Power Systems and Clean Energy,* vol. 8, p. 796–808, 2020.

[54] J. Cordier, S. Klass and R. Kennel, "A Discrete-Time Model of Induction Machines Including Winding Distribution Harmonics," in *2019 IEEE 13th International Conference on Power Electronics and Drive Systems (PEDS)*, 2019.

[55] S. D. Pekarek, O. Wasynczuk, E. A. Walters, J. V. Jatskevich, C. E. Lucas, N. Wu and P. T. Lamm, "An efficient multirate simulation technique for power-electronic-based systems," *IEEE Transactions on power systems,* vol. 19, p. 399–409, 2004.

[56] J. A. Sabate, V. Vlatkovic, R. B. Ridley, F. C. Lee and B. H. Cho, "Design considerations for high-voltage high-power full-bridge zero-voltage-switched PWM converter," in *Fifth Annual Proceedings on Applied Power Electronics Conference and Exposition*, 1990.

[57] L. Costa, G. Buticchi and M. Liserre, "Bidirectional series-resonant DC-DC converter with fault-tolerance capability for smart transformer," in *2016 IEEE Energy Conversion Congress and Exposition (ECCE)*, 2016.

[58] D. Cittanti, M. Gregorio, E. Armando and R. Bojoi, "Digital multi-loop control of an LLC resonant converter for electric vehicle DC fast charging," in *2020 IEEE Energy Conversion Congress and Exposition (ECCE)*, 2020.

[59] A. Bahrami, "EV Charging Definitions, Modes, Levels, Communication Protocols and Applied Standards," *Changes,* vol. 1, p. 10–01, 2020.

[60] *Tritium PKM150 - Product Specifications,* 2022.

[61] *PHIHONG EV Chargers - 2020-2021 EV Charging Solution.*

[62] M. I. Rahman, K. H. Ahmed and D. Jovcic, "Analysis of DC fault for dual-active bridge DC/DC converter including prototype verification," *IEEE Journal of Emerging and Selected Topics in Power Electronics,* vol. 7, p. 1107–1115, 2018.

[63] Q. Liu, Q. Qian, M. Zheng, S. Xu, W. Sun and T. Wang, "An improved quadrangle control method for four-switch buck-boost converter with reduced loss and decoupling strategy," *IEEE Transactions on Power Electronics,* vol. 36, p. 10827–10841, 2021.

[64] S. A. Gorji, H. G. Sahebi, M. Ektesabi and A. B. Rad, "Topologies and control schemes of bidirectional DC–DC power converters: An overview," *IEEE Access,* vol. 7, p. 117997–118019, 2019.

[65] S. P. Engel, M. Stieneker, N. Soltau, S. Rabiee, H. Stagge and R. W. De Doncker, "Comparison of the modular multilevel DC converter and the dual-active bridge converter for power conversion in HVDC and MVDC grids," *ieee transactions on power electronics,* vol. 30, p. 124–137, 2014.

[66] C.-W. Chen, K.-H. Chen and Y.-M. Chen, "Modeling and controller design of an autonomous PV module for DMPPT PV systems," *IEEE Transactions on power electronics,* vol. 29, p. 4723–4732, 2013.

[67] L. Callegaro, M. Ciobotaru, D. J. Pagano and J. E. Fletcher, "Feedback linearization control in photovoltaic module integrated converters," *IEEE Transactions on Power Electronics,* vol. 34, p. 6876–6889, 2018.

[68] S. Pugliese, G. Buticchi, R. A. Mastromauro, M. Andresen, M. Liserre and S. Stasi, "Soft-start procedure for a three-stage smart transformer based on dual-active bridge and cascaded H-bridge converters," *IEEE Transactions on Power Electronics,* vol. 35, p. 11039–11052, 2020.

[69] M. Liserre, G. Buticchi, M. Andresen, G. De Carne, L. F. Costa and Z.-X. Zou, "The smart transformer: Impact on the electric grid and technology challenges," *IEEE Industrial Electronics Magazine,* vol. 10, p. 46–58, 2016.

[70] M. La Mendola, M. Di Benedetto, A. Lidozzi, L. Solero and S. Bifaretti, "Four-port bidirectional dual active bridge converter for EVs fast charging," in *2019 IEEE Energy Conversion Congress and Exposition (ECCE)*, 2019.

[71] E. Kaufhold, J. Meyer, P. Schegner, A. S. Abdelsamad and J. M. A. Myrzik, "Comparison of solvers for time-domain simulations of single-phase photovoltaic systems," in *2020 International Conference on Smart Grids and Energy Systems (SGES)*, 2020.

[72] G. De Carne, M. Langwasser, M. Ndreko, R. Bachmann, R. W. De Doncker, R. Dimitrovski, B. J. Mortimer, A. Neufeld, F. Rojas and M. Liserre, "Which deepness class is suited for modeling power electronics?: A guide for choosing the right model for grid-integration studies," *IEEE Industrial Electronics Magazine,* vol. 13, p. 41–55, 2019.

[73] G. De Carne, G. Lauss, M. H. Syed, A. Monti, A. Benigni, S. Karrari, P. Kotsampopoulos and M. O. Faruque, "On modeling depths of power electronic circuits for real-time simulation–a comparative analysis for power systems," *IEEE Open Access Journal of Power and Energy,* vol. 9, p. 76–87, 2022.

[74] G. Buticchi, D. Barater, L. F. Costa and M. Liserre, "A PV-inspired low-common-mode dual-active-bridge converter for aerospace applications," *IEEE Transactions on Power Electronics,* vol. 33, p. 10467–10477, 2018.

[75] A. Benigni, T. Strasser, G. De Carne, M. Liserre, M. Cupelli and A. Monti, "Real-time simulation-based testing of modern energy systems: A review and discussion," *IEEE industrial electronics magazine,* vol. 14, p. 28–39, 2020.

[76] T. Dragičević, X. Lu, J. C. Vasquez and J. M. Guerrero, "DC microgrids—Part II: A review of power architectures, applications, and standardization issues," *IEEE transactions on power electronics,* vol. 31, p. 3528–3549, 2015.